Doctoral Dissertation
Doctoral Program in Electrical and Electronic Engineering (36th cycle)

Aqueous Based Hybrid Micro-Supercapacitors

A circuital element for a sustainable electronics

Davide Arcoraci
* * * * *

Supervisors
Prof. Andrea Lamberti, Supervisor
Prof. Candido Fabrizio Pirri, Co-supervisor

Doctoral Examination Committee:
Prof. Eugenio Gibertini, Politecnico di Milano
Dott. Francesco Lufrano, CNR-ITAE Messina

Politecnico di Torino
July 2024

I hereby declare that the contents and organisation of this dissertation constitute my own original work and does not compromise in any way the rights of third parties, including those relating to the security of personal data.

.....

Davide Arcoraci
Turin, July 2024

La più bella felicità dell'uomo pensante è di aver esplorato l'esplorabile e di venerare tranquillamente l'inesplorabile.

J. W. von Goethe

Acknowledgements

Un ringraziamento particolare va al Prof. Andrea Lamberti e Prof. Fabrizio Pirri, i primi sostenitori di questa ricerca e fondamenta di un meraviglioso gruppo di ricerca, da loro ho percepito un rispetto e fiducia profonde, qualità che oggi io reputo d'oro, e che spero non perderanno mai, siate orgogliosi del vostro impegno in questo ateneo. Questo lavoro non sarebbe mai stato possibile senza l'incoraggiamento dei miei, lontani ormai nel tempo, compagni di magistrale, Nicolò Cacocciola Michela Fracasso e Alessandro Vizzino, mi hanno invogliato a intraprendere la tortuosa avventura del dottorato, senza il loro incoraggiamento non sarei qui a scrivere queste parole. Ovviamente Pietro Zaccagnini, per mille motivi, dalla messa in pratica della ricerca, all'entusiasmo trasmessomi per l'elettrochimica. Cari tutti Mara, Alessandro, Marco, Stefano, Cristina, Luisa, Micaela, Roberto, Davide, Simone, Anna, ognuno di voi nella giusta misura è stato protagonista del lavoro qui raccontato. E in questo stralcio di testo sono costretto a limitarmi. Per tutti gli altri amici scusatemi so di voi, ci sarà la sede opportuna per dedicarvi un grazie.
Quindi, a tutta la ciurmaglia del DISAT ingresso 2, ufficio dottorandi terzo piano, a tutto il suo microcosmo esteso, i soli le lune le costellazioni vicine gli astri e le meteore di passaggio, le quasar e le pulsar un grande grazie. Tutti quelli che mi hanno parlato con sentimento supportato, sopportato, amato, odiato, gioito e riso con me. Un grazie di cuore. Ringrazio la Sicilia la terra che mi ha equipaggiato di questo bellissimo carattere, da me spesso descritto come un festival di difetti, ed il Piemonte un luogo che con le sue montagne suggestive e vini pregiati è riuscito a smussare. Il festival è divenuto una sagra insomma.
In fine… ringrazio te gentile lettore che avrai la pazienza di leggere fino in fondo questa tesi spero di ispirarti con questa tematica. Buona lettura.

Contents

Chapter 1

Introduction

State of the Art

A noteworthy work was initially conducted by D. Pech in 2010 [1] using an electrophoretic process an gold on a rigid substrate, and later by Toupin et al. [2], pursuing an making clear the concept of pseudocapacitors and hybrid capacitors. Subsequently, Zaccagnini [3] studied flexible substrates and laser scribing for large-scale fabrication. Micro-supercapacitors excel in three major application areas: protection circuits for electronics, wearable devices, and biosensing and healthcare applications.

This work touches on all these application fields and provides a method for fabricating supercapacitors, demonstrating that by adopting simple techniques on different substrates such as polyimide and silicon wafers, it is possible to achieve micro-fabrication with high tolerance without compromising the environmental aspect. It is shown that working on the layer between the active material and the current collector can yield up to a fourfold increase in performance reaching tens of $mFcm^{-2}$. Additionally, the device presented shows good cycling stability over 1000 cycles. The study demonstrates that mixing dendritic current collectors with metal oxide materials can enhance the performance of planar supercapacitors for the 400%. Besides, mixing micro-structured current collectors with metal oxides can lead to simplified area balancing techniques for planar electrochemical cells, aimed at developing on-chip devices with a large operating voltage window 1.5 to 2 V, high energy storage capability, and efficiency. The silicon substrate provides mechanical support and paves the way for on-chip applications, while the dendritic gold current collector significantly enhances the surface area for efficient ion adsorption and desorption along the electrode-electrolyte interface. Nowadays, the next major challenge for this research is exploring and insert sustainable gel electrolytes and developing sealing techniques for these electrolytes in order to have in a single process a large number of devices produced.

1.1 Energy and Sustainability

”Sustainability, the long-term viability of a community, set of social institutions, or societal practice. In general, sustainability is understood as a form of intergenerational ethics in which the environmental and economic actions taken by present persons do not diminish the opportunities of future persons to enjoy similar levels of wealth, utility, or welfare.”

Font from encyclopedia Britannica[4]. The broader context to which the work presented in this thesis is to conceptualize and develop processes related to energy storage devices, in particular on supercapacitors, SCs. Applying a miniaturization and low-impact approach; with the aim to explore this technology, and its future use, as close possible compliant with the given definition of sustainability. The aim is also to define the concept of a self powered device for sustainable electronics, and validate the fundamental role that a miniaturizated supercapacitor, renamed micro-supercapacitors, will have for the development of this technology. An other key concept for the readings that places man as a user the way and the processes through these functionalities,as are achieved. Modern technologies value a lot those aspects, therefore the smart systems is linked to the smart use, that must embrace to concepts like low impact, green-like, eco-friendly. The final goal will be make, the entire life cycle of the product and its use starting from production to disposal, sustainable.

In environmental sciences and economic sciences, the terms ”sustainability” refers to the condition of a certain development that is capable to ensure the satisfaction of the needs of the current generation without compromising the ability of future generations to fulfill their own needs.

The notion of sustainability was initially broached at the inaugural United Nations Conference on the Environment in 1972. However, it wasn’t until 1987, with the release of the ”Brundtland report,” that the concept of sustainable development was explicitly outlined. Following the UN Conference on Environment and Development in 1992, it emerged as the guiding principle for research and development. Sustainability, viewed through an environmental lens, underscores the importance of ecological systems, which exhibit characteristics such as carrying capacity, self-regulation, resilience, and resistance. These factors collectively impact the stability of the ecosystem. Implicit sustainability arises from a balanced ecosystem; furthermore, the more stable it is, the better its self-regulation capabilities are, especially in comparison to external factors, which frequently disrupt its equilibrium. The factors that disrupt ecosystems’ balance even more are the relationships they establish with another type of complex system. The interaction between these two complex systems increases the likelihood of disturbances and raises the risk of irreversible alterations. Over the years, the concept of sustainability has undergone a profound evolution. Initially centered predominantly on ecological aspects, it has evolved towards a more comprehensive meaning that considers not only the

environmental dimension but also the economic, social, and especially, in today's context, the technological dimension. In essence, sustainability implies a constant and preferably growing well-being in environmental, social, economic, and technological terms. It involves the perspective of ensuring that future generations inherit a quality of life at least as good as the present one. Furthermore, taking in to account the relationship between sustainability and electronics a complex topic that involves various aspects. Here are some key points that illustrate this connection. Sustainable production: the electronics industry can work to improve sustainability through eco-friendly production practices. This includes adopting low-impact production processes, responsibly using resources, and reducing waste. Sustainable materials material choices are crucial. Adopting recyclable, low-impact, or sustainably sourced materials contributes to the sustainability of electronics. Responsible electronic waste management is also a critical aspect. Energy efficiency, improving the energy efficiency of electronic devices contributes to sustainability. Producing and using devices that require less energy reduces environmental impact and promotes sustainable energy resource consumption [5]. Modular design and upgrades, creating electronics with a modular design, allowing for high reparability idex and upgrades rather than complete replacement, contributes to sustainability by reducing the overall amount of electronic waste. Recycling, responsible electronic waste management is crucial. Properly recycling electronic components reduces the environmental impact of electronic waste, which often contains harmful substances. Social impact, sustainability in electronics can also consider social aspects, such as social justice in production and the promotion of ethical working conditions throughout the supply chain. In summary, sustainability in electronics involves reducing environmental impact, improving energy efficiency, responsibly managing electronic waste, and considering social aspects in production and product lifecycle. The approach and methodology adapted throughout this thesis work are to miniaturize and make the electrochemical systems known as supercapacitors as sustainable as possible (low impact). Aimed at evaluating the hypothesis of scalability and transportability, this approach therefore contributes to and consolidates what we know today as self-powered devices. [6, 7, 8, 9].

1.2 Supercapacitors, Smart-Devices and IoT

In, principle, by super-capacitor we mean a device capable of storing electrical/chemical energy within its volume, in which making a comparison with the performance offered by so-called "traditional" capacitors are able to easily exceeds the thresholds of 100 F/g or, 20 Wh/kg. The supercapacitor also called ultra-capacitor or electrochemical double-layer capacitor, EDLC. Are governed by the same fundamental equations as conventional capacitors but use electrodes with extraordinary surface area, this is possible for example involving activated carbon which has a surface area per unit of gram equal to 2000 m^2. Plus, supercapacitor can achieve

exceptionally large unit volume capacities, while working at medium/low voltages 0 to 5 V. Thanks to this, they have higher energy density compared to conventional capacitors and higher power density compared to batteries [10]. Supercapacitors belong to the macro area of Energy storage devices, ESDs. By energy storage device we generically identify a device capable of storing energy of a different nature within its volume and releasing the same energy when the user of the device requests it. Currently are adopted for portable and remote electronic systems, also equipped on circuit boards as energy/power supplies or energy/power backups [7]. These are utilized to produce precise information through data fusion, employing energy harvesting solutions and energy storage systems to extend the lifespan of the sensing platform. The next move will be the reduction of power consumption of the ESDs reduction [11, 12]. Currently, the market is focusing for a specific sector with specific applications such as wearable and healthcare electronics. This trend has led to the development of ESDs that have specific mechano-chemical requirements [13]. At present, comparison is necessary, so is needed to involve secondary battery and capacitor and use this technologies mainly to supply power and guarantee energy backups to electrical systems. Looking at the Fig. 1.1. Batteries are mainly exploited for prolonged, in time, applications because of their high energy density capabilities. Furthermore, in some cases electrochemical capacitors are used, as substitute of batteries in power backup operations do not require prolonged functioning. In these case we talk about on-demand power consumption. Although electrolytic capacitors have high-power capabilities, their low energy density often necessitates the use of multiple devices in parallel to achieve the required functionality. In contrast, supercapacitors (SCs) offer significantly higher energy densities and sufficiently high-power densities. Furthermore, SCs have a longer life cycle compared to batteries, particularly when energy storage mechanisms are confined to the surface.

In the context of current policies, the development of low-impact processes is crucial. However, for a long period, technological advancements and profitability have taken precedence over environmental concerns. Additionally, a fabrication process can be considered sustainable if the electricity consumed is sourced from renewable energy.

If the primary source of electrical energy is derived from fossil fuels, electrochemical processes and their products inherently contribute to environmental impact [8]. In light of the shift towards a zero-carbon energy sector [15], known as the energy transition, it is crucial to develop sustainable and low-impact electrochemical processes to align with the sustainable development goals. Recently, many efforts have been done to achieve good performances in this field regarding power and energy densities by using a sustainable chain production that becomes the driving force of new research challenges. Throughout the discussion developed here we will refer mostly specifically to devices capable of store electrical energy and chemical energy as a type of stored energy. Introducing the **hybrid-supercapacitors** we mean a

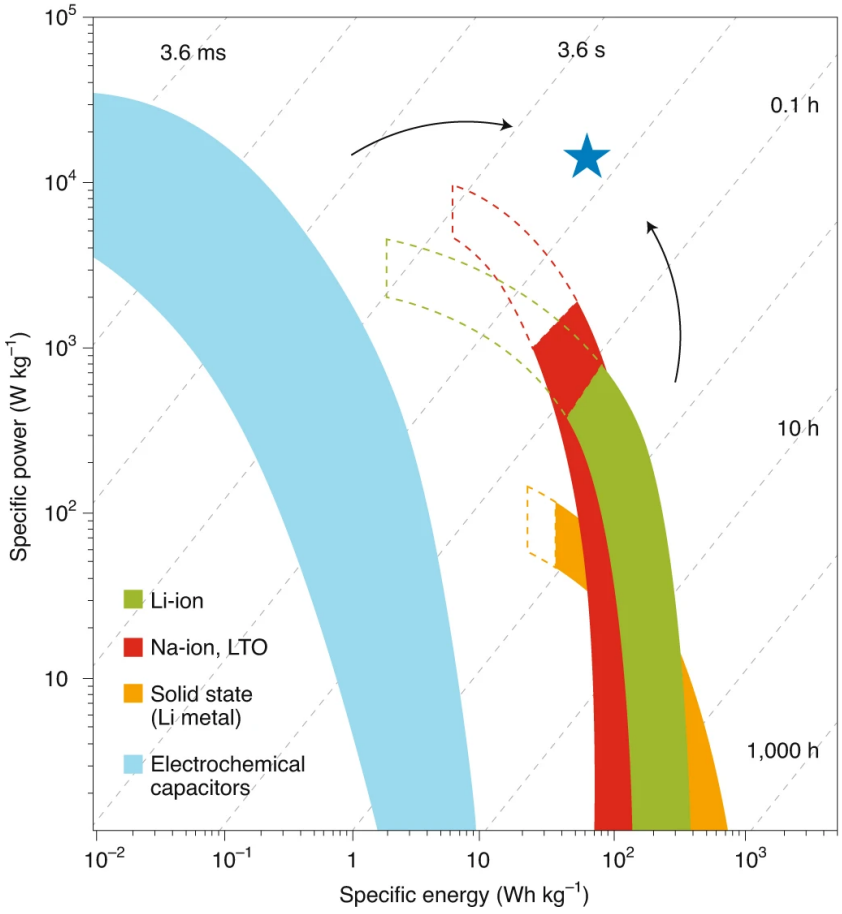

Figure 1.1: Classical Ragone plot shows the relation between specific power and specific energy fo various energy storage system P. Simon and Y. Gogotsi [14].

device capable of store electrical/chemical energy within its volume, that mix two different mechanism despite the "standards" electrical double layer supercapacitors. The reason why research is trying to merge the two different mechanisms, despite the technological complexity, lies in achieving specifications that favor specific energy storage capabilities, in order to extend the range of use. And these reason global hybrid-supercapacitor market size is experiencing significant growth and will grow considerably in the next few years. One electrode displays electrostatic capacitance, whereas the additional has electrochemical capacitance. Due to its high-power density and high energy density, a hybrid capacitor is fit for both applications. In addition, hybrid-supercapacitor is proficient of working in extreme temperatures, extending from -55°C to +200°C. Moreover, hybrid capacitors have an excellent frequency response of 5 kHz and are compact in size with respect to

aluminum electrolytic capacitors. Hence, owing to profit associated with hybrid-supercapacitors, it is highly accepted across several application segments particularly in the next energy generation, and automotive transition sector. Based on architecture, the Hybrid capacitor market can be divided into Hybrid capacitor module, and Board mounted hybrid capacitor. And these depend on the application, the market is categorized into Off-grid lighting, memory back-up, solar charge applications, on the basis of industry vertical into automotive and transportation, power generation and distribution, consumer electronics, and Others. And Geographically, the market is analyzed across several regions such as North America, Europe, Asia-Pacific, and Latin America, Middle East & Africa. Key players operating in the global hybrid capacitor market are Maxwell Technologies Inc., Ioxus Inc., Nesscap Co. LTD., YUNASKO, Panasonic Corporation, CAP-XX, Supreme Power Solutions Co. Ltd., Nippon Chemi-Con Corporation, NEC-Tokin, LS Mtron.

These companies have adopted several strategies such as product launches, partnerships, collaborations, mergers & acquisitions, and joint ventures to strengthen their foothold in the global market.

Nowadays Smart devices or being more precisely smart electronics system, refer to electronic devices that incorporate advanced functionalities, often featuring wireless connectivity, adopting internet protocol or also offline transmission protocol such us WiFi, Bluetooth and NFC. and the ability to interact with other devices or digital platforms. These devices are designed to simplify daily life, enhance efficiency, and provide new opportunities for interaction with the environment. Common examples include smartphones, smart TVs, smart home devices, such as smart thermostats, connected lights, security cameras, smartwatches, and other connected objects that can be controlled or monitored through apps or voice commands. In this "artificial ecosystem", incorporating the supercapacitors as a sub-element of the supply module can play a pivotal role in establishing a sustainable use, as initially mentioned. Referring to the Bluetooth protocol for simplicity, we can delineate the functionality of a smart device based on its energy request. When the device is in idle mode, there is a low power demand, suitable for prolonged use, we can call it also **"idle −> energy mode"**. Conversely, when the device is in communication mode, a substantial energy demand is anticipated over a short duration so we identify a **"transmission −> power mode"**. In this task distribution aimed at ensuring uninterrupted operation, the incorporated battery within the system is designated to support the energy mode, while the supercapacitor is assigned to operate in transmission power mode. These two operating regimes have a range of required power ranging from 10 μW *to* 1000 μW. These approach posing the right harvester in the system can led to a complete off grid smart-device.[16]

1.3 Miniaturization hypothesis, electrochemistry & microelectronics

Conventional supercapacitors, due to their large size, pose limitations for various applications such as flexible and wearable electronics, as well as integration with on-board devices [17, 18, 3, 19] The miniaturization of electronics has led to the shrinking of energy storage devices adopted in power supply or backup solutions in the Internet of Things, IoT. At present, the miniaturization trend is evolving at different scaling rates, with the integration of electronic devices developing fastest. Micro-batteries have been developed in the last decade, but they suffer from low power capabilities and short life cycle [20, 21, 22] Micro-supercapacitors have a small footprint, relatively high energy density, and the ability to quickly discharge to provide high-power densities [1]. Moreover, the manufacturing methods employed for conventional supercapacitors are not compatible with micro-system fabrication. Therefore, the demand arises for on-chip supercapacitors that can be seamlessly integrated using techniques compatible with standard microelectronics devices[23]. As expected, micro-supercapacitor operate on the same fundamental principles as their conventional counterparts but diverge in their design, architecture, and fabrication technologies. Following the work, we will describe a μSC fabricated mainly via electrochemical steps in aqueous environment. Supercapacitors properties and electronics power requirements led research focusing on the development of miniaturized supercapacitors, called micro-supercapacitors,μSCs, suitable for power supply and especially as power backups. Micro-supercapacitors represent a valuable alternative to low-energy-density electrolytic capacitors. In this scenario, since the Supercapacitor, is an electrochemical device that envisions a medium between its two electrodes, either in a gel or aqueous phase, it becomes essential to question whether an electrochemical system can adhere to the scaling laws dictated over the years by electronics. This study aims to validate the scaling hypothesis applied to electrochemical systems and provide a foundation for the performance metrics that miniaturized electrochemical devices can offer. Additionally, it seeks to outline the open challenges and identify the next steps that can be taken to advance this technology.

1.3.1 Definition of micro-supercapacitor

Here is a definition of what is meant by micro-super capacitor. By micro-supercapacitor, we can therefore mean devices that:

- An object that adopt the well-known development and fabrication processes adopted by microelectronics industry;
- An objects capable of going well beyond the capacitance standard per unit of area achievable with actual technology;

- Therefore an object that in very long life cycle inherent utilization over 1 000 000 cycles;
- An object whose dimensions are controllable on a micro unit scale;
- An object that can handle very high current rate respect its volume.

This set of characteristic features allow us to identify μSC. μSCs potentialities are in the exploitation of these devices increasing for many applications in microelectronics, such as wearable electronics energy storage recovery self-powered sensors and protection circuit.

1.4 From *consumer electronics* toward the *sustainable electronics* concept.

Examining how these two regimes can harmoniously coexist, deriving power from distinct energy storage modules, all while leveraging a common energy harvester as the source that binds them together. Here too, taking as an example a device for wearable electronics, we can see how the human body itself in its daily activity becomes an integral part of the electrical power supply of the smart devices adopted compatible harvesting systems such as Die Sintetized Solar Cell, triboelectric harvester and solar panels. They therefore define a device that can be powered off-grid with virtually unlimited operation in time [24, 9]. Beyond the purely application aspect, it is crucial to consider the industrial and technical aspects that are often overlooked by companies even today. Particularly in the electronics industry, driven by increasing demand in both mature and emerging markets, many crucial issues arise. This demand, coupled with intense competition for the lowest price, poses numerous challenges for companies that outsource production and move operations abroad to maximize profits and optimize the supply chain. Adding to this, the increasingly shorter product lifecycles, sustainability becomes an even more critical factor for this sector. On the supply chain front, it becomes clear that the sector needs better corporate regulation to monitor its supplier base. This can help prevent violations of human rights in the workplace and environmental risks. In the final phase of the product lifecycle, the sector has not maintained consistency in efforts to recycle or withdraw discontinued products. Through regulation, companies will be obliged to recover more devices, improving withdrawal rates and increasing recycling and reuse. The entire supply chain lacks coherence regarding corporate responsibility, sustainability, and human rights programs. Just as there are organizations like ISO and TL that assess specific corporate aspects or programs and financial and regulatory requirements, it becomes essential for government bodies to also support companies in meeting the objectives of a sustainable supply chain. In evaluating companies, a framework is used. This framework includes the evaluation of supplier relationship management, supply chain management, labor and

human rights risk, and sustainability. Most companies in this sector fall into the middle range, however, there is a need for improvement especially in scores related to labor, human rights, and sustainability. Any issues in the supply chain can impact the slim profit margins typical of the electronics sector. Currently, there are two ISO standards available, ISO 14001 for environmental management systems and ISO 50001 for energy management, but they are not yet widely implemented by evaluated companies. Although they do not directly regulate CO_2 emissions or energy use, working towards these standards could represent a significant step towards greater sustainability in the electronics sector.

Chapter 2

Theoretical Models

The present chapter focuses on various models that have historically been developed and have evolved over the years, in order to give a brief understanding of electrochemical system, the behavior and contribution of both double-layer capacitance and pseudo-capacitance. Through an examination of these models that have been developed and refined over time, we can define how double-layer capacitance and pseudo-capacitance, work and their respective roles in energy storage systems. This comprehensive analysis allows us to unravel the complex interplay between these two distinct mechanisms and their combined impact on the performance of electrochemical capacitors. Moreover, our understanding of double-layer capacitance and pseudo-capacitance, from their initial conceptualizations to their integration into practical applications. In essence, through a thorough examination of the historical models and their evolution, we can gain valuable insights into the nuanced behavior of double-layer capacitance and pseudo-capacitance, enhancing our understanding of these fundamental aspects of electrochemical energy storage.

2.1 Physico-Chemical Models for Energy Storage Devices

Supercapacitors, also known as ultra-capacitors or electrochemical double-layer capacitors EDLCs, represent a significant advancement in capacitor technology, particularly when compared to traditional electrolytic capacitors. Unlike electrolytic capacitors, supercapacitors adopt electrolyte, that can be solid or liquid. The energy storage mechanism of supercapacitors relies on two distinct capacitance components, each associated with different charge storage principles. The first the electrical double-layer capacitance, EDLC, is type of capacitance that arises from the electrostatic separation of charges at the interface between a conductor's surface and an electrolyte solution, forming what is known as the Helmholtz double layer[25]. It represents a form of energy storage of electrostatic nature. The second

mechanism, the **pseudo-capacitance**, unlike double-layer capacitance, pseudo-capacitance involves electrochemical charge transfer, involving electrons, between the electrolyte ions and the electrode. The charge transfer is facilitated by chemical reactions occurring on the electrode surface, predominantly reduction-oxidation, red-ox, reactions and ion adsorption from the electrolyte. By leveraging these two distinct charge storage mechanisms, supercapacitors can achieve remarkable energy storage capabilities. They exhibit large capacitance values, often reaching into the farad range, and can store and deliver electrical energy rapidly. This unique combination of features makes supercapacitors highly versatile and suitable for various applications requiring high power density, rapid charge/discharge cycles, and long operational lifetimes. Furthermore, supercapacitors fills the gap between short-time energy devices respect to long-time energy devices, in other words from capacitors and batteries, offering a balance between energy storage capability and power delivery. This makes them particularly attractive for use in hybrid energy storage systems, full electric vehicles, renewable energy applications, and portable/wearable electronic devices. So, it is easy to see how capacitance at the potential applied to the device influences the energy stored by the system, the capacitive term intervenes linearly while the potential term offer quadratic trend. Nowadays, mixing the two charge storage mechanism researcher try to extend the operating potential window of the device, in order to raise the specific energy stored, as much as possible without compromising the long-term cycling stability [26, 27].

$$E = E(C, V) = \frac{1}{2} C \Delta V^2 \tag{2.1}$$

In summary, supercapacitors represent a promising technology with wide-ranging potential in the realm of energy storage. Their ability to combine electrostatic and electrochemical charge storage mechanisms opens up new possibilities for innovation in various industries and contributes to the ongoing pursuit of more efficient and sustainable energy storage solutions.

2.1.1 Helmholtz Model

Helmholtz proposed the first model of charge separation at the interface between two metals in 1853. Later, in 1879, he replaced the metal-metal interface with the metal-aqueous solution interface. To model explain how the interface between a metal and an electrolyte solution behaves like a capacitor, capable of accumulate electrical charge.

In this model, the metal electrode possesses a certain density of positive charge that is exactly balanced by an amount of ions present in the electrolyte solution, the charge are free to move, these ions moving toward the electrode balance equally but oppositely the charge present on the surface. However, the ions are not in direct contact with the electrode, because the presence around the ions of a **solvation**

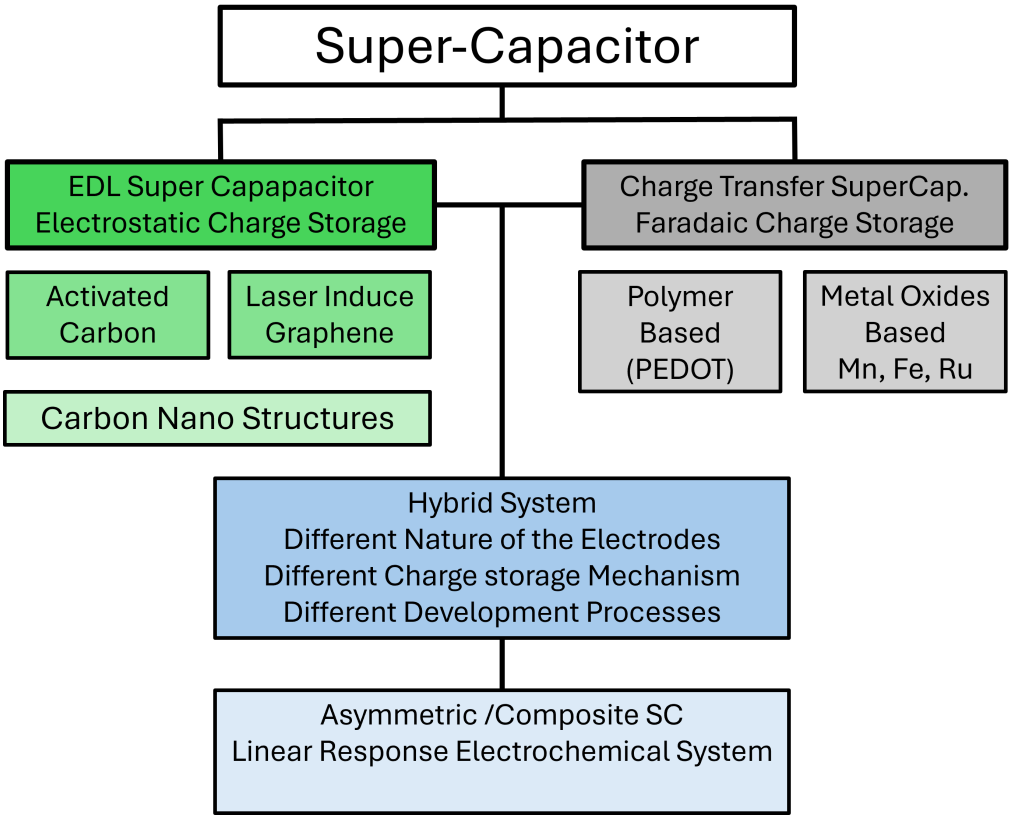

Figure 2.1: Table for the utilization of supercapacitors based on the materials involved.

shell that is formed by the solvent molecules. This creates a potential difference across the interface. The imaginary line crossing the centers of these solvated ions, surrounded by solvent molecules due to electrostatic attraction, at the minimum distance from the electrode, defines the boundary known as the *Outer Helmholtz Layer* see Fig. 2.2.

The region within this boundary is called the electric double layer because it consists of a layer of charges on the electrode surface and a monolayer of ions in the electrolyte.

Helmholtz's model, has some limitation, does not fully describe the correct functioning of the double-layer capacitance. Experimental data do not confirm the model, because capacitance discharge due to electrochemical reactions occurring at the interface, and the also because the double-layer capacitance depends not only on the composition but also on the electrolyte concentration, and is further dependent on the applied potential[25]. The double-layer dielectric as thickness d with the order of an half nanometer for example referring to Na^+ ions. There are uncertainties about what value to assign to thicknesses of the layer, d is equal,

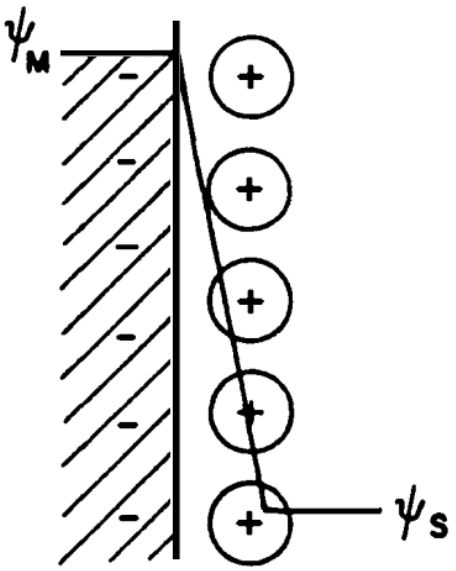

Figure 2.2: Elementary section description of Metal-Liquid interface eith the formation of the Helmoholz layer.

$$q_M = q_S \tag{2.2}$$

$$\psi(x) = (\psi_S - \psi_M)\frac{x}{d} + \psi_M \tag{2.3}$$

$$C = \kappa_0 \frac{A}{d}\varepsilon_r \tag{2.4}$$

and it is also strong related on the molecular basis and the zeta-potential of the molecule. This is a significant conclusion regarding the state of water within the double layer at polarized electrode interfaces. Similar findings are applicable to other charged electrodes, such as gold and carbon.

Gouy-Chapman Model

Louis George Gouy and David Chapman in 1910, introduced a new model that specifically accounted for the dependency of capacitance on potential and electrolyte concentration.

However, in the Gouy-Chapman model, ions are treated as point charges and distribute themselves from the electrode to the solution under the influence of two forces.

The first depends on the excess charge on the electronic conductor, which tends to accumulate charge on the electrode. The second si mitigated by thermal agitation, which tends to disperse the charge. So we can visualize, a rigid, compact double layer between the electrode surface and the Helmholtz Layer, and a diffuse double layer between the Helmholtz layer and the bulk of the solution. However, this dependency does not match experimental observations. While the Gouy-Chapman model is less rigid than that of Helmholtz, significant differences persist between the model and experimental data. The main limitation arises from the assumption of ions as point charges.

Stern Combination

An additional step for a complete description was achieved with Stern's model in 1924. According to the Stern model, there is an excess charge localized at the outer Helmholtz layer that alone is not able to balance the charge present on the electrode. The remaining charge necessary for equilibrium is found between the Outer Helmholtz Layer and the bulk region of the solution, so is possible to introduce a **diffuse layer**. In Stern's model, within the compact double layer between the electrode and the Outer Helmholtz Layer, starting from electrode, applying the Helmholtz model, the potential varies linearly with distance; whereas in the diffuse layer, the potential varies exponentially according to the Gouy-Chapman law see Fig. 2.3. The electrical equivalent consists of two capacitors in series.

Bockris-Devanthan-Muller Model

In 1963, Bockris, Devanathan, and Muller proposed a model known as the B-D-M model of the double layer that included the action of the solvent on the electrolyte interface. According to this model, solvent molecules, such as water, exhibit a certain alignment with the electrode surface. This alignment is particularly evident in the first layer of solvent molecules, which show a strong orientation to the electric field depending on the charge. This orientation significantly influences the solvent's permittivity, which varies with the strength of the electric field. It is important to note that some of these solvent molecules can be replaced or removed by the adsorbed ions, as described in the previous model. The Inner Helmholtz Layer passes through the center of these molecules and the adsorbed ions, representing a crucial reference point in the double layer structure. It is worth noting that, despite the significant contribution of the Bockris-Devanthan-Muller model in understanding the solvent's action at the electrolyte interface, there are more complex models that can describe the double layer capacity more accurately.

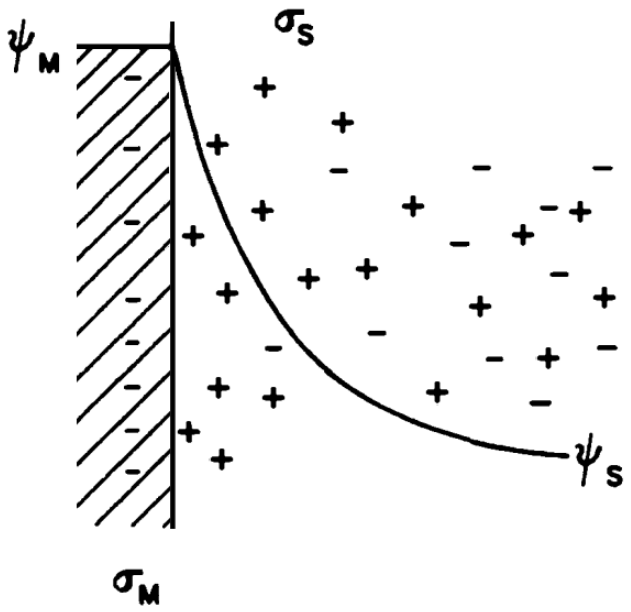

Figure 2.3: Gouy model graph.

$$q_M = -q_S = \left(\frac{2k_BTc\varepsilon}{\pi}\right) sinh \frac{ze(\psi_s - \psi_M)}{2k_BT} \tag{2.5}$$

$$C = \varepsilon_r \varepsilon_0 \lambda_D^{-1} cosh \frac{ze(\psi_s - \psi_M)}{2k_BT} \tag{2.6}$$

$$\lambda_D = \left(\frac{e^2 z^2 c\varepsilon}{2\pi k_BT}\right)^{1/2} ;\ Debye\ lenght \tag{2.7}$$

$$\psi(x) = (\psi_M - \psi_S) e^{-x/\lambda_D} \tag{2.8}$$

2.1.2 Pseudocapacitance

An other mechanism through is possible store charge on an interface electrolyte electrode by mean of chemical reaction is **pseudo-capacitive** effect.

In addition to the double layer capacitance, which forms due to the orientation of electrolyte molecules near the electrode surface, there is also a pseudo-capacitance arising from reversible Faradaic reactions between the electrolyte and the electrode. Pseudo-capacitance arises when the charge, Q, transferred during the process, is approximate as continuous function of the potential, V, so that a derivative, dQ/dV, give the electrical properties of a capacitive surface. Following some examples are treated. These reactions involve the transfer of electrons from electrolyte ions to

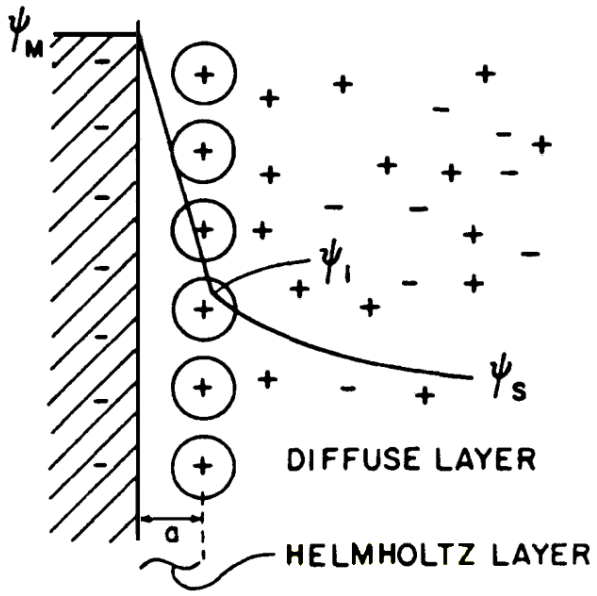

$$q_M = -q_S = [q_H + q_G] \tag{2.9}$$

$$\frac{1}{C} = \frac{1}{C_H} + \frac{1}{C_G} \tag{2.10}$$

Figure 2.4: Graph of the combination fo Helmholtz and Gouy model.

the electrode, generating a Faradaic current.

It's important to note that this current is not caused by the direct movement of charge but by reactions occurring at the electrode-electrolyte interface. This Faradaic charge transfer depends on the applied voltage, resulting in a capacitance-like phenomena to what is observed in capacitors. This capacitive behavior is primarily caused by reduction-oxidation reactions and ion adsorption phenomena. A comprehensive explanation of oxidation-reduction reactions, commonly referred to as redox reactions. In these chemical processes, electrons are exchanged between two distinct chemical species, which can manifest as molecules, ions, or atoms. A redox reaction is comprised of two fundamental sub-reactions: Oxidation, this involves a chemical species that lose electrons. Reduction, conversely, this entails a chemical species that gain electrons. It's essential to understand that in any given redox reaction, if one substance undergoes oxidation by losing electrons, another substance must simultaneously undergo reduction by gaining the same amount of electrons. An example is the manganese oxide reduction [2]

$$MnO_2 + xA^+ + xe^- \rightleftarrows A_xMnO_2 \tag{2.11}$$

Consequently, oxidation and reduction reactions must occur concurrently, as they

are inherently interconnected processes. This process play a pivotal roles in various chemical and biological systems, including electrochemical processes but also metabolic pathways. Through these reactions, energy and charge is transferred and chemical transformations occur, influencing diverse phenomena [28].

2.1.3 Dunn's Model

Here we give a model, the Dunn's model useful to distinguish the two behavior proposed previously. Referring to the total stored charge at the interface electrode-electrolyte we can recognize three contribution for the phenomena: the Faradaic contribution from the ions insertion process, the Faradaic contribution from the surface-charge-transfer process with the boundary atoms, referred to as pseudo-capacitance, and the non Faradaic contribution from the double layer effect. These capacitive effects were characterized by analyzing the cyclic voltammetry data at various scan-rates, that si the rate at we reach certain voltage in a certain time interval. According to the Dunn's method. That introduce a formula for pseudo-capacitance is an expression used to quantify the pseudo-capacitive capacity of an electrochemical material.

So, the method introduce a formula that provides a relationship between the electric current generated during a cyclic voltammetry measurement and the scan rate of the applied potential. The formula is expressed in terms of a power law, so according with the following equation:

$$i = nFACD^{1/2}\nu^{1/2}(\alpha nF/RT)^{1/2}\pi^{1/2}\chi(bt) \tag{2.12}$$

where, n is the number of electrode involved in the reaction, F th Faraday constant, A is the surface area of the electrode, C is the surface concentration of the electrode material, D is the chemical diffusion, ν the scan rate, α is the transfer coefficient, R is the molar gas constant, T is the temperature, X(bt) is the function that represent normalized current, for a totally irreversible system, b is an adjustable parameter. So i possible represented the pseudo-capacitive contribute in terms of two parameter

$$i(\nu) = a\nu^b \tag{2.13}$$

for the contribute of the electrical double layer we can introduce a formula linear depending with the scan-rate value.

$$i(\nu) = AC_d\nu \tag{2.14}$$

where C_d i s the capacitance, A the surface area. So, we can combine the two mechanism surface capacitive effects and surface charge transfer effect defying the equation:

$$i(\nu) = k_1\nu + k_2\nu^{1/2} \tag{2.15}$$

where: i is the current generated during cyclic voltammetry measurement, ν is the scan rate of the applied potential, k_1 and k_2 are constants representing the contributions of two distinct mechanisms to the generated current. The $k_1\nu$ part of the formula represents the contribution to the current due to surface capacitive effects, while the $k_2\nu^{1/2}$ part represents the contribution to the current due to diffusion-controlled insertion processes. By using this formula and measuring the current at various potential scan rates, it is possible to determine the values of and thus quantify the fraction of the total current due to pseudo-capacitance, allowing for a better understanding of energy storage mechanisms in electrochemical materials.

2.2 Equivalent Circuital Models

For our discussion, we'll introduce equivalent circuits for electrode-electrolyte interfaces. This graphical representation appears remarkably concise yet abundantly informative. The plane used to represent the frequency response of the equivalent circuit is referred as the Nyquist plot. Electrochemical Impedance Spectroscopy, EIS, is a method used for characterizing electrode-electrolyte interfaces. In this technique, a small signal with a low amplitude is applied to the system within the frequency range from 1 MHz to 1 mHz, usually from high to low. The ratio of the sinusoidal voltage to the corresponding current yields the complex impedance at a specific frequency. In a capacitor, there exists a phase shift ϕ between the current and voltage, where ϕ equals 90 degrees for an ideal capacitor. The simplest equivalent-circuit that can easily represent the electrochemical capacitor is as, a series of a resistance and a capacitor follows in Fig. 2.5. Fore every circuital model

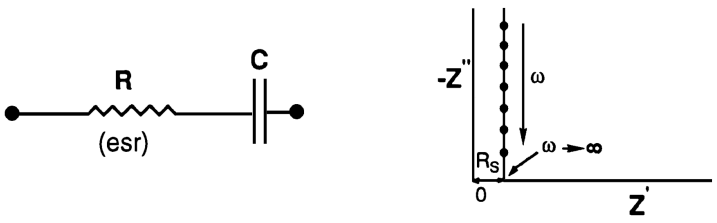

$$Z(\omega) = R_s + \frac{1}{j\omega C} \tag{2.16}$$

Figure 2.5: Nyquist Plot for two element equivalent circuit.

so we can define the Nyquist plot associated, to have directly and fast information of the behavior of the electrochemical system. Nyquist plot contain on x axis real part of the impedance, Z, and imaginary part on vertical axis. Typically the plot, consist of three distinct regions that we can separate from left to right, in:

- High frequencies;
- Medium frequencies;
- Low frequencies.

the point where the intercepts meet the x axis measure of the serial resistance R_s, associated to the electrolyte resistance 2.6, a semicircular feature in high-to-medium frequency give the charge transfer resistance R_F and line inclined at 45 degrees to real axis or a near-vertical line in low-frequency revealed Warburg's element resistance, W 2.7, which is frequency-dependent terms of the impedance Z(ω). And suggest that the surface can have Faradaic active response. These can involve Faradaic charge transfer processes arising from interface redox reactions of impurities or surface functionalities, as well as electron charge transfer reactions involved in charging or discharging a pseudo-capacitance. Hence the kinetic representation of frequency-response behavior is important in interpreting the impedance spectroscopy of various types of electrochemical capacitors that do not behave in an ideally polarizable environment, an other aspect which should not be ignored is that pores shape can strongly influence the bending of the Nyquist curve 2.8.

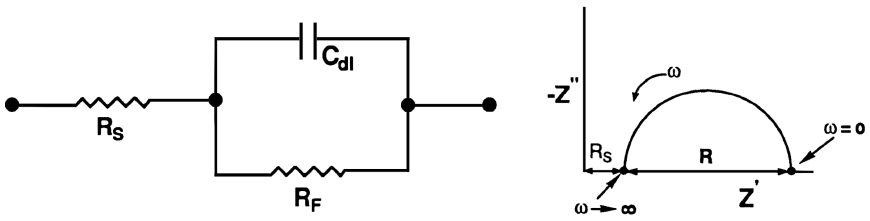

Figure 2.6: Three elements equivalent circuit.

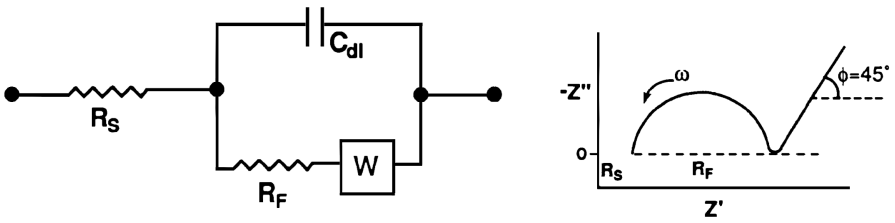

Figure 2.7: Four elements equivalent circuit, including warburg element.

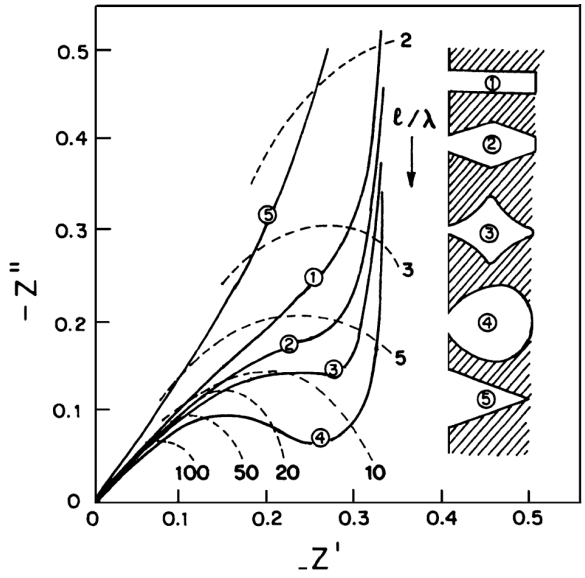

Figure 2.8: Graph of the bending of the Nyquist plot respect to the surface pores shape.

2.3 Aqueous System, Pourbaix Diagram

An other theoretical block, useful for the analysis and development of electrochemical system are Pourbaix's Diagrams. In 1945, Marcel Pourbaix introduced the potential-pH diagram of elements in the presence of water in his "Atlas of Electrochemical Equilibrium in Aqueous Solutions," now known as the "Pourbaix diagram" [29].

This graph applies principles of thermodynamics to ascertain the potentials associated with the equilibrium states of all feasible reactions involving a specified element, its ions, and its solid and gaseous compounds in aqueous solutions, varying with pH. This segment will elucidate the basics of Pourbaix diagrams, illustrate their interpretation, and furnish examples for the most notable metals. Generally, Pourbaix diagrams delineate the thermodynamic circumstances of metals regarding **immunity**, **corrosion**, and **passivation** [30]. Each Pourbaix diagram presents the equilibrium potential of cathodic reactions, such as oxygen reduction and hydrogen evolution, which are contingent on pH, as stipulated by the Nernst equation.

$$E = E^0 + \frac{0.05916}{n} log\left(\frac{\Pi[ox]^{v_{ox}}}{\Pi[red]^{v_{red}}}\right) \tag{2.17}$$

Therefore, the two equations are represented by two parallel dashed lines having a slope of -0.059 V pH at 25 °C and spaced 1.23 V.

Figure 2.9 shows these two dashed lines indicating limits for hydrogen and oxygen evolution.

At potentials above line b, oxygen formation occur,and the acidity of the system increase.

$$2H_2O \rightleftarrows O_2 + 4H^+ + 4e^- \tag{2.18}$$

below line a, water hydrogen formation occur, in this case the alkalinity of the system is favored.

$$2H_2O + 4e^- \rightleftarrows H_2 + 4OH^- \tag{2.19}$$

The area between the two dashed lines are the limit of water stability, in which the only oxygen reduction and hydrogen oxidation occur. The distance between two lines is exactly 1.23 V, that is also thermodynamic potential of water splitting. Three region can be distinguished in the plot: immunity, corrosion and passivation, representing the fields of thermodynamic stability of the metal, of its ions and of its oxides and hydroxides, respectively. Referring to metals, the Pourbaix diagram, E vs pH, displays the area of stability of the chemical species involved as a function of potential and pH, namely:

- metal, immunity zone;
- metal ions, corrosion zone;

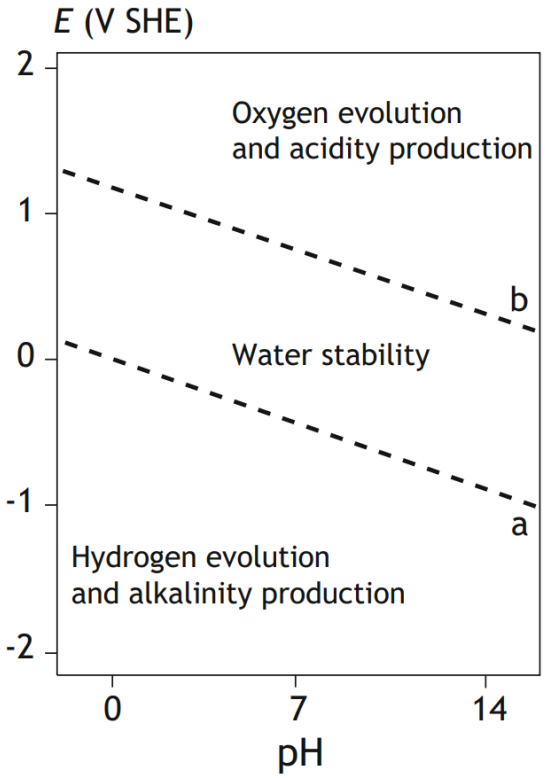

Figure 2.9: Water limit in Pourbaix diagram.

- oxides and hydroxides, passivation.

it is worth highlighting the difference between passivation and passivity. **Passivation**: indicates, in general, the formation of oxides on the surface of a metal. With the term **Passivity** is refered to the formation if this oxide but forms a continuous and adherent layer. Fig. 2.10 illustrates the general potential-pH equilibrium diagram for the metal-water system at 25°C. The equilibrium regions are determined by electrochemical or chemical reactions. In a chemical reaction, only neutral molecules and ions participate, excluding electrons.

In contrast, an electrochemical reaction involves not only molecules and ions but also electrons. This means that non-equilibrium conditions, stability regions, and reaction kinetics can vary. For instance, the Pourbaix diagram of iron, as determined experimentally in laboratory settings with agitated, oxygenated water, shows a broader passivity zone compared to the one predicted by thermodynamics.

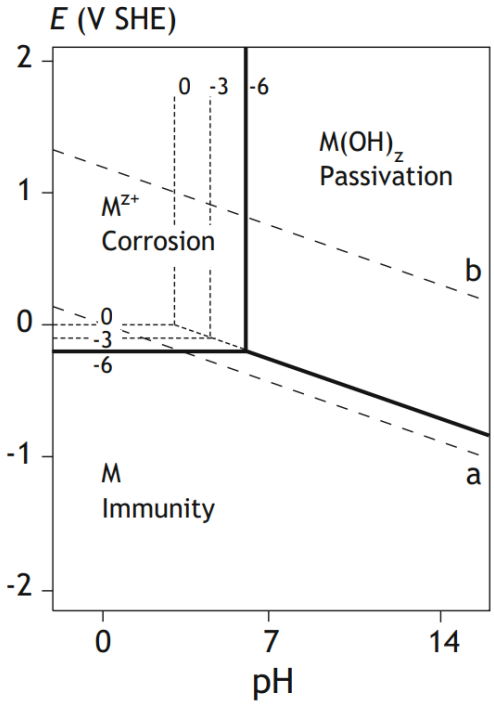

Figure 2.10: Pourbaix diagram for a general metal.

Pourbaix Gold

Gold, Pourbaix diagram 2.11 shows that even in the presence of oxygen, the stable species is metallic gold. If we compare the equilibrium potential of the 2 reaction $Au^+ + e \rightarrow Au$, the dissolution for gold and the formation of oxygen. This is because the equilibrium potential relevant to the dissolution reaction, fixing the gold ions concentration at $10^{-6} molL^{-1}$, is higher of equilibrium potential of the oxygen reduction reaction.

$$O_2 + e + OH^- \rightarrow H_2O \tag{2.20}$$

Nevertheless, the characteristics of gold alter when complex chemical compounds are present, as seen with cyanides. In cyanide solutions, gold undergoes corrosion due to the formation of complex Au CN, which possesses a stability constant of 1038. The concentration of gold ions in solution is significantly reduced, resulting in an equilibrium potential lower than that of oxygen reduction.

This elucidates the rationale behind the utilization of sodium cyanide (NaCN) in gold mining operations. Consequently, gold emerges as a valuable asset in water-based electrochemical applications [31].

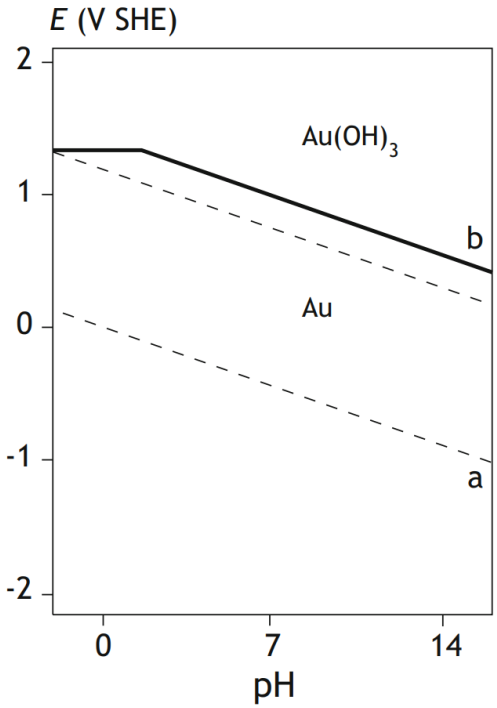

Figure 2.11: Gold Pourbaix Diagram

Pourbaix Iron

The Pourbaix diagram of iron is reported in Fig. 2.12. Corrosion is possible at low and high pH with formation of Fe^{2+} (or also Fe^{3+} at high potentials) and $HFeO_2$, respectively.Iron is stable in the immunity zone and can resist corrosion in passivation zone after the formation of Fe_3O_4 and Fe_2O_3 oxides, which form at low and high potentials, respectively. In the presence of some species, such as Ca^{2+}, Mg^{2+} or sulphate, SO_4^{2-}, the passivation zone broadens due to the formation of protective layers.

Pourbaix Manganese

In this case the equilibrium line of the manganese exist between the horizontal line at -1.1 V vs SHE.

$$Mn^{2+} + e^- \rightarrow Mn_{(s)} \tag{2.21}$$

There is no dependence for the reduction equaiton respect to the pH.

The vertical line straight at ph equal to 7.5 is the equilibrium line between the manganese ions and the manganese hydroxide, the line reaction in this case is no potential dependent.

$$Mn^{2+} + 2OH^- \rightarrow Mn(OH)_2(s) \tag{2.22}$$

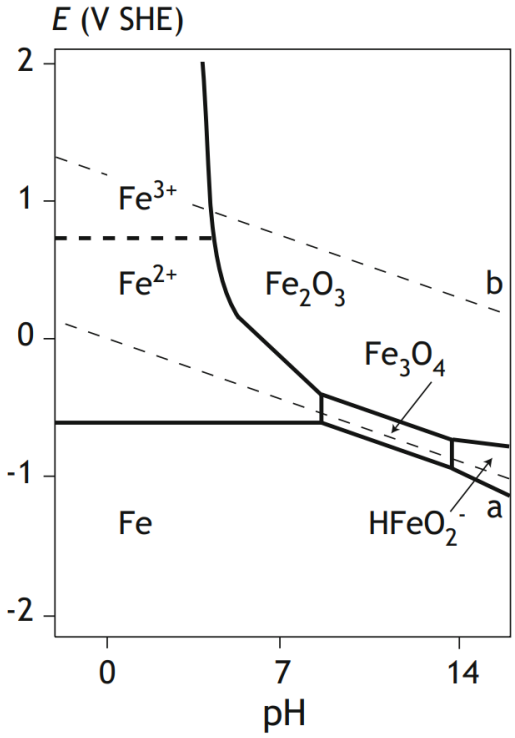

Figure 2.12: Iron Pourbaix Diagram.

$$Mn^{2+} + 2OH^{-} \rightarrow Mn(OH)_2 \tag{2.23}$$

Mn^{2+} become solid at ph higher than 7.5.

In conclusion, from the preliminary analysis of these diagrams it becomes fundamental to better understand and configure the water-based hybrid electrolytic cells so as to be able to predict its possible operating parameters.

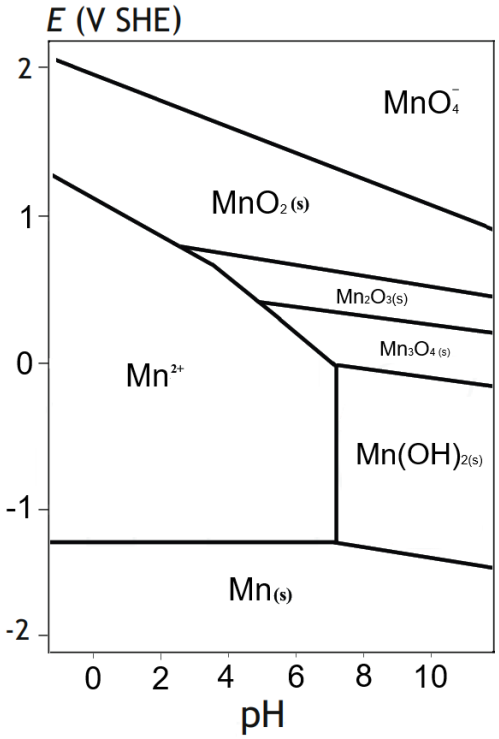

Figure 2.13: Manganese Pourbaix diagram.

Chapter 3

Materials

In the research and development of supercapacitors and micro-supercapacitors, the role of materials plays a crucial importance. These devices, used for energy storage, require advanced materials that can provide high performance in terms of capacity, energy density, efficiency, and durability over time [32, 33, 34, 26]. Among the materials involved, those for pseudo-capacitors and aqueous-based electrolytes play a crucial role [35]. Materials for pseudo-capacitors, including activated carbons and metal oxides such as manganese oxide and iron oxide [36], are designed to provide significant electrical capacity through reversible Faradaic reactions.

These materials are selected for their ability to accommodate electrical charges and facilitate electron transfer during the charging and discharging process, contributing to the overall capacity of the device. Aqueous-based electrolytes are used to create an ionic environment that promotes the movement of ions fast diffusion of cations in surface of metal oxide. These electrolytes are preferred for their high ionic conductivity, safety, stability, as well as their availability and relatively low cost. The use of aqueous electrolytes also helps to increase the efficiency and safety of the energy storage system. Within the realm of active materials, activated carbons are a common choice due to their high surface area, which allows for greater ion adsorption and improved charge storage capacity. Metal oxides such as manganese oxide and iron oxide are appreciated for their electrochemical properties[26], which facilitate reversible redox reactions and contribute to the capacity of pseudo-capacitors. This introduction aims to explore in detail the materials used in the manufacture of supercapacitors, micro-supercapacitors, and aqueous-based pseudo-capacitors, highlighting the distinctive characteristics of each type of material and their role in ensuring optimal performance for advanced energy storage devices [37]. The choice of material and electrode structure is fundamental for supercapacitors, as their capacity relies on the quantity and quality of free surface area. Additionally, it is necessary to select the pore size to facilitate ion movement in solution and the size and shape of the solid part to facilitate electron current flow. The

substances used as binders also have an effect on both porosity and current conduction. The most common used material for electrodes is carbon, which offers the following advantages, Low cost, Easy availability, Long-standing experience in usage. It is important for carbon based electrodes to have a distributed porosity of appropriate dimensions to ensure a large contact surface with the electrolyte, easily accessible for ions.

3.1 (3D) Dendritic Gold as Current Collector

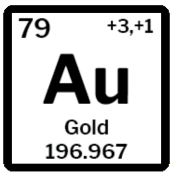

Deposition of gold by electrochemical mean has satisfied many of the demands of the electronics industry. gold has the third best electrical and thermal conductivity of all metals at room temperature, and it is recycled globally of about 24% RMIS-Gold. It has high ductility and excellent wear resistance, which are important for electrical contacts. The inertness of gold prevents the formation of insulating surface oxides as compared to metals like aluminum. gold is an excellent metal suitable for wire bonding for the integrated circuits industries. The wires can be bonded to pure, **soft** gold pads by thermocompression in a range between 300 to 400 °C high pressure let to form the stable weld, or thermosonic bonding in a lower range from 150 to 200 °C, through vibrations and frictional energy.

The electrodeposition of pure gold is a crucial method for pads on silicon wafer bonding connections. Most traditional pure gold electroplating processes in the electronics industry use cyanide-based salts.

The complex $[Au(CN)_2]^-$ has an exceptionally high stability constant of10^{39}, rendering the solution highly stable and altering the standard reduction potential of Au(I) from 1.71V to –0.61V (SHE).

Moreover, solutions that do not contain cyanides, can be incompatible with resists adopted in microelectronics, the cyanides can attack the interface between the resist and the substrate, causing the resist to lift and depositing gold under the resist layer. However, cyanide-based baths pose significant health and safety risks, which often outweigh the benefits they offer.

Sulfite-based gold or Cloride-based processes have been the traditional alternative for silicon wafer technology. But, the over mentioned sulfite-based/cloride-based processes suffer of issues related to the solution stability and also they necessity for high-thermal treatment to achieve the desired deposit hardness.

Soft gold electroplating finds primary application in wire bonding and surface mount applications, particularly in scenarios where numerous bump bonds are required on a chip. The gold must possess sufficient softness to allow the bumps to deform easily, accommodating minor variations in thickness. Therefore, the demand for cyanide-free gold electroplating processes has increased significantly [38]. In the realm of gold plating applications, there lies a promising opportunity to

explore the manipulation of deposition conditions to induce dendritic growth on the contacts. This dendritic growth, while initially perceived as a deviation from the desired uniformity, can, in fact, be harnessed to significantly improve the interaction properties of the metal surface with an electrolyte. This phenomenon is closely correlated with the electrochemical behavior of the surfaces, offering intriguing possibilities for enhancing performance. What makes this approach particularly appealing is its utilization of techniques already well-established in the domain of microelectronics processes. However, the intended functionality differs markedly. Instead of aiming for the traditional objectives of uniformity and smoothness, the focus shifts towards deliberately inducing controlled dendritic growth. This opens the way to innovative application possibilities that leverage the unique characteristics of dendritic structures. By strategically incorporating dendritic growth into the gold plating process, significant advancements can be realized across various domains. For instance, in electronic devices and components, enhanced surface interaction properties can lead to improved conductivity, reduced impedance, and better overall performance. In the field of sensors and detectors, the increased surface area afforded by dendritic structures can amplify sensitivity and response rates. Furthermore, the adoption of dendritic growth in gold plating processes can offer compelling cost advantages. Rather than necessitating the development of entirely new methodologies or materials, this approach builds upon existing infrastructure and techniques. This streamlining of processes translates to reduced research and development costs, as well as more efficient utilization of resources. Some basically information about gold : Gold in nature is present primarily in the +1 and +3 oxidation states. As mentioned the mainly ion for electrodeposition is $[Au(CN)_2]^-$. Two other gold complexes for electrodeposition are, gold sulfite (log(K)=10) and gold thiosulfate (log(K)=28).

$$[Au(CN)]^- \rightarrow Au^+ + 2CN^- \tag{3.1}$$
$$[Au(SO_3)_2]^{3-} \rightarrow Au^+ + 2SO_3^{2-} \tag{3.2}$$
$$[Au(S_2O_3)_2]^{3-} \rightarrow Au^+ + 2S_2O_3^{2-} \tag{3.3}$$

In this work we try to develop adopt a free cyanide gold plating solution to develop a sustainable micro-device.

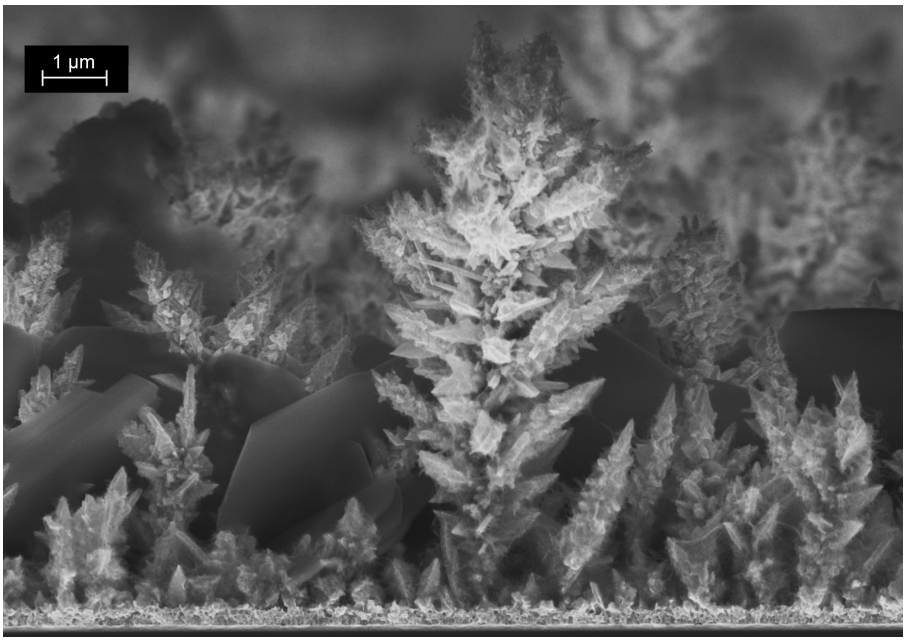

Figure 3.1: Dendritic gold growth on silicon wafer.

3.2 Activated Carbon

The choice of material and electrode structure is crucial for supercapacitors, as their high specific capacitance relies on a high surface area.

Besides, the pore size distribution must be tailored to facilitate the diffusion of ions into the carbon pores and their surfaces should also facilitate the electronic conductivity. The substances used as binders of carbon particles can also have an effect on both the porosity and the electronic conductivity of materials. The most commonly used material for electrodes are the carbons, which offers the following advantages:

- Low cost
- Easy availability
- Green Like

It is important for carbon electrodes to have a distributed porosity of appropriate dimensions to ensure a large contact surface with the electrolyte, easily accessible for ions. To increase the surface area of electrodes, materials containing carbon nanotubes, carbon onions and graphene are being developed although the high porosity of carbons leads to a low packing density, which disadvantages volumetric

capacitance. Other research aims to obtain electrodes made of nanostructured carbon films. The presence of many empty channels between the grains of this film suggests high porosity and low material density.

Compared to nanotube-based technology, which requires a complex fabrication process, deposition from supersonic cluster beams appears to be a simpler and more versatile technique. The high porosity of these deposited carbon layer allows to obtain high active surface area (1000 to 3000 m^2/g), leading to the following values in terms of magnitude order[39]:

- Specific capacitance of 100 F/g;
- Maximum energy density of 10 Wh/kg;
- Maximum power density of 100 W/kg;
- Other materials used include various types of polymers and metallic oxides.

Other approaches include using different materials for each electrode or composite materials in each electrode. Of course, research activity is ongoing and there are no definitive solutions but to a diversification of materials adopted strongly related to the final energy storage application.

Figure 3.2: Activated Carbon powder.

3.3 Manganese Oxide

Very common in the form of Pyrolusite, MnO_2, Hausmannite (Mn_3O_4), $MnCO_3$. Manganese present different properties: its a metal with low ductility, in metallurgy is used in alloys with iron (steels) because it provides hardness and mechanical resistance. About the presence in soil, is the 12th most abundant element on Earth and the third transition metal after iron and titanium, in 2023 has been signed as critical raw material by the (EC) RMIS.

In nature, various minerals containing manganese are found, corresponding to an overall abundance of 0.106%. Twelve of these minerals are economically extractable, with the main ones being pyrolusite (MnO_2), manganite ($Mn_2O_3 \cdot H_2O$), hausmannite (Mn_3O_4), rhodochrosite ($MnCO_3$), and manganese nodules. The highest oxidation state of Mn corresponds to the number of electrons in 3d and 4s orbitals, present in oxycompounds like MnO_2, MnO_3F, and Mn_2O_7, partly analogous to the corresponding halogen compounds. Manganese is relatively abundant and is found in nature as oxides, hydrated oxides, or carbonates. From these, or from Mn_3O_4, the metal is recovered by reduction with Al. Manganese is quite electropositive and is easily attacked by non-oxidizing dilute acids (HCl, H2SO4, etc.). The most common stereochemical characteristics of manganese compounds are: Octahedral as in $[MnCl_6]^{2-}$ Mn(II), Mn(III), Mn(IV), Tetrahedral as in $[MnO_4]^{2-}$ and MnO_4^- Mn(VI), Mn(VII), Mn(II) salts are soluble in water. The sulfate, $MnSO_4$, is very stable and is used in analysis. The phosphate and carbonate are slightly soluble.The equilibrium constants for the formation of Mn(II) complexes are relatively low because the Mn^{2+} ion exhibits significant ligand field stabilization energy. However, polydentate ligands such as en, ox, or EDTA- form isolable complexes. In organic media, it is easier to isolate complexes like MnX_3^- (o) or $[MnX_4]^{2-}$ (yellow-green) or (pink polymers), $[MnCl_6]^{4-}$. Mn^{2+} ions can occupy tetrahedral cavities in certain glasses. Tetrahedral Mn(II) has a fluorescent yellow-green color, much more pronounced than the pink color of the ion in octahedral coordination.

By heating any of the oxides or hydroxides of Mn, black crystals of Mn_3O_4 (hausmannite) with a spine structure Mn(III) $Mn(III)O_4$ are obtained. Upon exposure to air, $Mn(OH)_2$ oxidizes to a hydrated oxide that dehydrates to $MnO(OH)$ (manganite). Aqueous ions and complexes of manganese(III) The manganese(III) ion is obtained by oxidation, electrochemical or with $S_2O_8^{2-}$, of Mn^{2+} or by reduction of MnO_4^-. It is a good oxidizing agent ($E^\circ = 1.58$ V) and tends to disproportionate into MnO_2 and Mn(II) (log(K) = 9). It is more stable in organic solvents, and numerous complexes are known. The acetate is obtained from $KMnO_4$ and Mn(II) acetate in acetic acid.

Manganese(III) and (IV) complexes are important in photosynthesis, where they control the formation of oxygen from water. The most common compound of manganese(IV) is manganese dioxide , MnO_2, a dark green solid found in nature as pyrolusite. It is obtained by the action of O_2 on Mn at high temperatures, by heating MnO_2, or by reduction of basic aqueous solutions. It has a rutile structure, similar to other dioxides (Ru, Mo, W, Re, Os, Ir, Rh). It does not adhere to stochiometric ratios and can exchange cations. Mn exists in various forms (alpha, beta, gamma) with different surface areas and catalytic activities, with pyrolusite being the least reactive. MnO_2 is inert to most acids but dissolves

upon heating, reducing itself. With H_2SO_4, it forms manganese(III) sulfate or releases oxygen and forms $MnSO_4$. It is widely used as an oxidation catalyst. It is used as a component of Leclanchè batteries, as a pigment in construction, in glass manufacturing, and in electronics ($MnFe_2O_4$ceramic ferrites). Mn_2O_3 is prepared from Mn by heating in air or in vacuum in a range between 206 and 505 °C at P(O)=n10^{-5} bar[40]. Mn_3O_4 is prepared from other oxides by heating in air at 1000°C. MnO is prepared from other oxides by treatment with H_2 at temperatures below 1200°C (above which metallic Mn is obtained).

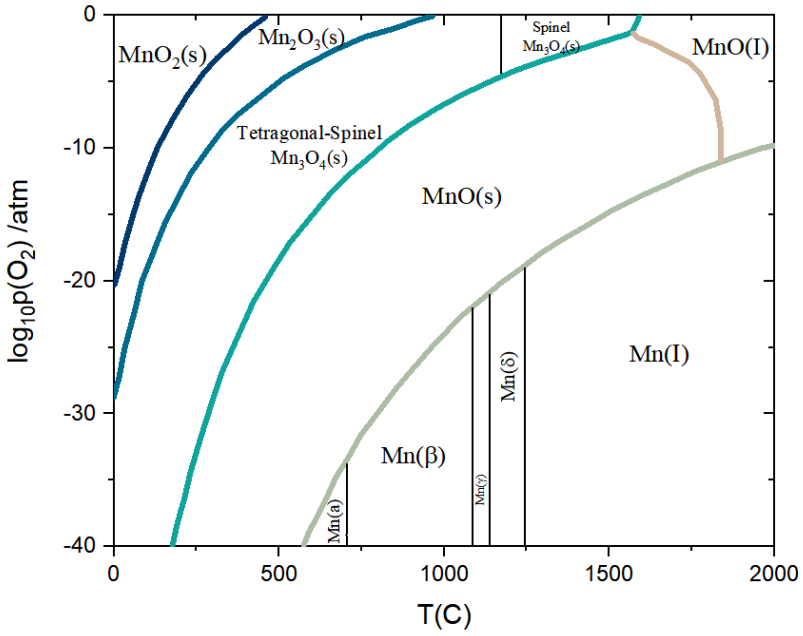

Figure 3.3: Manganese phase diagram.

MnO2 is used for decolorizing commercial glass. When added to molten glass, it produces reddish-brown Mn(III) that masks the blue-green color of iron impurities. The metal is used to make many important alloys. In steels, Mn improves quality in rolling and forging, resistance, toughness, stiffness, wear resistance, hardness, and tempering. With Al and Sb, especially in small amounts of Cu, it forms ferromagnetic alloys. Metallic Mn is ferromagnetic only after special treatments.

MnO_2 (pyrolusite) is used as a depolarizer in dry-cell batteries and to "bleach" colored glass green from iron impurities.

Permanganate is a powerful oxidizing agent and is used in quantitative analysis and in medicine as $KMnO_4$. Other bio aspects is that Mn is essential element for humans and animals. It is fundamental for bones formation. It is estimated that a normal 70 kg person has a total of 12-20 mg of Mn in their body. Although

manganese is an essential nutrient, exposure to high levels through inhalation or ingestion can have negative health effects. Chronic exposure to lower levels of Mn causes difficulties in performing rapid hand movements and partial loss of coordination and balance, as well as an increase in general symptoms such as memory loss, anxiety, or insomnia.

Figure 3.4: Manganese oxide aspect.

3.4 Iron Oxide

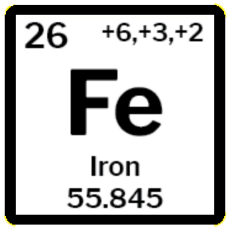

Iron is an abundant metal inside the Earth, making up nearly 35% of its mass. It is also a chemical element that is abundant in the Earth's crust, where it accounts for almost 5% of the weight. In its pure form, iron would appear silvery-white, but in nature, it is always found in various compounds such as oxides, hydroxides, carbonates, and sulfides. Some physical properties, Iron is generally hard, dense, and heavy. The color can vary depending on the type of iron oxide present, with hematite typically being red or reddish-brown, magnetite black or dark gray, and goethite brown or yellowish-brown. Iron can have various textures, including crystalline, granular, or massive. There are numerous minerals that contain iron. Among the most common are pyrite (chemical formula FeS_2), which contains iron and sulfur and often appears as golden-yellow cubic crystals, and magnetite, which is shiny black and is a combination of iron and oxygen (chemical formula Fe_3O_4).

Recently, iron oxides have been tested with various successes as electrode materials for lithium-ion batteries[41]. Reports on the use of iron oxides as electrodes in supercapacitors are currently subject of study. Some study like [42], that synthesizing Fe_3O_4 in sub-micrometric particles and are presenting preliminary results

of their electrochemical performance in aqueous electrolytes. This study also focused on the electrochemical characterization of a hybrid supercapacitor using a composite Fe_3O_4 negative electrode and a composite MnO_2 positive electrode in neutral electrolyte. Fe_3O_4 thin film is currently being investigated for applications in catalysis, electrochemical capacitors, and magnetic devices.

In recent decades, various methods have been proposed by researchers to produce thin Fe_3O_4 films, including chemical vapor deposition (CVD), molecular beam epitaxy, pulsed laser deposition, and sputtering [43, 44]. However, equipment and technology required for synthesizing Fe_3O_4 thin films via CVD and sputtering are both expensive and complex. In contrast, electroplating offers a more sustainable alternative with advantages such as operational simplicity, cost-effectiveness, and scalability for large-scale production. Moreover, the hydrothermal formation of Fe_3O_4 films remains an area that lacks comprehensive study [42].

3.5 Polymide (KAPTON®)

Kapton® is a polyimide film utilized in flexible printed circuits and flexible electronics. Originally developed by the DuPont Corporation in the 1960s, Kapton® exhibits stability over a broad temperature range, spanning from -269 °C to +400 °C. It finds applications in electronics manufacturing, space exploration, electric vehicle industries, and 3D printing. Its advantageous thermal properties and low outgassing make it a common choice for cryogenic and high vacuum environments. Besides, Kapton® has an inert structure and is very stable and non-flammable as a material for electronics. The synthesis of Kapton® exemplifies the utilization of a dianhydride in step polymerization. Chemically known as poly (4,4'-oxydiphenylene-pyromellitimide), Kapton® is formed through the condensation of pyromellitic dianhydride (PMDA) and 4,4'-oxydiphenylamine (ODA). Kapton® E, on the other hand, incorporates biphenyltetracarboxylic acid dianhydride (BPDA) and p-phenylenediamine (PPD) in addition to PMDA and ODA, enhancing dimensional stability and flatness in flexible circuitry applications. Compared to Kapton® H, Kapton® E offers lower coefficients of thermal expansion (CTE) and hygroscopic expansion (CHE), as well as reduced moisture absorption [45]. As insulating foil, Kapton® remains stable across a wide range of temperatures, from -269 to +400 °C. Kapton® insulation ages poorly: an FAA study shows degradation in hot, humid environments or in the presence of seawater.

3.6 Electrolytes

The term electrolyte generally refers to substances that undergo electrolytic dissociation in solution, meaning the breakdown of molecules into ions. Specifically, they are divided into cations, positively charged ions, and anions, negatively charged

ions, making the electrolyte ionic conductive. Ionic conductivity refers to the ability of an electrolyte solution to conduct electricity due to the movement of ions. The higher the number of ions in the electrolyte, the higher its conductivity, but the mobility does not follow the same trend. Ion mobility is a measure of how quickly an ion can move through an electrolyte solution when subjected to an electric field. It is influenced by several factors: size of the ion, viscosity of the solvent and temperature. Ion mobility, does not necessarily increase with the number of ions. Instead, it depends on the specific characteristics of the ions and the medium. For instance, adding more ions to a solution can lead to interactions among ions, which might reduce mobility due to increased collision rates and the formation of ion pairs or clusters. Electrolytes are capable of conducting electric current once

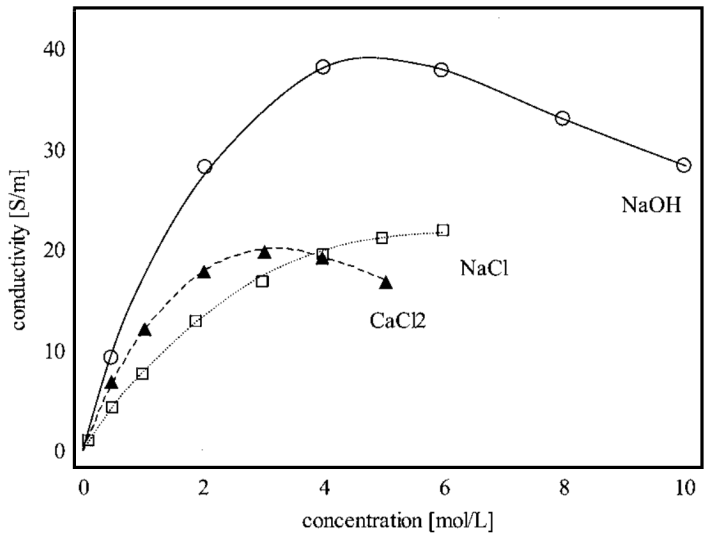

Figure 3.5: Conductivity of aqueous electrolyte in function of the molar concentration.

dissolved in a solution due to the presence of positive and negative ions in the generated solution, derived from the dissociation and ionization of the electrolyte. In supercapacitors, the electrolyte serves as the electrical connection between the two electrodes, and its solvent molecules form the monolayer that separates the electrode from the layer of solvated ions in the Helmholtz layer; eventually releasing ions for the formation of pseudo-capacitance. The choice of electrolyte is as crucial as the choice of electrode material. The maximum voltage achievable by a supercapacitor depends on the breakdown voltage of the electrolyte, thus limiting the energy density (which depends on voltage) determined by the electrolyte. Power density, on the other hand, depends on equivalent series resistance, which is strongly related to the electrolyte's conductivity. There are generally four types of

electrolytes[46, 47, 48, 49]:

- **Aqueous**: these exhibit higher conductivity leading to high power density but have a low voltage window due to water decomposition per electrode (typically 1 V), resulting in low energy density.
- **Organic**: these are more expensive than aqueous electrolytes but have a higher breakdown voltage window of about 2.5-3 V and thus higher energy density. However, their low conductivity affects power density negatively.
- **Ionic Liquid**: Ils have very large voltage window up 5 V, are less conductive low vapor pressure, higher energy density, higher cost.
- **Polymer electrolyte**: less ion conductivity, they are easy to be integrated in microfabrication process and low conductivity some affect power density.

Chapter 4

Methods

In this section we present the approaches in which we set methods and processes to validate the scaling hypothesis proposed on chapter 2 on supercapacitors. Initially, due to its versatile properties, kapton was used to define areas with a total area of 1 square centimeter and a spacing of approximately 300 microns. This preliminary phase had two purposes, one was to demonstrate the compatibility of the use of micro-super capacitors with flexible electronics, and it also greatly speeded up the tests in the laboratory. This to then migrate onto silicon wafers and land on supports more similar to chip electronics. The investigation method adopted in this work therefore followed two paths, a definition phase and then validated a first migration on on-chip support with a miniaturization approach. Initially to study the limits of physical deposition, arrays with fractal designs with h-tree patterns were created to probe the stress limits of the metal film deposited on kapton. Although referring to a bulk configuration, the first innovative study, on the concept of hybrid capacitor, was originally proposed by Hong [37] and successively by Toupin and Brousse [50]. After this to give little bit of roughness and porosity is used an electroplating process (black gold deposition) to have more conductivity and finally the electroplating processes and electrophoretic deposition made, to obtain the surface coated by the active material, that are activated carbon and Manganese oxide to enhance the surface are of the electrodes self. At the end the system is closed in planar configuration for the tests.

4.1 Physical and Chemical Fabrication

4.1.1 Physical Vapor Deposition

The method used, for the fabrication of current collectors, is compatible with the micro-fabrication methods available in the semiconductor industry. The first step was a hot-pot thermal Physical Vapor Deposition (PVD): the process is aimed to deposit metallic current collectors over a Kapton® substrate. The Kapton®

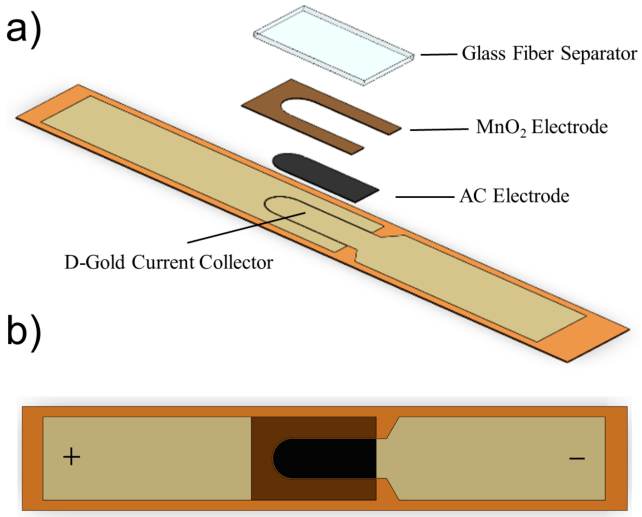

Figure 4.1: Single interdigit current collector.

substrate was 10 cm x 10 cm and it was cleaned by sonication for 1h and treated in an oxygen plasma for 5 min prior to the deposition process. Two metal layers of chromium and gold were deposited onto the substrate, from pellets precursor with a purity of 99.8 %. Less than 10 nm of chromium were used as adhesion layer, while 100 nm gold thin film were used as metal seed layer for the subsequent phases. A deposition rate of 1.9 $\mathring{A}/s$ has been set with a level vacuum in chamber of about $5 \cdot 10^{-4}$ Pa.

4.1.2 Photolitography

The patterning was accomplished using photolithography and wet etching techniques, as illustrated in Fig. 4.1. The design features a single-digit separation with a distance of approximately 100 µm between the electrodes. This single-digit geometry, depicted in Fig. 5.1, was patterned onto the metal film via photolithography. Specifically, AZ-1518 photoresist (Microchemicals GmbH, Germany) with a thickness of about 1200 nm was first spin-coated onto the surface at 4000 rpm for 45 seconds. Following this, the sample underwent a soft bake at 110 °C for 1 minute to allow the volatile chemicals to evaporate. Finally, the sample was exposed to UV light ($3mWcm^{-2}$).

Afterwards, the sample was immersed in an AZ400k developer solution for 35 seconds. The patterned interdigital Cr/Au current collector was then obtained through wet etching, first in a gold etch solution for 10 minutes, followed by a chromium etch solution for 35 seconds.

4.1.3 Electroplating Deposition

Electroplating is an electrochemical process for producing coating, usually of metal or alloys, upon a surface by applying a current or potential. The coating produced is usually for decorative and/or protective purposes, or enhancing specific properties of the surface. The surface that is coated can be conductors, such as metal, or non-conductors. Electroplating methods are widely used for many industries, such

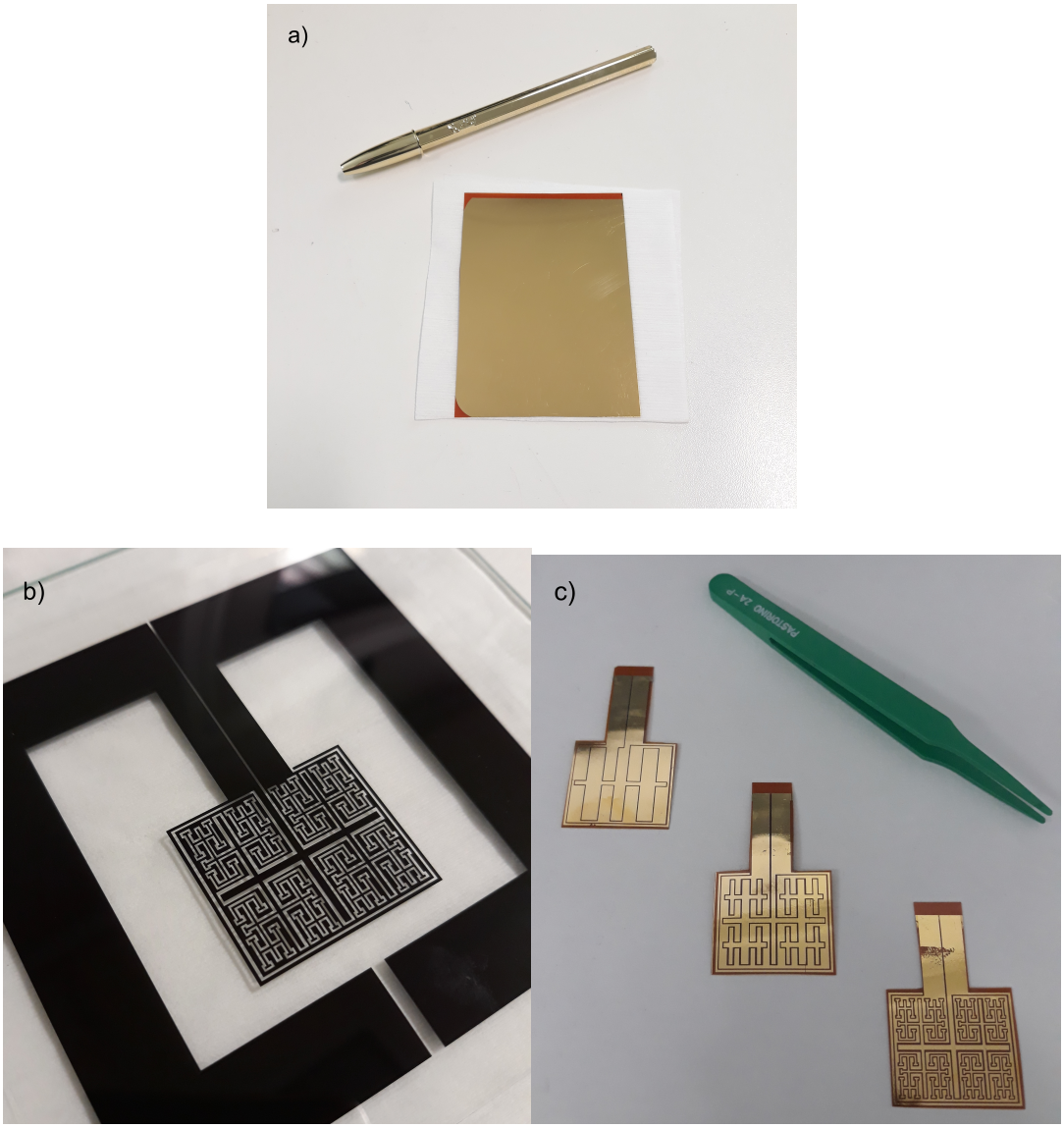

Figure 4.2: a) Foil of Kapton covered by gold b) Mylar Mask, c) H-tree fractal interdigitated current collector.

as automotive, jewelry, air space, machinery and electronics. The principal part of the electroplating process is the electrochemical bath. The electrochemical bath its a confinement of two electrode inside a volume containing a liquid, that is the electrolyte solution, giving electrical signals to the system is possible to obtain the desired reaction. The two electrode are called anode, and the cathode. In industrial production are important treatment before and after the deposition. We call the part that will be decorated cathode (negative terminal). The **anode**, however, can act in two way: as sacrificial anode (dissolvable anode) and as permanent anode that is inert in the bath solution. If is possible sacrificial anodes are made of the metal that is planned to be loaded. The permanent anodes close the electrical circuit, but cannot give new metal ions to keep the constant the solution concentration. Usually, Platinum and carbon based electrode are used as inert anodes. **The Plating solution** is the media interposed between the electrodes, containing metallic ions. Upon application of current or a potential drop, the positive ions in the solution will move toward the electrode where the reduction occurs the negative and the anions go on the positive electrode. This flux of ions through the solution

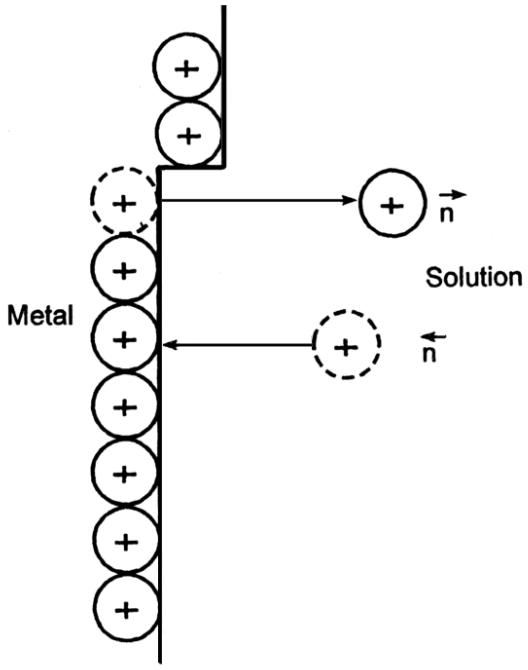

Figure 4.3: Plating interfaces diagram.

constitutes the electric current in the electrochemical cell the circuit. The migration of electrons into the anode through the metal wire and an electric generator and then back to the cathode constitutes the current in the external circuit. The metallic ions in the solution carry a positive charge and are thus attracted to the

cathode. Electrodeposition, also known as electrochemical deposition, involves the reduction of metal ions from electrolytes onto a substrate. During this process, electrons are provided to cations at the cathode, causing them to migrate to the anode. In its most basic form, the cathodic reaction in an aqueous system can be represented as follows:

$$M^{n+}_{(aq)} + ne^- \rightarrow M_{(s)} \tag{4.1}$$

The anode material can be either a sacrificial anode or an inert anode. For the sacrificial anode, the anode reaction is:

$$M_{(s)} \rightarrow M^{n+}_{(aq)} + ne^- \tag{4.2}$$

If the equilibrium potential of the electrode is V and the potential of the same electrode as a result of current flowing is V*I, then the difference between these two potentials, is called overpotential. The cathode potential of a Au cathode, is measured versus a reference electrode, a high-input-impedance device so that a negligible current is drawn through the reference electrode. For high negative overpotential values, the current density i correlates with the surface area S.

Returning to the electrode preparation process, following photolithography, a commercial Au-precursor solution, NB Semiplate Au 100 TH, MicroChemicals GmbH, was employed in a three-electrode configuration setup for electrodeposition. The working electrode was connected to the target electrode, with a pure gold sheet, 50 μm thick, serving as the counter electrode, and an Ag/AgCl electrode used as a reference. Galvanostatic deposition was conducted by applying a current density of 1.4 mA/cm^2 between the working and counter electrodes for 450 s, while maintaining a 4 cm distance between the electrodes. As depicted in the figure (Fig. 4.4), the current density was adjusted to generate a deposition rate curve, aiming to determine the optimal mass loading parameters. The deposited layer exhibits dendritic growth, manifesting a distinct tree-like structure (Fig. 3.1). This morphology arises from rapid growth, leading to specific crystallographic orientations.

4.1.4 Active Material Deposition

ElectroPlating Deposition

For the deposition of the active materials onto the current collectors, two approaches were used. For the positive electrode, manganese was chosen as precursor for the active material[51]. A neutral, pH = 7, plating solution of Manganese(II) Acetate 0.1 M and Sodium Sulfate 0.1 M, the sodium sulfate adding act as, supporting salt, were used as precursor. Both salts were provided by MERK- TALY. Milli-Q water was used as solvent. The setup configuration for the galvanostatic electrodeposition, was made up by three electrode parallel plates. Working electrode, connected to the interested electrode, applying a negative density current of -0.9 mA/cm^2 for

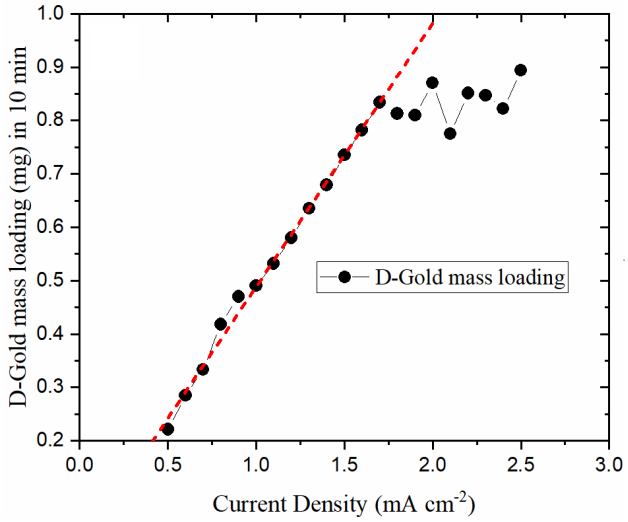

Figure 4.4: Dendritic Gold deposition curve obtained changing density current during the process. Solution used NB Semiplate Au 100 TH provided by Microchemical GmbH.

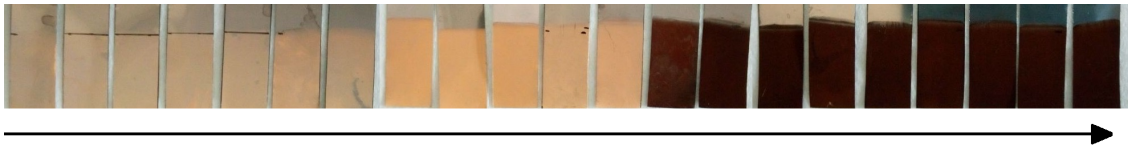

Figure 4.5: Plating palette on Ti foils varying deposition current density.

1000 s between working and counter electrode so the electrode during the plating assume negative polarization respect to the reference, manganese cations move on the surface and reduce. Here reported the plating reaction.

$$Mn^{2+}_{(aq)} + 2e^{-} \rightarrow Mn_{(s)} \tag{4.3}$$

The distance between Working Electrode and Counter Electrode was fixed to 4 cm. After plating, samples were cleaned, by deionized water and dried in an oven at 60 °C for few 48h, and mass loading was measured before and after the process with a Kern ALJ 210-5A Analytical balance with a linearity parameter of 0.1 mg. Trials were made to define deposition rate curves: one involves Manganese, the second one Gold (Fig.4.7). Moreover, different salts have been involved to find the right stability of the solution, such as K_2SO_4 or $MgSO_4$. After plating of Mn a thermal process was applied in Buchi Glass Oven, to convert the metallic manganese in oxidized form, with the sequent temperature curve: starting reaching for 1 h at 60 °C then 4 h at 300 °C and finally 1 h at 60 °C h [52, 50] after the

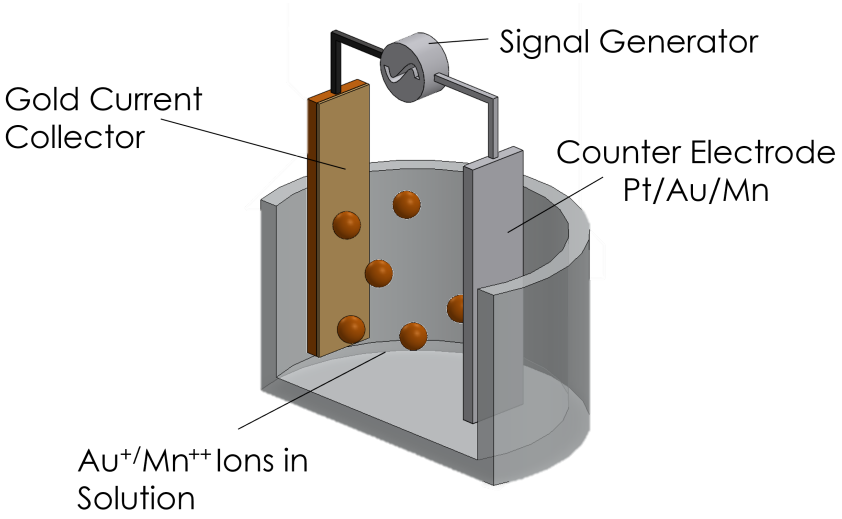

Figure 4.6: Plating set-up cell section.

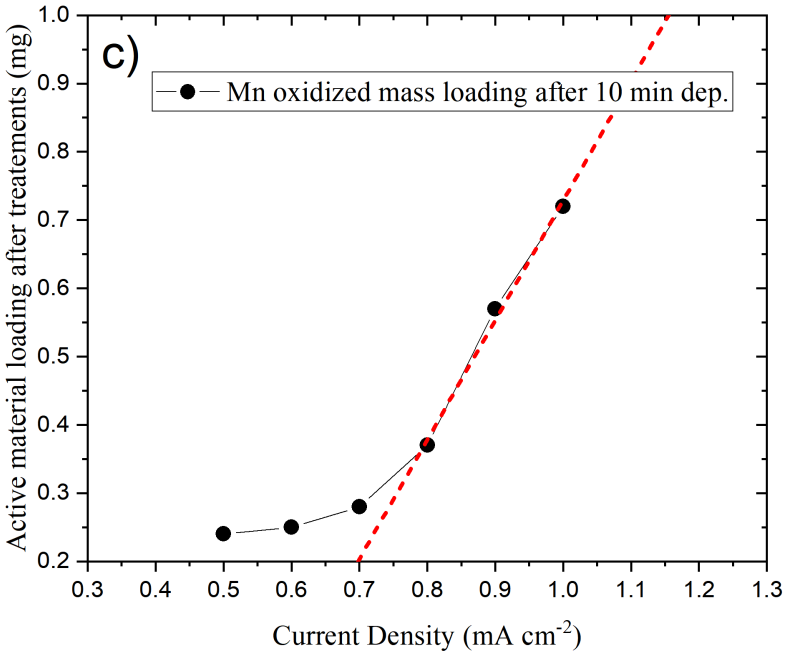

Figure 4.7: Manganese oxide phase, deposition curve after thermal treatment, changing density current during the process, using an aqueous solution of $Mn(CH_3COO)_2$ and Na_2SO_4 provided by SigmaAldrich in milli-Q water.

thermal process the sample, are weighed and data about the oxidized form are reported di in the curve 4.7.

Electrophoretic Deposition

Electrophoretic deposition is a technique used to create coatings, laminated structures, or concentration gradient structures, as well as solid pieces, applying electric field starting from a colloidal suspension in an aqueous or organic medium. The technique involves the use of two conductive surface, one of which pose the surface where coating will be done, both are immersed in a stable suspension made by micro-particles. A potential difference ΔV is applied between the electrodes. The particles, which acquire a positive or negative surface charge upon contact with the dispersion medium, move towards the electrode with the opposite charge and deposit onto the surface [53]. The surface on which the deposition takes place can serve as a simple support or be an integral part of the final application. In the first case, the material it is made of is quite irrelevant: it is sufficient for it to be conductive (stainless steel, platinum, Graphite, etc.) and has the shape of the required surface. At the end of the deposition, the product must be carefully removed to avoid delamination or washing away of the deposit [54]. If the electrode is part of the device, it must be made of the required conductive material. However, it will be seen that deposition can also be achieved on a non-conductive substrate by modifying the electrophoretic cell set-up. The technique is based on the combination of two effects: **Electrophoresis**, which is the motion of charged particles in presence and under the action of an electric field. **Deposition**, which is the accumulation and consecutive agglomeration of particles on a surface. The first attempt to interpret the process can be attributed to Hamaker in 1940 [55]. In 1939, they described the deposition of suspended particles on an electrode as a phenomenon similar to sedimentation, where the force produced by the electric field replaces gravity: particles near the electrode deposit due to the pressure exerted on them by other particles. These authors observed that, in some cases, the deposited layers resemble a viscous fluid and suggested that this is due to the fact that the potential energy curve of the suspension is always positive. Koelmans et al. 1954,[56] proposed an electrochemical mechanism for deposit formation based on the Derjaguin, Landau, Verwey, and Overbeek theory: the theory explain how increasing of the electrolyte concentration near the electrode surface, this variation can induce for a system coagulation with a consequent reduction of Z-potential. Other authors suggest the neutralization of particle charge when they touch the electrode, Grillon in 1992 [57], involve secondary processes at the electrode leading to polymerization and particle deposition Shimbo, in 1985, [58], or combine neutralization and polymerization mechanisms Mizuguchi 1983 [59]. Most of these theories have been invalidated by subsequent experiments and studies. According to Sarkar [60], the most plausible explanation is based on the Derjaguin-Landau-Verwey-Overbeek heory; The stability of a colloidal suspension is attributed to the balance of repulsive and attractive forces with the formation of an electrical double layer.

When particles move under the action of the applied potential difference between the two electrodes, the electrical double layer is distorted, thinning in front and thickening behind the particle. The decrease in thickness, due to both dynamics and the "reactions" that occur between the ions in solution, allows the particles to approach each other and the electrode so there is a predomination of the Van der Waals forces in order to have the formation of a deposit4.8. Concerning the preparation of the negative electrode casting technique empowered with electrophoretic process where made. The active material for the negative electrode was deposited through drop casting technique. A water-based colloidal solution containing 0.9% weight of Kuraray's Activated Carbon was utilized, with a minimal water binder content of 0.03% weight of Acrylic Acid Modified Cellulose. The dispersion was stirred in vial over a night. A volume of 100 μL of this dispersion was applied onto the surface [1]. An electric field, induced by a DC voltage of approximately 50 Vcm^{-1}, was established between the electrode cast and a needle electrode. The positive potential was applied to the substrate electrode, while the negative potential was applied to the needle immersed in the meniscus. This strong electric field initiates an electrophoretic process, facilitating the contact of the carbon particles with the surface of the current collector. The deposition is carried out by applying the electric field for an half an hour, then the sample is left to dry, by repeating the process it is possible to control the mass loading on the electrode. Zeta potential measurements were conducted to examine the polarization shell of the activated carbon, revealing a zeta potential of around -30 mV in deionized water.

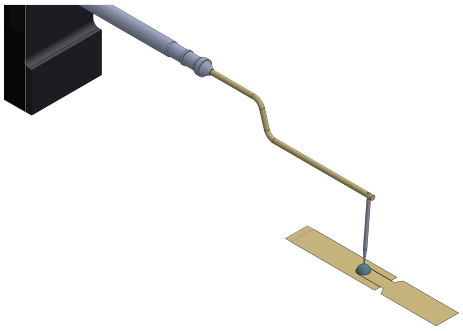

Figure 4.8: Electrophoretic set-up, with needle, applied on the single inter-digit device.

Two different electrodes were prepared one with thermal treatment and one without thermal treatment for XPS measurement, (Fig. 4a) to understand the oxidation state of the active material surface before and after the thermal process [61]. After this analysis a planar hybrid device was built. Besides, the studies

suggest an asymmetrical configuration using activated carbon and manganese oxide in neutral aqueous media to extend the operating voltage window (1.6 V) and so to achieve higher energy density. Similarly, the research presented here aims to enhance energy performance in planar devices.

4.2 Physical Characterization

In the realm of material science and engineering, the physical characterization of materials plays a pivotal role in understanding their properties and behavior. Various sophisticated techniques are employed to delve deep into the structural, morphological, and compositional aspects of materials. These techniques not only provide valuable insights into the fundamental properties of materials but also facilitate the development of new materials with tailored properties for specific applications. From microscopic analyses to spectroscopic methods, these characterization techniques enable researchers to unravel the intricate details governing material performance, paving the way for advancements in diverse fields ranging from electronics to biomedical applications.

4.2.1 Electrical Characterization

Van Der Pauw

Vander Pauw method, [62] was applied on the square metal film obtained through the technique. The technique consist in a four wire measurements. Injecting a current between the two nodes Fig. 4.10, **1,2**, and measuring the potential drop in the opposite two nodes **3,4**, then the measurement is repeated rotating the injection point and the voltage drop points, for reciprocity. Tens of measurements have been performed resulting in a sheet resistance of the metal film of about 300 $m\Omega square$.

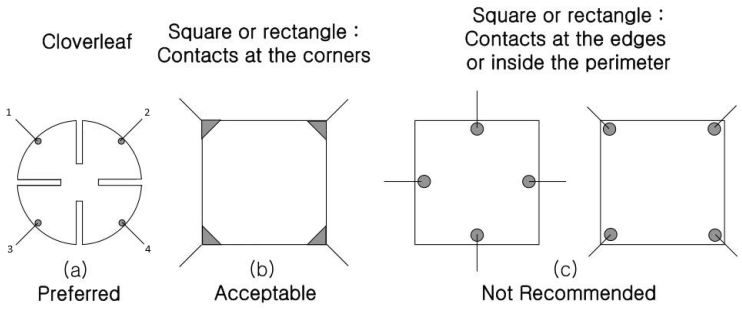

Figure 4.9: Van Der Pauw set up and geometries.

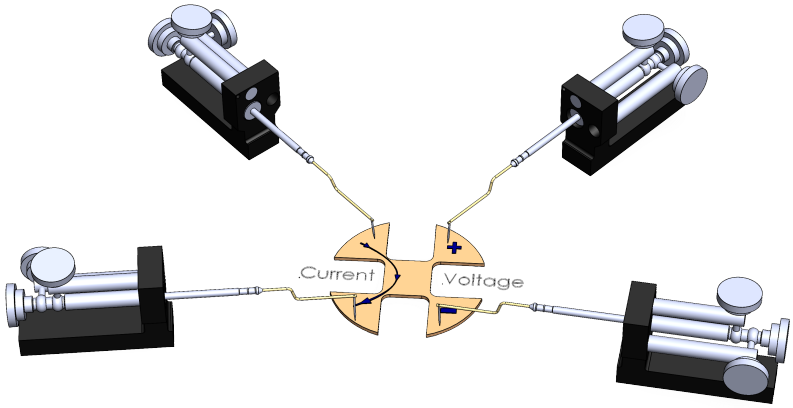

Figure 4.10: Van Der Pauw set up and geometries

$$R_{12,34} = \frac{V_{34}}{I_{12}} \tag{4.4}$$

$$e^{-\pi R_{12,34}/R_s} + e^{\pi R_{23,41}/R_s} = 1 \tag{4.5}$$

4.2.2 X-Ray Photo-Electron Spectroscopy

X-ray Photoelectron Spectroscopy (XPS) analyses were conducted utilizing a PHI 5000 Versaprobe spectrometer (Physical Electronics, Chanhassen, MN, USA) equipped with an Al k-alpha monochromatic source (1486.6 eV). To mitigate the electrical charging effect induced by the photo-electrons extracted during the measurements, the samples under examination were subjected to a combined electron and Ar ion gun neutralizer system. Semi-quantitative atomic concentration and fitting procedures were performed using the dedicated software Multipak 9.7.0.1 Version. The core-level peak energies were calibrated with respect to the C1s peak at 284.8 eV (attributed to adventitious carbon), and the background contribution in high-resolution (HR) scans was subtracted using a Shirley function.

4.2.3 X-Ray Diffraction

XRD patterns of the electrodeposited manganese oxides were collected on a Empyrean powder x-ray diffractometer with Cu Kα radiation source with a wave length, λ = 1.54052 Å, other specs of the where voltage 40 kV, current and 30 mA, and a 0.013 step size of 2θ angle from 10 to 100. The samples were placed onto a zero-background stage holder to avoid further signals. After data acquisition QualX software with, **RRUFF** and **COD** database, were used for the phase identifications. For the quantitative phase analysis and the refinement, **MAUD** open software was employed. Fityk free software was employed for the deconvolution of the peaks and used only for graphical purposes. For the Rietveld refinement, the Crystallographic Open Database (COD) was used, the COD numbers employed are:

- 00-900-8518
- 00-210-5394
- 00-900-9111
- 00-900-8463
- 00-900-1963
- 00-151-0524

4.2.4 Micro Raman

Micro-Raman spectroscopy was performed by using a Renishaw InVia Qontor Raman microscope. A laser diode source, with a wave length λ=532 nm, was used with 5 mW power, and sample inspection occurred through a microscope objective, with a magnification of 50x. Including backscattering light collection setup. After data collection the Raman spectra analysis was carried out with Fityk software

[63]. Lorentzian functions were used as fitting functions. All the data reported in the result section are with baseline correction.

4.3 Electrochemical Characterization

Both positive and negative electrodes were analyzed separately in three electrodes configuration to obtain for each electrode the charge storage performance. An electrochemical characterization system with three electrodes consists of three distinct electrodes: the working electrode, the counter electrode, and the reference electrode. The working electrode is the main node controlled directly by the potentiostat, where electrochemical reaction that interacts with the solution are investigated. It is where the desired process takes place, such as the oxidation or reduction of a chemical species. The auxiliary electrode, also known as the counter electrode, is used to close the circuit and provide and the necessary current to the system for the desired reactions to occur on the working electrode. This electrode is typically made of an inert material that does not actively participate in the electrochemical reactions. The reference electrode is used to maintain known the potential of the working electrode during electrochemical measurements. This electrode has a well-defined and constant reduction potential against which the potentials of the working and, counter (if is possible) electrodes are measured. This system allows for precise control of experimental conditions and reliable measurements of electrochemical potentials and currents during electrochemical reactions. The electrochemical synthesis and subsequent characterizations of individual electrodes were initially conducted using a potentiostat/galvanostat by Metrohm Multi Autolab Cabinet/M101. Each electrode was immersed in an electrolyte-filled beaker arranged in a three-electrode cell configuration, with a platinum rod serving as the counter electrode and Ag/AgCl as the reference electrode. Parameters such as Open Circuit Voltage (OCV) and Potentiostatic Electrochemical Impedance Spectroscopy (EIS) were measured to determine the equivalent series resistance of the electrodes. Subsequently, electrochemical characterizations of the 2-electrode device were carried out using an Arbin BT2000 potentiostat/galvanostat.

4.3.1 Impedance Spectroscopy

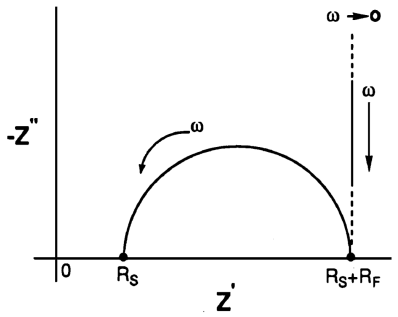

Figure 4.11: General Nyquist diagram from PEIS measurement for a supercapacitor.

The characterization method known as Electrochemical Impedance Spectroscopy, EIS, is highly effective for thoroughly analyzing the electrochemical performance of supercapacitors. EIS operates by applying a small (i.e. 10 mv) signal to the cell, across a broad frequency spectrum and measuring the resulting current variations due to the sample's impedance as a function of frequency. PEIS, were performed with a frequency range, from 1 MHz to 10 mHz with a sinusoidal signal, with an amplitude of 10 mV. Nyquist plot shows the relationship of imaginary transfer function, Z, to real transfer function Z_{Im} and correlates with the system dynamic. The intercept point of the curve in the Nyquist plot with the real axis is the equivalent series resistance, ESR.

The ESR value primarily hinges on the resistance of the electrolyte and the contact resistance at the interface between the active material and the current collector. The presence of a second intercept signifies the charge transfer resistance R_{ct}, computed by the disparity between the two intercept points. R_{ct}'s magnitude is depicted as the diameter of the semicircular segment on the Nyquist plot in the high-frequency range, primarily influenced by the electron transfer mechanism. At intermediate frequencies, the plot provides insights into ion diffusion across the electrolyte-electrode interface. In the right part of the plot, refered to lower frequency, the straight curve is by diffusion processes. In this work we present, measurements performed by use of two potenziostat, **Biologic** and **Metrohm Autolab**.

4.3.2 Cyclic Voltammetry

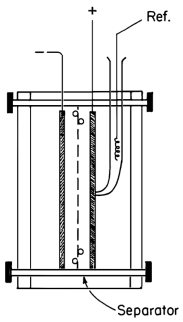

Concerning a electrochemical cell formed by tree electrode, when a positive voltage is applied to electrochemical system, opposite charges start to move through the surface and tend to accumulate on the electrodes under test. The electrodes are separated by a separator to prevent short-circuits and thus an electric potential is produced between the two electrodes to achieve the function of energy storage. Capacitance is defined as the ratio of stored charge transferred to the applied voltage on the electrodes of the cell, C = dQ/dV. At first glance, performances of electrochemical cell can be measured by using standard Cyclic Voltammetry. In practical Cyclic Voltammetry test consist in applying a staircase signal, voltage sweep, dV/dt, on the working electrode of the cell, the rate in which the voltage raise or go down is called **scan-rate**. As consequence fo the applied voltage a current ca be measured by the instruments between the working and the counter electrode. Reversing the voltage sweep is possible to explore the behavior in discharge. In Fig. 4.12a is show, the typical behavior of the electrical double layer capacitor (EDLC) is evaluated based on the corresponding current response at a fixed scan rate (10 mVs^{-1}). From the Fig.4.12b, the typical behavior of the pseudo capacitive electrochemical system is evaluated based on the corresponding current response at a fixed scan rate. The capacitance, C, can be calculated by the following:

$$C = \frac{Q}{\Delta V} = \frac{1}{\Delta V} \cdot \int I_d dt \tag{4.6}$$

Where Q represents the supercapacitor's charge in coulombs at its maximum voltage, measured by the CV system in use. ΔV denotes the voltage drop across the device's terminals, expressed in volts. The capacitance, C, can also be determined from the difference in current at a specific point, typically the midpoint, of the potential's rising and falling curves [64].

$$C = \frac{1}{SR} \cdot \int I_d(V) dV \tag{4.7}$$

4.3.3 Galvanostatic Charge Discharge with potential Limitation

A galvanostatic charge-discharge test is a classical chrono method test performed on supercapacitors for performance evaluation such as charge capability and life.

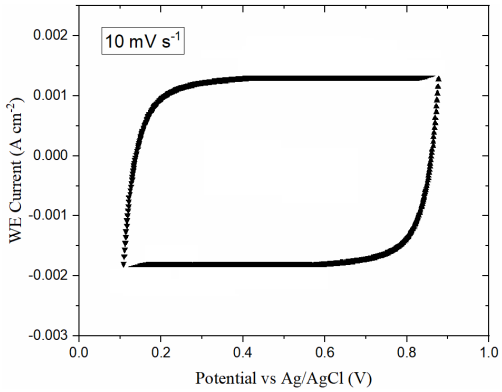

(a) General cyclic voltammetry for an electric double layer capacitor.

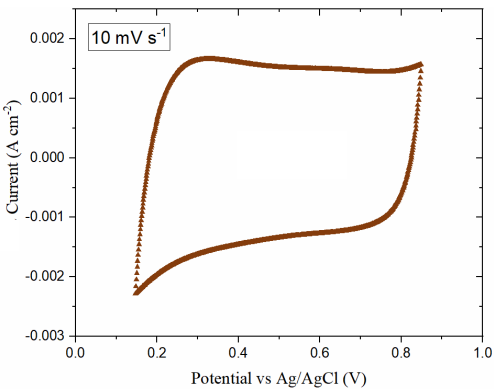

(b) General Cyclic voltammetry for a Pseudo capacitive material.

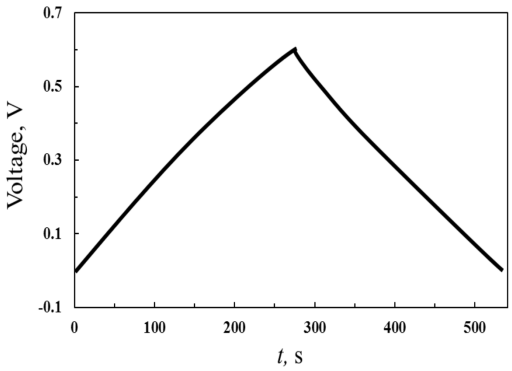

(c) Galvanostatic charge/discharge measurement, GCD, general profile.

Figure 4.12: General curve for cyclic voltammetry and charge discharge measurments.

Like the name said the measurement consists in two steps: the first charging a cell with a constant current imposed between the two terminals, and the second step, discharging phase, at a fixed negative current inside a specific voltage range. The capacitance C can be directly calculated by the following equation:

$$C_s = \frac{1}{m} I \cdot \frac{\Delta t}{\Delta V} \tag{4.8}$$

where I is the discharge current in amperes, ΔV is the voltage of the discharge, Cs is the specific capacitance of the electrode, m is the average mass of active material each electrode. They were utilized to assess the capacitance of each sample in this research. The operational voltage range is dictated by the electrolyte employed in the supercapacitor. The rated voltage incorporates a safety margin to prevent

reaching the electrolyte's breakdown voltage, the threshold at which the electrolyte decomposes or unwanted chemical reactions take place. Standard supercapacitors based on aqueous electrolyte typically have a rated voltage of ∼1 V , while those using organic solvents usually operate around ∼2.5 to 3.0 V. Asymmetrical (or hybrid) supercapacitors can operate in neutral aqueous electrolytes in a voltage window between 1.5 and 2.0 V.

Chapter 5

Experimental

5.1 Project Flow

In the context of my research on the development of sustainable micro supercapacitors, Has been adopted a methodological approach based on a structured and targeted project flow. This project flow has been designed to guide and coordinate all crucial phases of the development process, ensuring effective resource management and optimal achievement of objectives in terms of sustainability. Below, a list of the main steps and activities included in the project flow for the development of low impact micro-supercapacitors will be presented:

- Definitions of materials and potential applications.
- Analysis for compatibility and impacts of the materials chosen.
- Preliminary electrochemical characterization, EIS, CV, GCD on single electrode surface.
- Conceptualization of chemical/physical processes for the fabrication of a device
- Layout design through CAD for test cell.
- Layout design and fabrication of the masks for the photolitohography.
- Definition of a measurement protocol for the electrical characterization
- Definition of a measurement protocol for the electrochemical characterization.
- Development of 3D CAD for the set-up.
- Package and the electrical and functional properties have been verified.
- Figure of merit and long term tests are carried out.
- Final conclusion and future outlook.

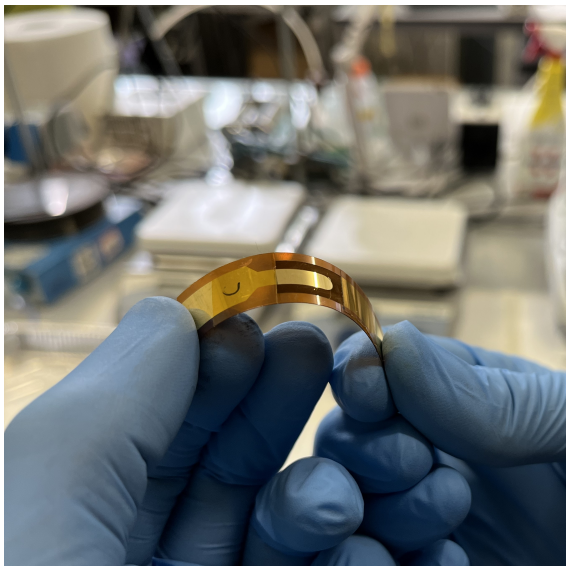

Figure 5.1: Picture of a single digit device plated by dendritic gold.

5.2 Material Characterization

The figure labeled as 5.2 displays a tilted FESEM (Field Emission Scanning Electron Microscopy) image depicting a selectively grown layer comprising Dendritic Gold and Manganese oxide. To ascertain the thickness of the deposited layer, SEM (Scanning Electron Microscopy) and confocal microscopy were employed. The morphological examination and elemental analysis of the electrode surface were conducted utilizing a Zeiss field emission scanning electron microscope. Figure 5.2a shows the different shapes if they develop during the plating process of Dendritic Gold, corresponding to a mass loading of $\sim 1to2mg/cm^2$, to 5.2b in greater detail where the layer of gold metal film (100 nm) deposited is shown. Figure 5.2c show alpha manganese oxide morphology. In fig. 5.2a is shown, alfa manganese oxide deposited on dendritic gold the morphology is similar to the layer without dendritic gold, suggesting that over a certain mass loading the manganese plating does not follow the dendritic profile and change morphology during thermal treatment.

5.2.1 XPS on Manganese Dioxide Electrode

The surface chemical composition of the electrodes underwent assessment through XPS analysis to ascertain the surface chemical makeup and manganese oxidation states of the deposited materials. Examination of the survey spectra revealed the presence of Mn, along with O, C, and occasionally trace amounts of Au ($<$ 1 at.%) originating from the substrate, as well as remnants of precursors and solvents utilized during the deposition processes (such as Na, K, and S). It's known that

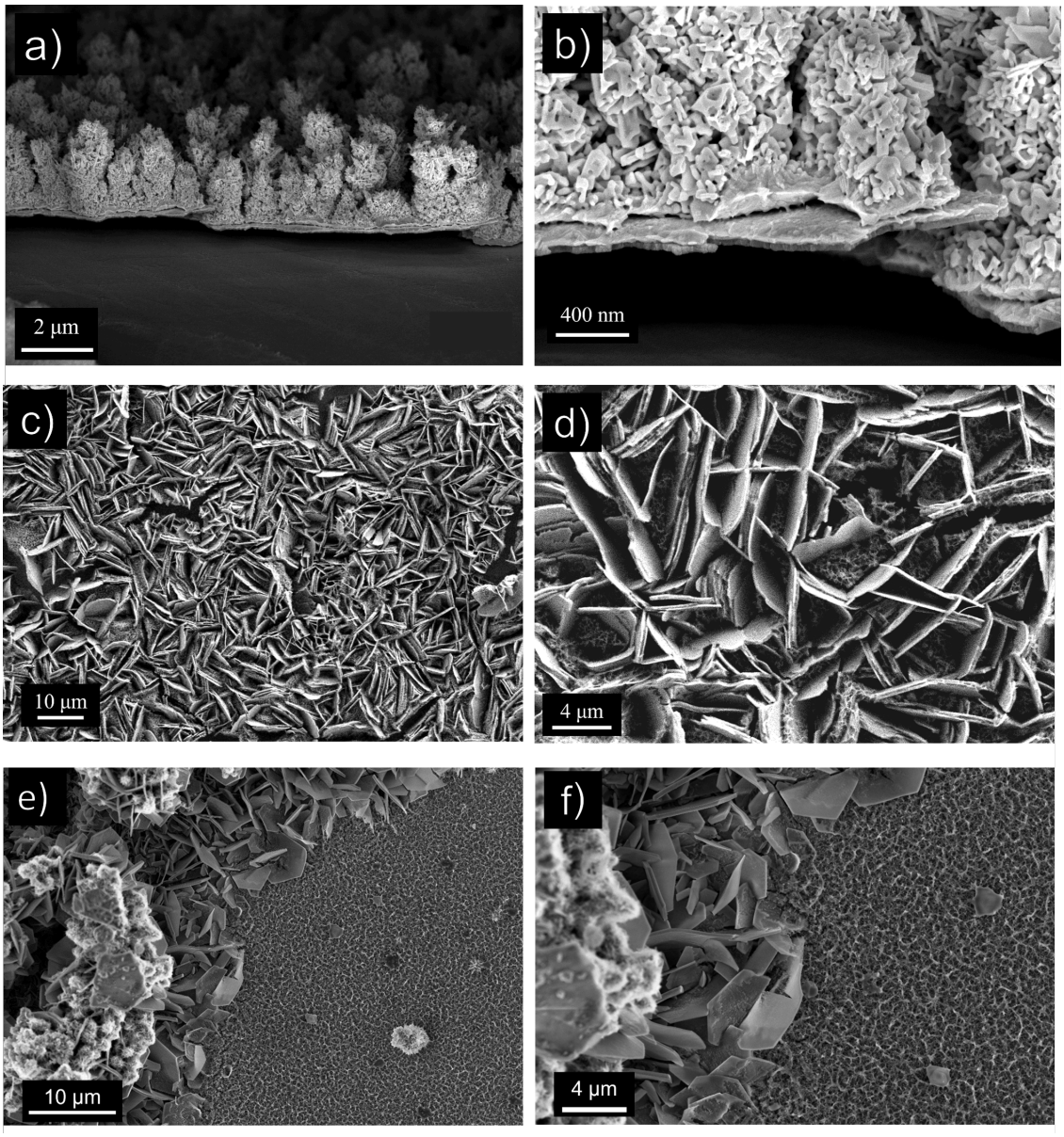

Figure 5.2: (a, b) FESEM image for grown D-Gold on thin film gold. (c, d) FESEM image for grown MnO_2 on thin film gold current collector. (e, f) FESEM images with different magnification of grown MnO_2 on Dendritic Gold current collector

manganese poses challenges for complete characterization via XPS due to its six oxidation states, multiplet splitting (for oxidation states II, III, IV, and VI) overlap, and broadening caused by the simultaneous presence of multiple oxidation states. Hence, relying solely on Mn 2p doublet analysis may not suffice to definitively determine Mn oxidation states. The analysis of Mn 3s doublet provides additional

insights, as the relative separation distance between the two peaks on the binding energy scale offers another piece to solve the intricate puzzle. From Fig. 5.3, it's evident that the two Mn 2p signals exhibit noticeable discrepancies between the thermally treated (red line) and the as-prepared (blue line) samples. A relative

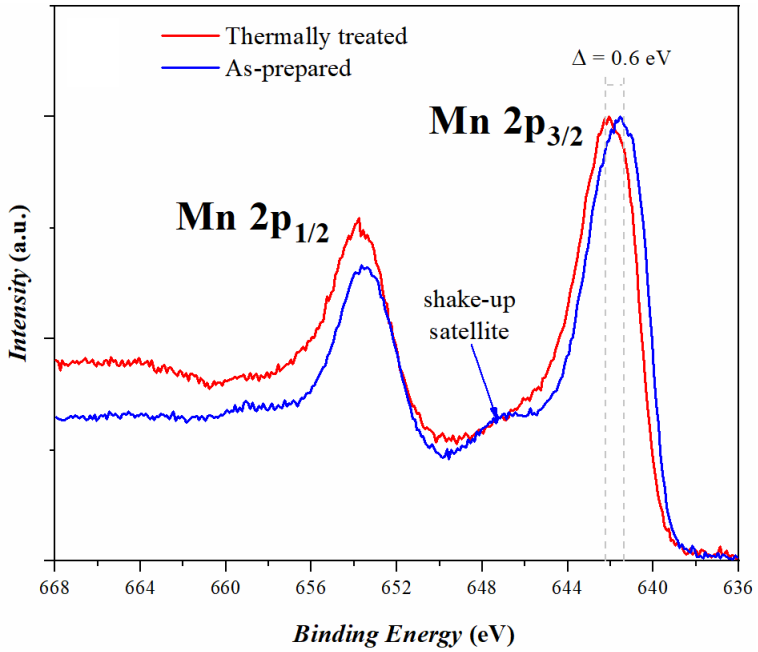

Figure 5.3: XPS spectra of Manganese 2p.

energy distance of 0.6 eV can be inferred between the two Mn 2p3/2 peaks together with the presence of a satellite structure (5.2 eV apart from Mn 2p3/2 maximum), for the as-prepared sample, above 644.0 eV, which is commonly attributed to shake-up losses due to MnO phase [65]. Considering the Mn 3s doublet depicted in Fig. 5.4, we observe two distinct values for the relative spacings (ΔE) between the two doublet peaks: 5.23 eV and 5.65 eV for the thermally treated and as-prepared samples, respectively. These values align well with those proposed by Chigane and Ishikawa in [66], further affirming the transformation of MnO into Mn_2O_3 through thermal treatment. While numerous attributions exist in the literature for these values [67, 68], based on the oxidation state and crystallographic phases, employing the formula from [69] to calculate the Average Oxidation State (AOS) as: AOS = 8.95 – 1.13 ΔE, enables us to assess the predominant oxidation state present on the surface of our samples. The calculated AOS values are 3.04 and 2.56 for the thermally treated and as-prepared samples, respectively. This suggests that the active material treated thermally demonstrates an average oxidation state corresponding to Mn(+3), as observed in compounds like Mn_2O_3 or MnOOH. Conversely, the electrode prepared as-is showcases an oxidation state reflecting a

blend of Mn(+3) and Mn(+2). The detection of the shake-up satellite associated with the MnO structure had already hinted at the presence of a Mn(+2) component. Moreover, if we recall the relative distance highlighted in Fig. 5.3 between the two

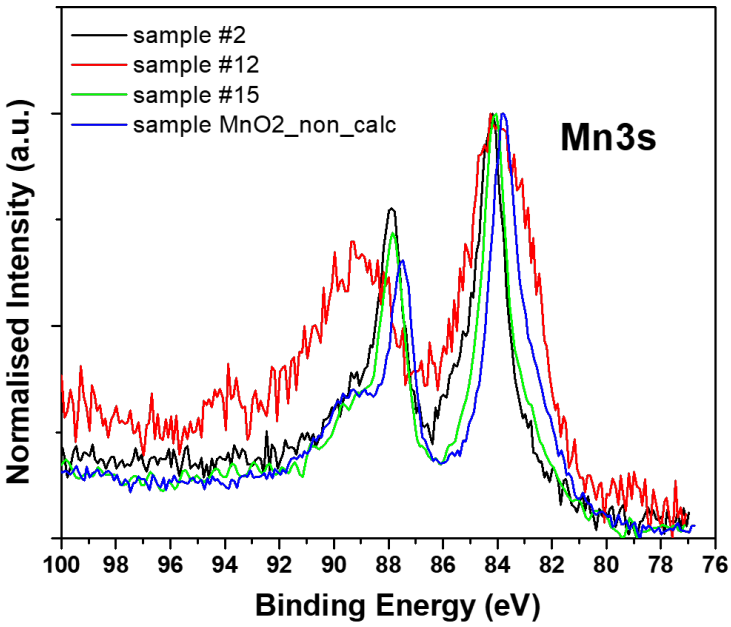

Figure 5.4: XPS spectra of Manganese 3s.

Mn $2p_{3/2}$ components ($\Delta = 0.6$ eV), we can find out the same relative distance between MnO and Mn_2O_3 or MnOOH reported in M. Biesinger et al. detailed work on transition metal oxides [65].

5.2.2 Raman on Manganese Dioxide Electrode

The Raman spectra of manganese oxides has three main regions: 200-450 cm^{-1} it is possible to find the skeletal vibrations, 450-550 cm^{-1} there are the deformation modes of the Mn-O-Mn structures and in the region 550-750 cm^{-1} the Mn-O stretching.

Literature findings vary concerning the claimed phases in both natural and synthetic samples. Xin et al. conducted thorough chemical and physical analyses of synthesized manganese oxides/hydroxides, with their work serving as a reference for the Raman spectra [70]. Using a 532 nm continuous green laser, powders were compressed and examined on a glass substrate, with the Raman shift scale calibrated using a crystalline Si-wafer. The structure of manganese oxides consists of

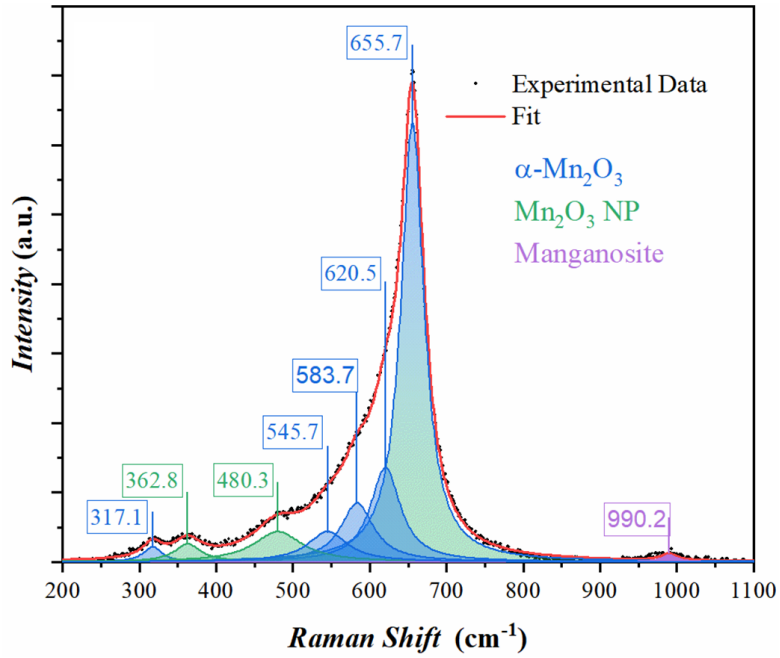

Figure 5.5: Raman Spectra for electroplated Manganese dioxide.

MnO_6 octahedral building blocks, which share edges and corners in various configurations. These octahedral structures exhibit six normal vibrational modes: v1, v2, v3, v4, v5, and v6. Among these, only v1, v2, and v5 are Raman active, while v3 and v4 are Infra Red (IR) active. However, the nominally inactive modes may become active in layered and/or tunnel structures. Our sample displayed a prominent peak at 655.7 cm^{-1} attributed to the v1 vibrational mode of Mn3+, with two less intense shoulders at 620.5 cm^{-1} and 583.7 cm^{-1} also attributed to the v1 vibrational mode of Mn^{3+}. According to data from [70], the possible phase is αMn_2O_3. This characteristic peak is also observed in Mn_3O_4 phases, as reported in other literature sources [71, 70]. However, considering the oxidation state of manganese, this phase was not deemed relevant. Consistent with the XPS results, the absence of the v3 mode peak at 703 cm^{-1} suggests that the material is not a layered or tunnel structure. Additionally, the presence of the v5 peak at 317.1 cm^{-1} indicates skeletal modes with relatively low activity. The v2 mode was found at 545.7 cm^{-1} instead of 538 cm^{-1}, as qualitatively noted in the report by Ram et al. [72]. The spectra exhibit two relatively intense peaks in the 300 to 500 cm^{-1} range, which, according to Karuppaiah et al. [73], can be attributed to Mn_2O_3 nanoparticles. Further insights from Yousefi et al. [74, 75] suggest that the small peak at 990.2 cm^{-1} may correspond to the Manganosite phase, MnO, although its presence is not significant due to the relatively low intensity [37]. The common poor crystallinity

of electrolytic manganese oxides, coupled with crystallite sizes typically limited to the nanoscale and the presence of multiple phases, pose challenges for identification and characterization using XRD. Hence, IR, Raman, and XPS spectroscopies are more sensitive in this regard. To unravel some features of the complex dendritic electrode pattern, two additional measurements were conducted on samples prepared specifically for this purpose.

5.2.3 XRD

The reflections at the dendritic electrode are characterized by the presence of very strong and sharp peaks imposed by the dendritic gold and by weak, but very broad, reflections arising from the Kapton flexible substrate (evidenced in Fig. 5.6 with the patterned yellow and orange peaks, respectively) onto which the reflections of the manganese oxides are superimposed.

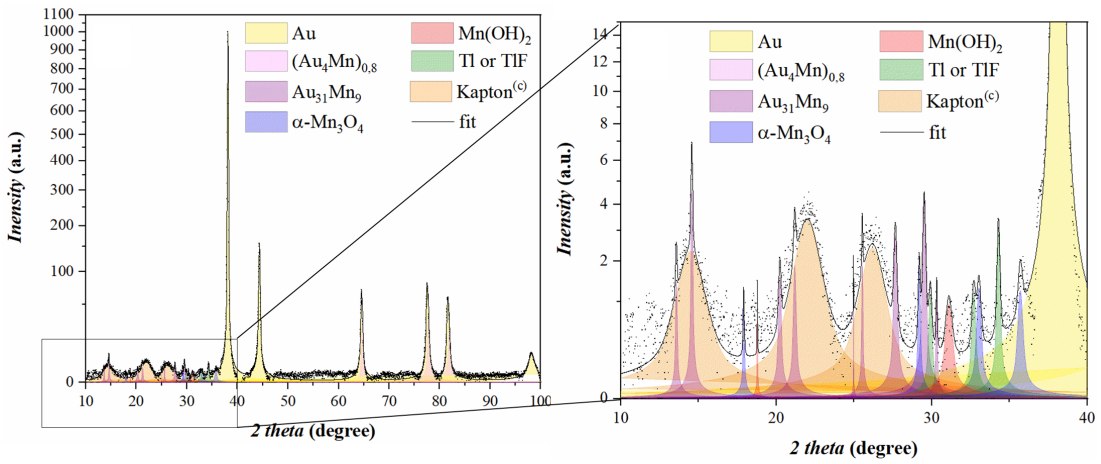

Figure 5.6: XRD pattern of manganese dioxide on dendritic gold.

It is noteworthy to mention that the reflections from the Kapton support remained identical before and after thermal treatment. They were subtracted along with the polynomial background during qualitative identification and quantitative analysis. To mitigate the intense signal generated by gold, electrochemical deposition of manganese oxide was also performed on a flat-smooth gold current collector with higher manganese-compounds mass loading. This approach allowed focusing more on the metal oxide electrodeposited rather than on the current collector. Subsequently, the same sample underwent annealing according to the standard procedure for preparing dendritic electrodes. Through these three measurements, the evolution of both the gold current collector and manganese-related phases under thermal treatment was tracked.

Combining qualitative, quantitative, and Rietveld refinement analyses, it was

determined that the flat current collector belongs to the gold Fm-3m space group with a face-centered cubic unit cell, having a cell parameter a = 4,099 Å, which decreased to 4,080 Å after thermal annealing. In contrast, the average crystal size increased from 758 to 833 Å, and the microstrain of the structure relaxed from 1.31μ to 1.20μ. The dendritic gold, on the other hand, exhibited a unit cell with a = 4.076 Å and significantly larger average crystal dimensions, above 1150 Å, with a microstrain of 1.35μ even after thermal treatment. Interestingly, in the dendritic electrode, metallic gold (22 % of the sample weight) was not the sole metallic phase. Two Au-Mn alloys, $(Au_4Mn)0.8$ and $Au31Mn_9$, were found to be present in significant quantities during the refinement, accounting for 4.45 and 1.8 % of the total sample weight, respectively. Regarding the manganese-based active material, two manganese oxyhydroxides, Hausmannite (αMn_3O_4) and Pyrochroite ($Mn(OH)_2$), were identified on both the flat and dendritic current collectors. Pyrochroite disappeared completely after thermal treatment on the flat gold, leaving a small residue on the dendritic current collector (0.2 %). Before thermal treatment, Pyrochroite exhibited a small average crystal size of about 110 Å, while αMn_3O_4 showed a large crystal size of 1075 Å, which significantly decreased to 164 Å post-annealing. This change in crystalline size, without altering other structural parameters of the phase, resulted in a noticeable color change from light orange to deep brown. To complete the Rietveld refinement of the dendritic electrode, one phase (0.1 % by weight) remained unidentified. It is equally plausible that this phase could be metallic Tl or TlF, originating as an impurity from the gold electroplating solution containing a Tl-based salt as a brightening agent. It is conceivable that the residual $Mn(OH)_2$ and the Tl-based compound may have been trapped in close porosities during the electrodeposition process due to the irregular shape or insufficient annealing time/temperature. All refined parameters of the identified phases in the three samples are presented in Table XRD in the supporting information. In wet synthesis of MnO_x nanostructures, the nonequilibrium crystallization at ambient temperatures leads to the formation of various metastable phases, often resulting in mixtures of manganese oxides with multiple valences. Pyrochroite is naturally abundant in aquatic and wet environments and readily transforms to higher oxidation states with fast kinetics. Hausmannite, on the other hand, is the most stable phase of manganese oxides, with the highest average oxidation state of Mn as +2.66. αMn_3O_4 corresponds to the I41/ space group and exhibits a spinel structure described by the formula, $Mn^{2+}(Mn^{3+})_2O_4$, wherein Mn^{2+} and Mn^{3+} ions occupy the tetrahedral and octahedral sites, respectively, with tetragonal distortion of Mn^{3+} ions due to the Jahn-Teller effect. Bixbyite, a trivalent oxide (αMn_2O_3), possesses a cubic structure with the Ia3 space group. In recent decades, it has garnered significant scientific interest due to its structural architecture's suitability for supercapacitors. Chen et al. proposed a phase change from precipitated wires of $Mn(OH)_2$ to αMn_3O_4 and eventually to αMn_2O_3 through thermal treatments

in air or a nitrogen atmosphere. Similarly, Ramirez et al. observed that amorphous MnO_x, when heated above 450 °C, crystallized into αMn_2O_3 under air and αMn_3O_4 under nitrogen. These reactions, conducted under flowing gases, aimed to supply reactants to the surface. However, during the annealing procedure at 300 °C for the dendritic electrodes, the atmosphere was static, potentially limiting the oxidizing agent's availability to promote further oxidation of Hausmannite into Bixbyite on the electrode surface. Moreover, for metal oxides with numerous oxidation states, surface phases often differ significantly from those in the bulk. Song et al. employed laboratory and synchrotron-based light analysis to study phases at different depths in their samples using small-angle and quartz capillary transmission XRD. They identified the co-presence of αMn_3O_4 and αMn_2O_3 at different depths and under varying annealing conditions.

Hence, in this study, evidence of oxidation state evolution from bulk through XRD (analysis depth > 2000 nm) to the surface via Raman (<1000 nm) and up to the interface through XPS (<10 nm) is presented, alongside the structural evolution of the current collector from flat to dendritic gold.

5.3 Dendritic Gold Electrochemical Characterization

A dendrite, characterized by its tree-like branching structure, is a common form observed across various scientific fields, including biology, metallurgy, and crystallography. An illustrative example of such structures in nature is found in the crystalline formations of snowflakes. In this study, we explore the electrochemical behavior of metallic dendrites formed during electroplating deposition and provide insights into the surface modifications achieved by coating these structures with active materials for supercapacitor applications. Porous metallic current collectors were prepared using plating solutions, where the working electrode was connected to the surface slated for coating, and a pure gold sheet, 50 μm thick, served as the counter electrode, with a reference Ag/AgCl electrode utilized. The deposition process was conducted in galvanostatic mode, applying a current density of 1.4 $mAcm^{-2}$ for 450 s, while maintaining a distance of 4 cm between the deposition electrodes. Variations in current density were implemented to generate a deposition rate curve, aiding in determining the optimal mass loading parameters. The resulting structure exhibits a dendritic morphology, showcasing its characteristic tree-like shape, as depicted in Figure 5.2a.

The distinctive shape of the dendritic metallic layer arises from its rapid growth, which induces specific crystallographic orientations. An advantage of this technique lies in its cleanliness and simplicity, rendering it easily adaptable to production lines equipped with microelectronic facilities. To characterize the dendritic metallic layer, preliminary cyclic voltammetry was conducted in 0.5 M sulfuric acid

(H_2SO_4). In Fig. 5.7, voltammograms of two different current collectors are depicted: the red curve illustrates the voltammograms of the flat gold, while the violet-gray curve represents those of the dendritic gold. Two distinct regions can be identified, which we refer to as the "oxygen" region and the double-layer region. The oxygen region initiates when the CV is swept over a potential exceeding 0.9 V vs Ag/AgCl for the D-Gold electrode, and over 1 V vs Ag/AgCl for the flat gold electrode. In this region, a thin anodic oxide film is formed through a simplified reaction preceding the evolution of O_2 gas. Consequently, a hydrated gold oxide monolayer is formed on the electrode, contributing to the evaluation of the real surface area. The left portion of the voltammograms, ranging from 0 to 0.7 V, showcases the double-layer region, where only capacitive processes occur. Overlapping the gray curve onto the red one provides initial evidence of the effective area increase. The electrochemical surface area (ECSA) was assessed by estimating the charge associated with the reduction of the gold oxide at 0.87 V vs Ag/AgCl, as depicted in Fig. 5.7. Two peaks are visible: one referring to the flat gold in red (Fig. 5.7b), and the other, in gray, corresponding to the dendritic gold. The charge attributed to the reduction process, i.e., the reduction of the oxide monolayer formed on the surface of the Au electrodes, measured 1.2 mC for flat gold and 4.5 mC for the D-Gold electrode. From this charge, the ECSA and the roughness factor, defined as the ratio between the effective area and the geometrical footprint area, can be evaluated [76, 77]. The equation used for the calculation is presented below.

$$A_{real} = \frac{Q_{red}}{\Gamma} = \frac{Q_{red}}{e \cdot d_m} \tag{5.1}$$

Where the Q_{red} is the cumulative charge involved in the reduction peak, e is the electron charge 1.6 10^{-19} C, Γ is the charge per surface area for a gold oxide layer the value is 384 $\mu C cm^{-2}$ and dm is surface metal atom density. From the flat gold electrode, with a geometrical area of 0.5 cm^2, resulted a roughness factor of about 6.6 and an ECSA of about 3 cm^2, and from the D-Gold electrode, with a geometrical area of about 0.54 cm^2, resulted a roughness factor of about 22, and a ECSA of about 12 cm^2.

The areal gain factor, in terms of area from thin film gold to dendritic gold is of about four times (4x). In terms of areal capacitance dendritic gold layer offers a specific capacitance of about 0.5 mF cm^{-2},this value was calculated through CV in Na_2SO_4 1 M in a potential window 0 to 1 V, reporting the absolute capacitance on to the foot print area. Further analyses were made tuning the D-Gold mass loading with respect to the active material.

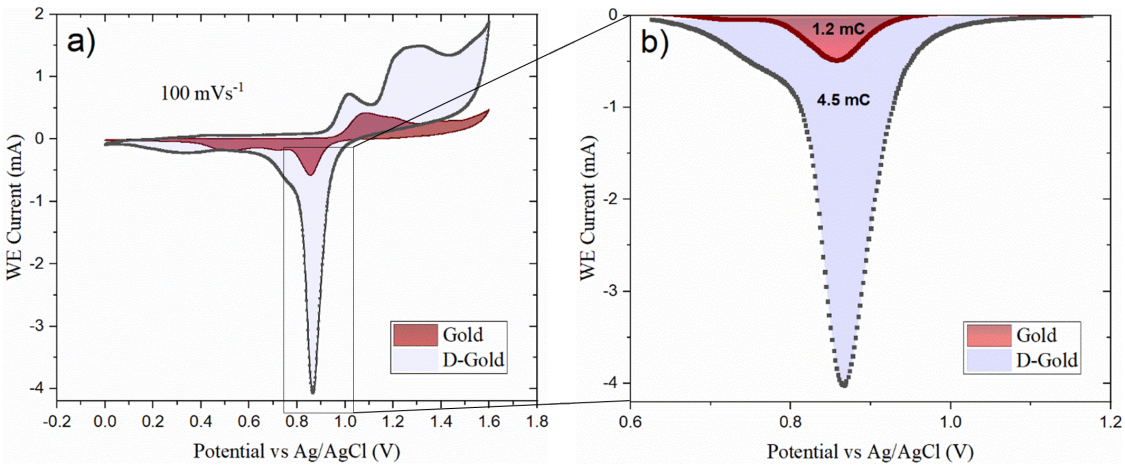

Figure 5.7: (a) CV of thin film gold and D-Gold overlapped at 100 mV s^{-1} in H_2SO_4 0.5 M, the electrode potential is referenced to Silver/Silver Cloride reference electrode. (b) Dettail of the reduction peak used for the calculation of the areal factor.

5.3.1 Activated Carbon Electrochemical Characterization

The negative electrode measurements, the electrochemical stability of the activated carbon electrode in the -1.1 V to 0 V vs Ag/AgCl voltage range was tested in Na_2SO_4 1 M giving a specific capacitance of about 55 $mFcm^{-2}$ with a scan rate of 5 mVs^{-1}. In this case it is useful to analyze between PEIS of AC based 5.8 electrode chart that give an idea of the different morphological pore structures led to a different PEIS curve. The typical semi-circular pattern of carbon-based electrode is absent in Mn_2O_3 based electrodes. This suggests a substantial difference in the porosity structure at the interface. PEIS of AC based electrode is more similar to line 4 in Fig. 2.8 describing an inner bulk porosity almost closed to the edge, while PEIS of Mn_2O_3 based electrode is similar to lines 1-2 in Fig. 2.8. Where a well-open rectangular pore structure is portrayed.

5.3.2 Manganese Oxide Electrochemical Characterization

The charge storage capabilities of the Mn_2O_3 coating on the F-Gold current collector, prepared according to the experimental section, were initially explored through cyclic voltammetry (CV) measurements. Furthermore, we examined how the capacitance performance varies with the mass loading of the pseudo-capacitive material. Preliminar PEIS test where made in different electrolyte before and after cycling, see 5.9b to explore differences in neutral environment of the pseudo activity for the material, no relevant differences where observed. In this context, it is instructive

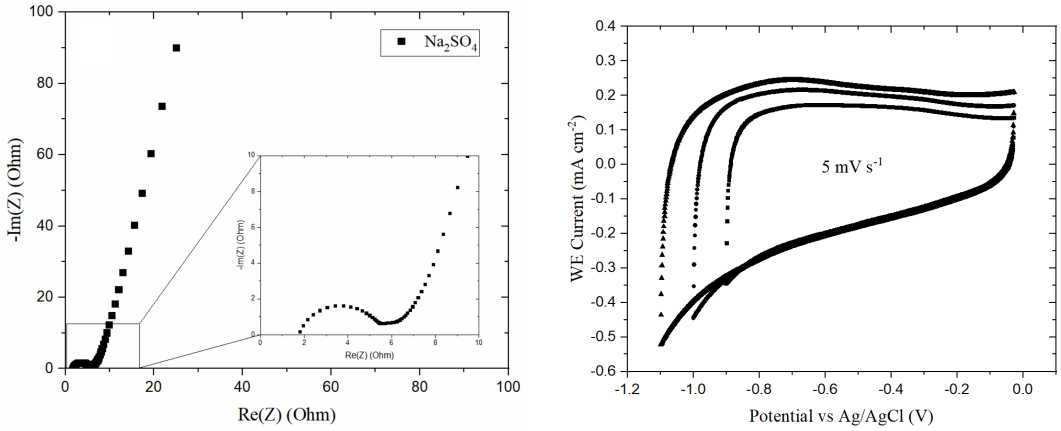

(a) PEIS curve of AC electrode after cycling.

(b) CV curves for AC electrode at a scan rate of 5 mV s^{-1}

Figure 5.8: PEIS and CV of AC base electrode.

to compare the potentiostatic electrochemical impedance spectroscopy (PEIS) of AC-based electrodes, which provides insights into the distinct morphological pore structures leading to different PEIS curves and to explore potential changes in surface oxidation states or activation phenomena of the active material. As suggested by Toupin et al. [50], these changes are observable during cycling between 0 and 0.9 V. Fig. 5.9a and 5.9b depict distinct slopes in the PEIS curves. After conditioning cycling, the slope increases in each curve, primarily due to the intercalation

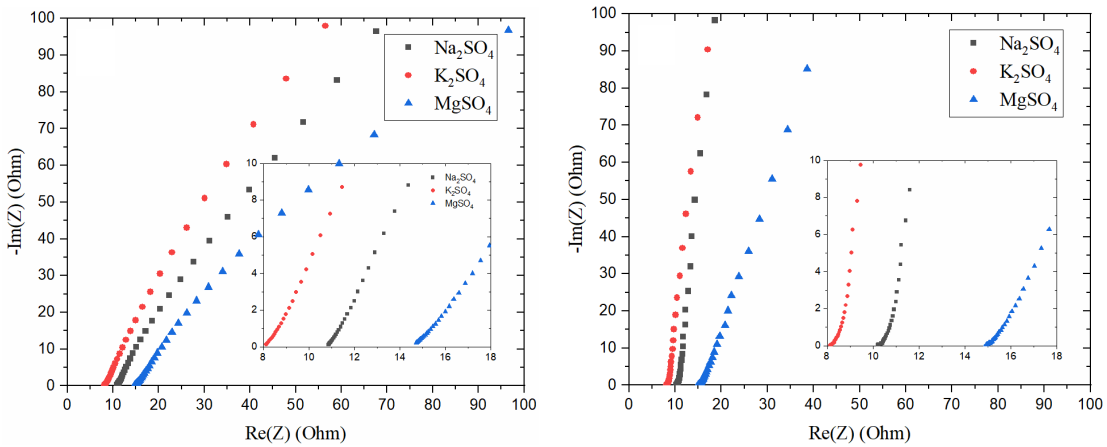

(a) PEIS manganese oxide before

(b) PEIS manganese oxide after

Figure 5.9: PEIS curve of Mn_2O_3 electrode before and after cycling, in different electrolytes.

of Na^+, K^+, Mg^{2+} cations into the bulk of Mn_2O_3 during the initial cycles. Additionally, it is noteworthy that Na_2SO_4 electrolyte exhibits a better slope compared to K_2SO_4 electrolyte in the lower frequency region.

The characteristic semicircular pattern observed in carbon-based electrodes is notably absent in Mn_2O_3-based electrodes, indicating a significant difference in porosity structure at the interface. The PEIS of the activated carbon-based electrode resembles the profile depicted by line 4 in Fig. 2.8, portraying an inner bulk porosity closely located to the periphery. Conversely, the PEIS of the Mn_2O_3-based electrode mirrors lines 1-2 in Fig. 2.8. Additionally, Fig. 5.10 presents typical cyclic voltammograms obtained at a scan rate of 10 mV s^{-1} within the range of 0.1 to 1.1 V vs Ag/AgCl.

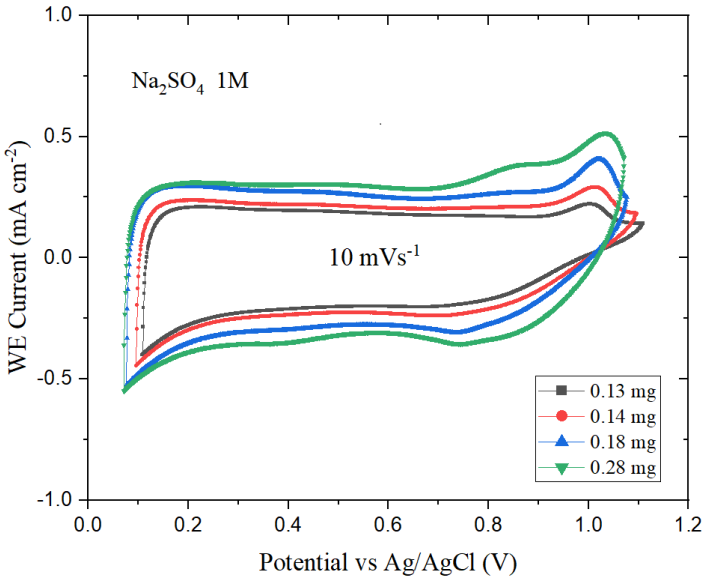

Figure 5.10: (a) CV curves of Mn_2O_3 loaded on to flat gold film, with differet Mn_2O_3 mass loading, at a scan rate of 10 mV s^{-1}.

The voltammetry profile displays an almost linear and well-defined structure, indicative of a good pseudocapacitive behavior. Fig. 5.11 illustrates the performance variation of this electrode with alterations in the Mn_2O_3 mass loading. It is evident from the results that the trend of gravimetric capacitance exhibits a linearly decreasing pattern. This experimental observation validates that only manganese atoms, present on the electrode surface, participate in the charge storage process. The red line, representing the areal capacitance, stabilizes at approximately 35 $mF\ cm^{-2}$ for electrodes with a Mn_2O_3 mass loading exceeding 0.25 $mg\ cm^{-2}$. To summarize, there are no significant benefits in terms of capacitance, in increasing the manganese mass loading beyond $0.25 mg\ cm^{-2}$ for planar

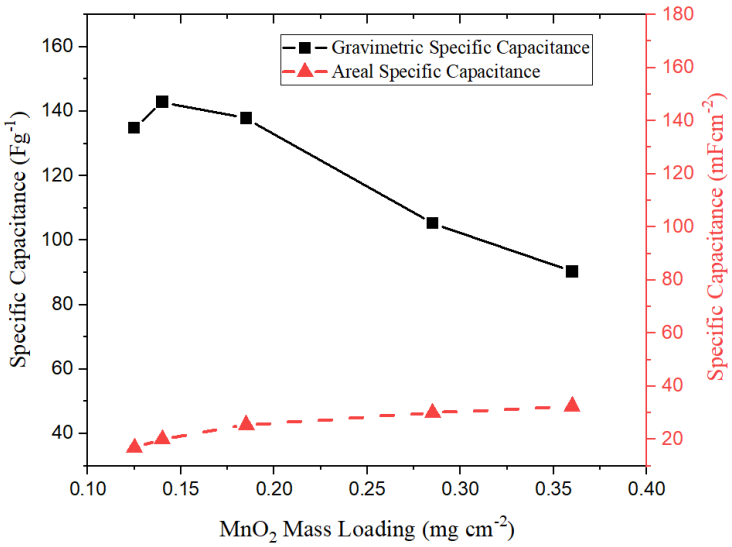

Figure 5.11: Gravimentric and areal capacitance performance in Na_2SO_4 at 10 mVs^{-1}in function of Mn_2O_3 mass loading.

micro-supercapacitors intended for specific applications, unless to reach well uniformity on the current collector avoiding exposition to the electrolyte. However, a swift deterioration was noted with the Flat-Gold electrode within the 0 to 1.1 V vs Ag/AgCl potential range. The extensive potential window results in electrode delamination and premature aging. It is presumed that this accelerated aging is caused by surface stress phenomena after numerous cycles, particularly near the O_2 gas evolution zone. Consequently, a restricted operating potential window of 0 to 0.7 V vs Ag/AgCl was selected to ensure prolonged cycle stability. Regarding subsequent analyses with the D-Gold treated electrode, a consistent Mn_2O_3 amount of 0.7 $mg\ cm^{-2}$ was utilized for the three electrode tests, in order to have well covering of the current collector avoiding to expose it to the solution. The three electrodes were fabricated with varying mass loadings of Dendritic-Gold, specifically 0.88, 1.56, and 3.34 $mg\ cm^{-2}$. The constant mass loading of Mn_2O_3 was deliberately chosen to emphasize the benefits associated with the Dendritic-Gold layer. A noticeable distinction in the shape of the cyclic voltammetry (CV) curves is evident between Fig. 5.10 and Fig. 5.12. The voltammogram in Fig. 5.12 exhibits a more "boxed" profile with higher specific current compared to the one in Fig. 5.10. It can be inferred that the enhancement effect provided by the Dendritic-Gold layer is limited up to 3 $mg\ cm^{-2}$ of deposited Dendritic-Gold material. Referring again to Fig. 5.12, the red and blue curves almost overlap without significant differences. However, notable distinctions are observed for the gray curve with 0.88 $mg\ cm^{-2}$ compared to the red and blue curves in terms of capacitance performance. Fig. 5.13 illustrates the gravimetric capacitance and specific capacitance per unit area

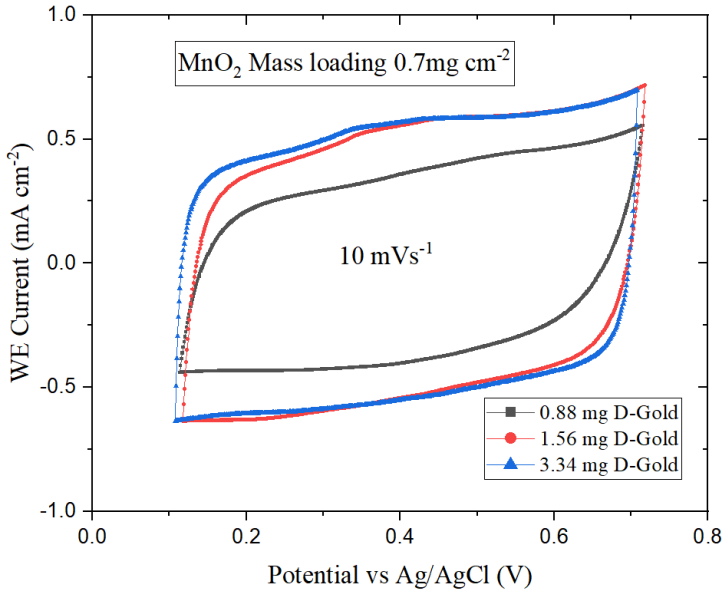

Figure 5.12: CV curves of Mn_2O_3 deposited on D-Gold Current collector, varying mass loading of Dendritic Gold, at a scan rate of 10 mVs^{-1}.

calculated from Eq. 4.8.

Significantly improved performances are noticeable, with areal capacitance tripled compared to the trendline in Fig. 5.11, and a stable gravimetric capacitance with a specific value of approximately 100 $mF\,cm^{-2}$ for the Mn_2O_3 electrode, it is important to note that the capacitance value pertains to the dendritic gold-treated electrode. The mass of the deposited gold, which is not included in the calculation, does not function as an active material but rather as part of the current collector. This contributes to the improvement factor, resulting in the increasing trend in gravimetric terms for the black curve in the figure 5.13. Additional voltammetry experiments were conducted with Dendritic-Gold multilayered electrodes in two other neutral water-based electrolytes, namely K_2SO_4 and $MgSO_4$ (Fig. 5.14).

5.4 Flexible hybrid device results

The hybrid device was built according to the procedure described in the experimental section. Electrodes were balanced in terms of charge, tuning the mass loading during the electroplating deposition techniques, the positive electrode was charged with 0.7 mg where the negative electrode was charged with 1.5 mg of AC, both electrode where charged with 1.86 mg cm^{-2} of dendritic-gold. The evolution of the

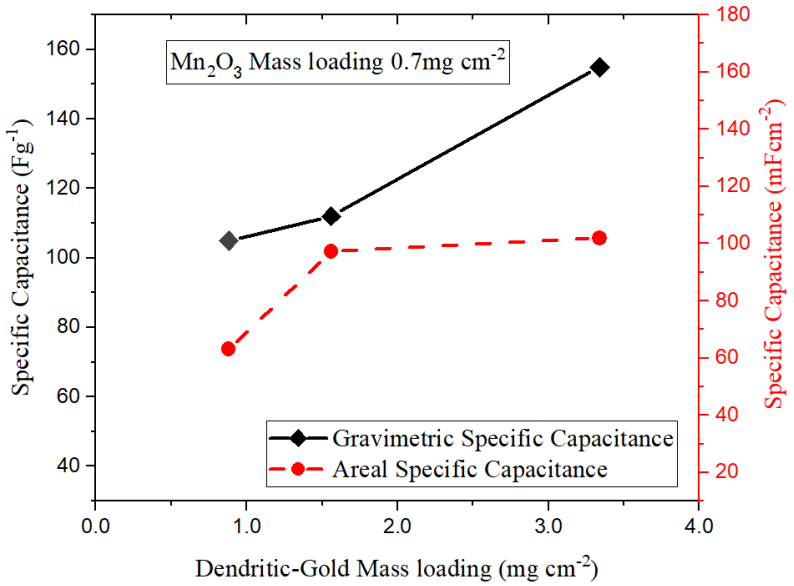

Figure 5.13: Gravimentric and areal capacitance perfomance in function of Dendritic Gold mass loading, with a fixed ammount of Mn_2O_3 0.7 mg cm^{-2}.

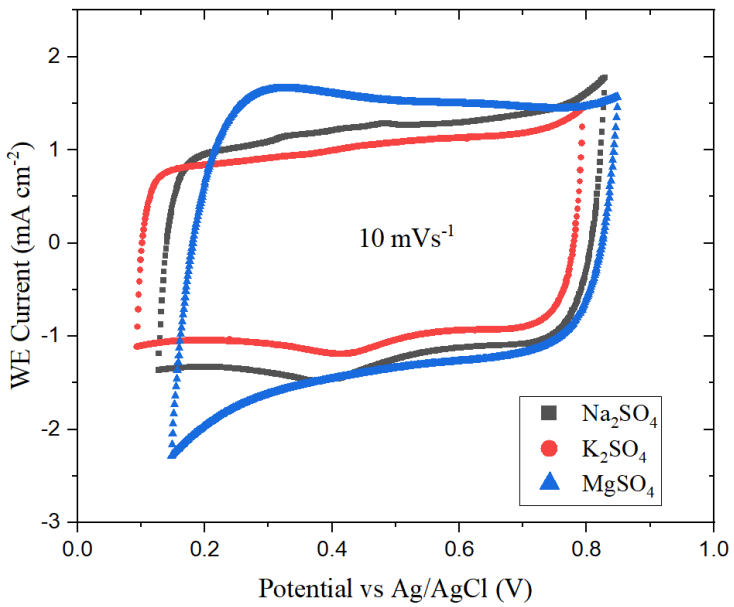

Figure 5.14: CV curves for Mn_2O_3 in different water based electrolyte. At a scan rate of 10 mV s^{-1}.

cell voltage during charge/discharge cycle is shown in Fig. 5.15c. The planar interdigitated micro-Supercapacitors was tested with 220 μL of 1 M Na_2SO_4 aqueous electrolyte infiltrated in the glass fiber separator.

PEIS was utilized primarily to assess the transport characteristics of the device, yielding an equivalent series resistance of approximately 7 Ω. Capacitance variations with the scan rate reflect the distinct ion diffusion dynamics across the interface. At lower scan rates, the maximum charge accumulation process, as depicted in Fig. 5.15c, allows for the full utilization of pseudo-porosity. The CCCD curves of the device exhibit a somewhat nonlinear behavior, indicating the occurrence of self-discharge phenomena and electrical losses at a rate of 50 $\mu A\ cm^{-2}$. Additionally, the potential presence of activated carbon particles,residual and anwanted from the electrophoretic process, within the separator could create minor resistive paths at the interface, contributing to charge losses. Numerous forthcoming analyses are required to comprehend and mitigate the self-discharge effect. Following an initial loss of 12% observed during the initial 100 cycles, the capacitance stabilized at 17 $mF\ cm^{-2}$ during cycling at 50 $\mu A\ cm^{-2}$. The specific capacitance was calculated using Eq. 4.8. The capacitance retention, illustrated in Fig. 5.15d, demonstrates long-term stability, with the device performance tested over 1500 cycles at a discharge current rate of 500 $\mu A\ cm^{-2}$. However, the maximum energy density calculated reached 5 μWh cm^{-2} with a discharge time of 550 s. This time scale aligns well with the operational requirements for the initially envisioned applications of MnO_2-based micro-supercapacitors, such as self-powered sensors, wearable electronics, or other applications with brief power demands where conventional batteries fall short. No observable gas evolution was detected during cycling. The device's energy and power densities, evaluated using appropriate equations, are depicted in the Ragone plot in Fig. 5.16, and are compared with the electrochemical performances of planar devices reported in literature from previous decades, tested under similar conditions. Table 1 presents a comparison of the device tested in this study with recent pseudocapacitive-based micro-supercapacitors. As suggested in a recent review by Gao and Liu [78], for solid-state supercapacitors, the capacitance should be computed considering the geometric area, given the significantly lower weight of the active material compared to other constituents of the device. In this context, the comparison was made solely based on the areal capacitance, electrolyte, and voltage windows of the various devices.

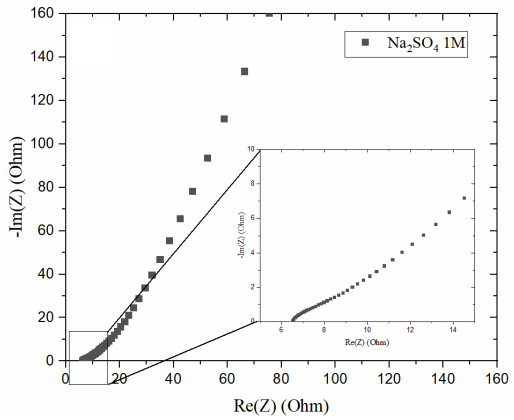

(a) PEIS of the hybrid device

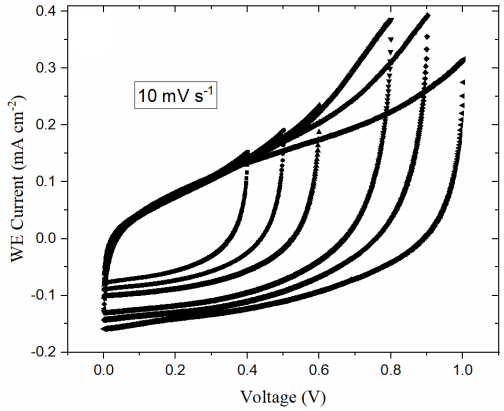

(b) Cyclic voltammetry conditioning cycling of the hybrid device

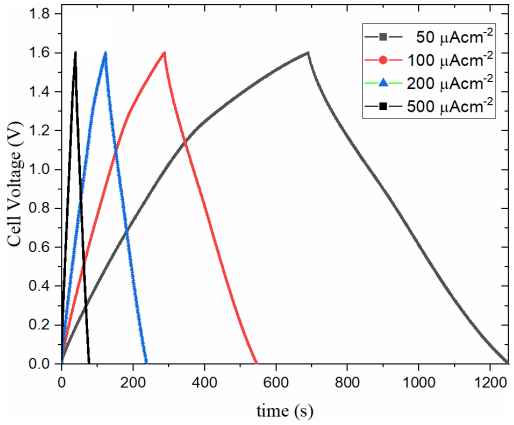

(c) CCCD curves of the hybrid device at a current density of 50–500 μAcm^{-2}

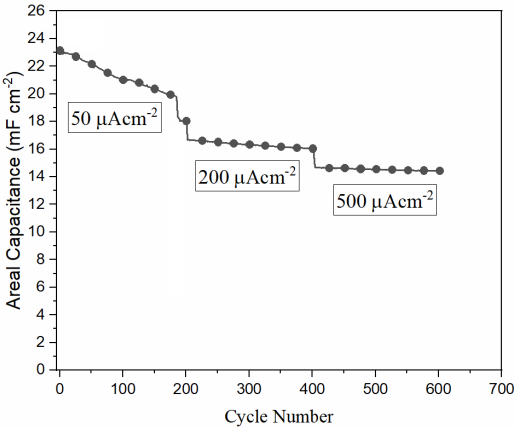

(d) Areal capacitance at different current rate

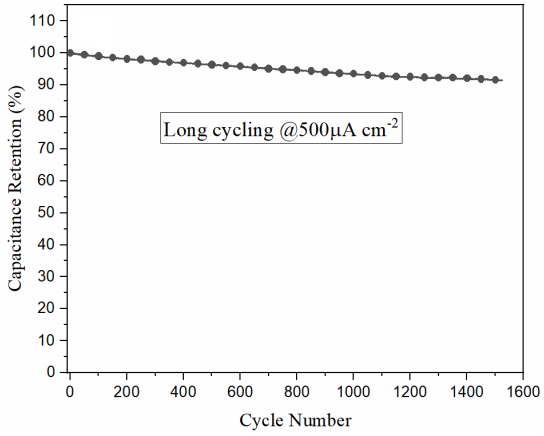

(e) Capacitance retention of the devices at a current density of 500 μAcm^{-2}

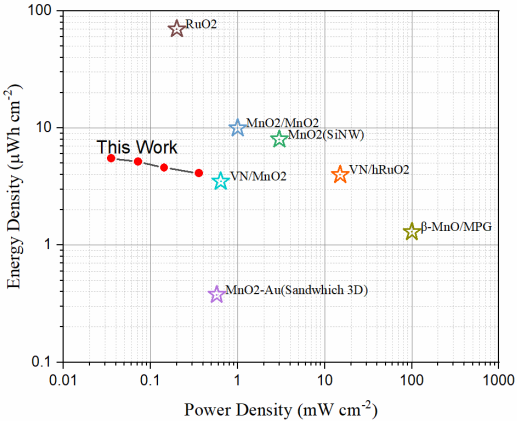

(f) Ragone plot of this work and micro-supercapacitors device in literature.

Figure 5.15: micro-supercapacitor AC//Manganese Oxide performances.

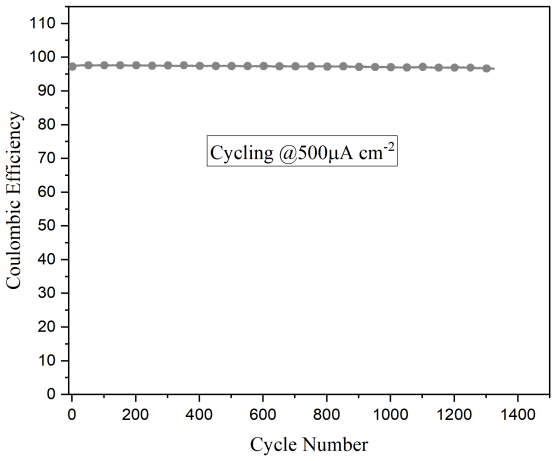

(a) Coulombic efficiency of the hybrid device

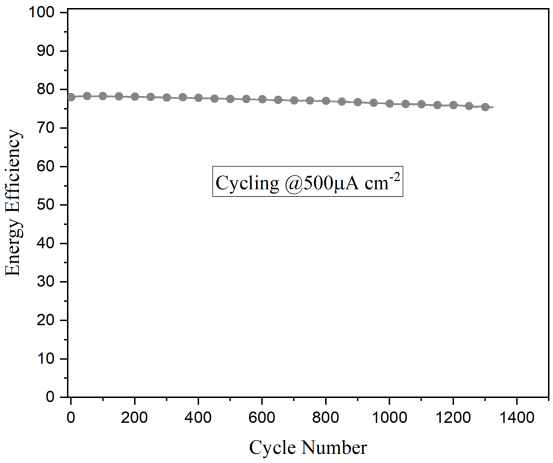

(b) Energy efficiency of the hybrid device

Figure 5.16: micro-supercapacitor AC//Manganese Oxide performances.

Table 5.1: Hybrid micro-supercapacitor comparison

Materials	Cap. $mFcm^{-2}$	Electrolyte	Vol. V	C_{1000}	Ref.
MnO/AC (2D)	20@50μAcm^{-2}	Na_2SO_4	1.6	0.7	[79]
MnO_2@$SiNW$ (3D)	13@10mVs^{-1}	$LiClo_4 - PMPyrBTA$	2.2	0.71	[80]
GQDs/MnO_2	1.1@15μAcm^{-2}	$Na_2SO_4 0.5M$	1	0.54	[81]
$MnO_2/C/AlNanowallArray$	1000@2μAcm^{-2}	$Na_2SO_4 1M$	1	0.01	[82]
MnO_2-Au (Sandwich-3D)	4.3@50μAcm^{-2}	$Na_2SO_4 1M$	0.8	0.05	[83]
rGO/Au-FS	0.77@1Vs^{-1}	PVA/H_2SO_4	1	1	[84]
$\delta - MnO_2$(2D)	0.26@5.4μAcm^{-2}	PEDOT	0.8	2.0	[13]
VN/MnO2(2D)	16@5.4μAcm^{-2}	$SiO_2 LiTFSIgel$	2.0	0.04	[85]
MnO_2/rGO	7.4@10mVs−1	PVA/H_3PO_4	0.8	0.9	[86]
RuO_2(2D)	812@1$mVs - 1$	$PVA - doped - (SiWa)$	0.9	1.5	[77]
$\beta - MnO/MPG$	6.5@1Vs^{-1}	KOH	1.5	0.04	[87]
$VN/hRuO_2$	200@μAcm^{-2}	KOH 1 M	1.15	0.04	[88]
MnO_2/MnO_2(ID)	50@10mVs^{-1}	EMImTFSI+liTFSI 0.5 M	1	0.04	[23]

5.5 Approaching on metal oxide on chip μSC

In this paragraph, we aim to overcome the limitations imposed by some aspect of the techniques used for hybrid supercapacitors. The adoption of electrophoretic techniques imposes a physical limit on the miniaturization process. We can identify this limit by referring to interdigitated planar devices with a resolution of approximately 50 microns. Going below this value and adopting colloidal suspensions with micro-sized particles entails, firstly, technological challenges in applying the deposition technique and, secondly, the risk of short-circuiting the two current collectors.

Iron Oxide Electrochemical Characterization

In this case, could be necessary to adopt the electroplating technique for both electrodes using solutions containing metallic salts. For this purpose Iron Sulfate plating solution was used with a concentration of 0.5 M and pH = 3 to prepare the negative electrode instead the AC based. Set up adopted is the same for manganese and gold discussed previously, using a sacrifical anode made by pure Iron. The density current applied during the process was from 10 - 15 mA/cm^2, charge loading 1 C/cm^2. In this context, iron oxide appears to be a promising candidate in terms of sustainability. Iron is employed similarly to manganese: it is deposited by plating and then thermally treated to be oxidized, as it exhibits pseudo-capacitance and thus responds linearly applying a constant current charging, thereby constituting asymmetric capacitors, measurement where made with swagelock T-cell with fat AC counter electrode and Ag/AgCl as reference electrode. In figure 5.18, the behavior

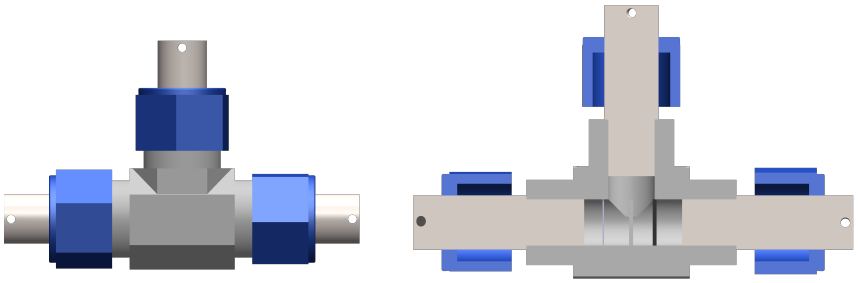

(a) Swagelock T-Cell (b) Section of Swagelock T-Cell

Figure 5.17: Swagelock set-up used for iron-oxide measurements in Na_2SO_4 1 M.

in neutral aqueous electrolyte of iron oxide is depicted, along with the performance metrics regarding long-term cycling. We can observe how the potential window is slightly shorter compared to that of manganese, ranging approximately from

-0.4 to -0.5 V vs Ag/AgCl, the peak going over 0.5 V vs Ag/AgCl is hydrogen accumulation on the surface. In terms of specific capacitance, it under performs compared to manganese, resulting in a dutiful balancing of the amount of active material placed on the two current collectors asymmetrically. In this case as well, there are three possible parameters to optimize, namely the geometry of the two current collectors, the depth of the added dendritic layer, and the maximum loading of the material itself. This will enable balancing of the eventual end device.

Although iron oxide shares development and manufacturing techniques, such as photolithography and plating, that are entirely comparable to those of manganese making, and this is a strong point of the material,It is also necessary to consider critical aspects, we observe that Iron Oxide have electrochemical behavior that is initially unstable, stabilizing after the first few cycles. But with loss in performances.

This phenomenon is largely due to a shift in the solution's pH, which increases on the negative side. This shift can lead to the formation of insoluble iron hydroxide, which allows for an increased number of cycles but results in greater resistance to ion transfer, reduced Coulombic and voltaic efficiency, and eventually lead to the cell failure.

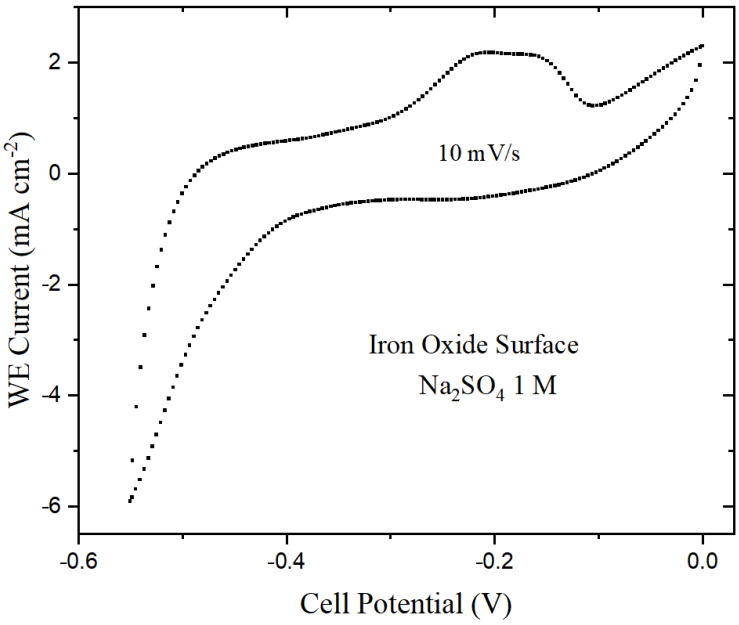

Figure 5.18: Cyclic voltammetry for Iron Oxide Electrode in neutral electrolyte.

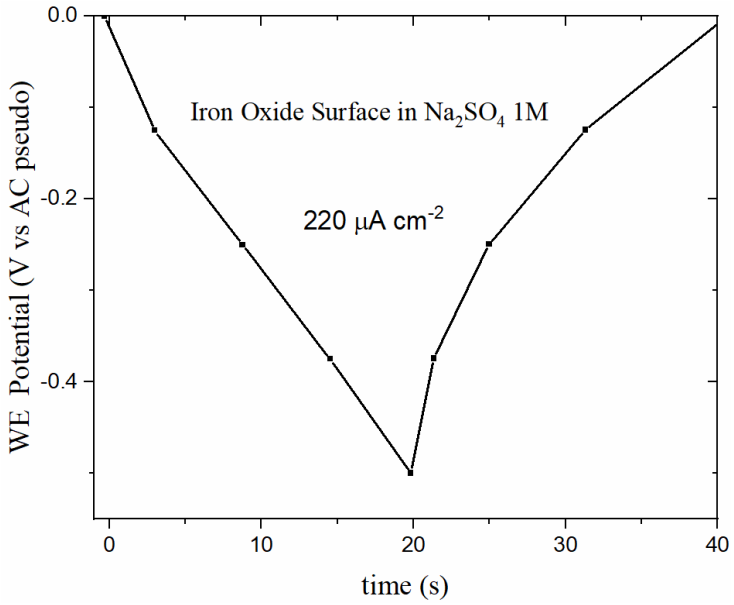

Figure 5.19: GCD curve of the Iron oxide electrode at current density of 220 μAcm^{-2}.

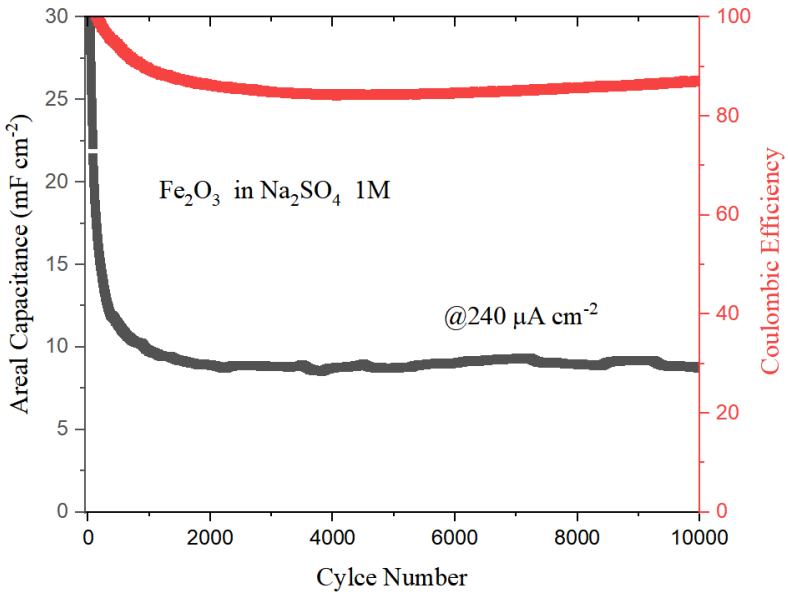

Figure 5.20: Areal capacitance of iron oxide in neutral electrolyte.

On chip Iron Oxide Manganese Oxide on silicon prototype

Metal oxide, like manganese oxide (Mn_2O_3) and iron oxide (Fe_2O_3) and , are promising for their substantial pseudo-capacitance and exceptional electrochemical performance in aqueous-based electrolytes. Our objective with these materials is to augment their energy storage capacity and cycling stability. The silicon substrate furnishes mechanical support and facilitates on-chip application, while the dendritic gold current collector provides a large surface area for effective ion adsorption and desorption at the electrode-electrolyte interface. The metal oxide is applied onto the enhanced gold current collector using a straightforward and economic method electroplating using a solution based on $FeSO_4 \cdot 7H_2O$, pH=3, molar concentration = 0.5 M.

The device was built according to the procedure described in the experimental section. Electrodes were balanced in terms of charge, tuning the mass loading during the electroplating deposition techniques, the positive electrode was charged with 4.6 mg/cm^2 where the negative electrode was charged with 19 mg/cm^2 of Iron, both electrode where charged with 1.8 mg cm^{-2} of dendritic-gold. The planar single interdigitated micro-Supercapacitors was tested with 100 μL of 1 M Na_2SO_4 aqueous electrolyte infiltrated in the glass fiber separator.

The performance of the micro-supercapacitor is assessed through various electrochemical tests, including CV, GCD, and PEIS. The results in fig. 5.21 show that the enhanced micro-supercapacitor with metal oxide materials exhibits significantly improved energy storage performance compared to the device with a flat metal oxide electrode. Fig. 5.23a. Example of single interdigitated micro-supercapacitor. The micro-device exhibits a high specific capacitance over 10 mF cm^{-2}. Moreover, the supercapacitor shows cycling stability with capacitance no negligible capacitance loss after 1000 cycles. This is due to the instability of the iron and probably formation of hydroxide on the surface of the electrode. The hypothesis of miniaturization can be considered successful, the area factor of the device shown in 5.22 compared to the device shown in fig.5.16 has a scaling factor of approximately 10 times in terms of area. This study demonstrates the potential of mixing dendritic current collectors with metal oxide materials can enhance the performance of planar supercapacitors. Concluding, mixing micro-structured current collectors with metal oxides can simplify the operation of area's balancing technique for planar electrochemical cells, designated to the development of on-chip devices with wide operating voltage window, high energy storage capability and efficiency.

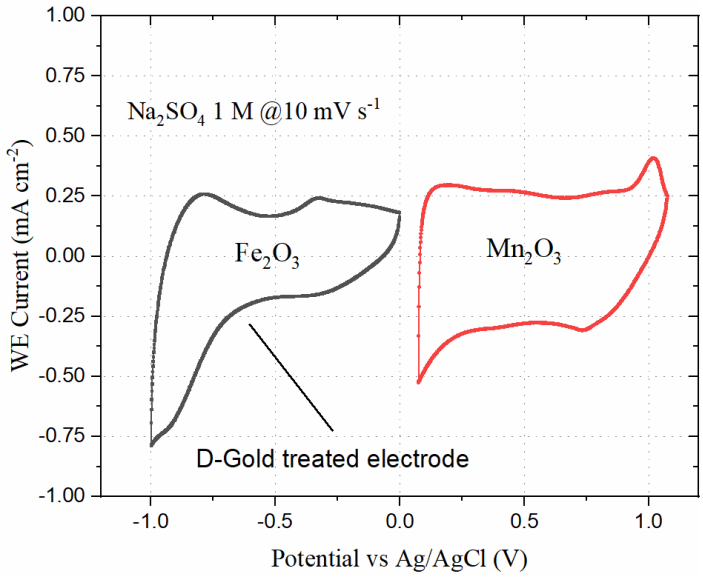

Figure 5.21: CV comparison between Manganes Dioxide and Iron oxide.

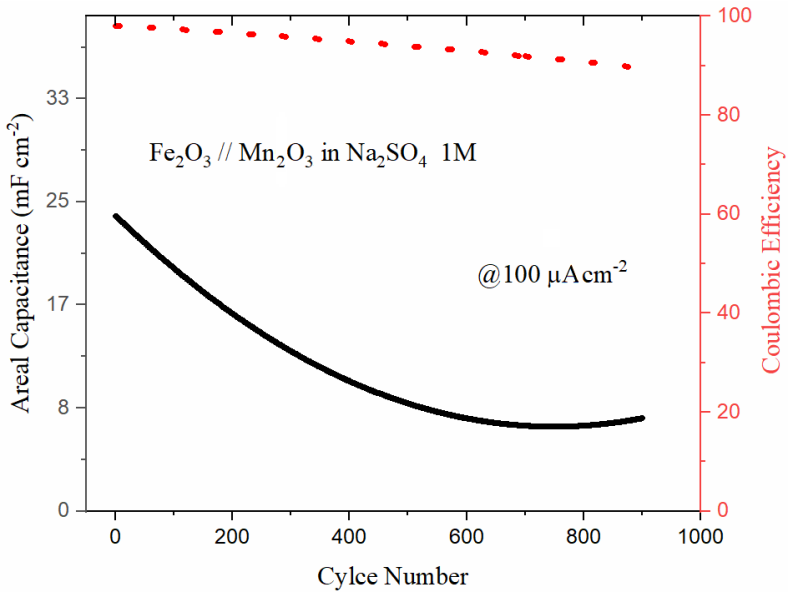

Figure 5.22: Areal capacity behavior as a function of the different cycles for the $Fe_2O_3Mn_2O_3$ hybrid device.

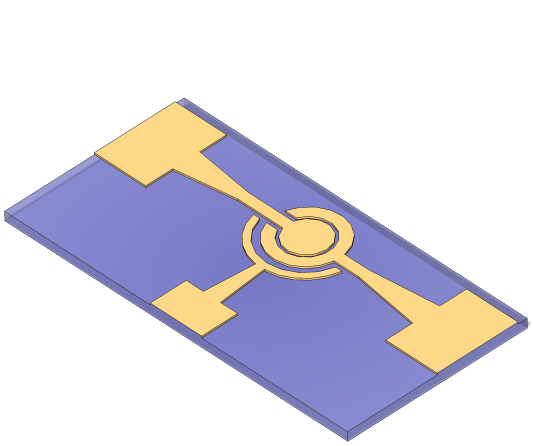

(a) Current collector patterned on silicon wafer

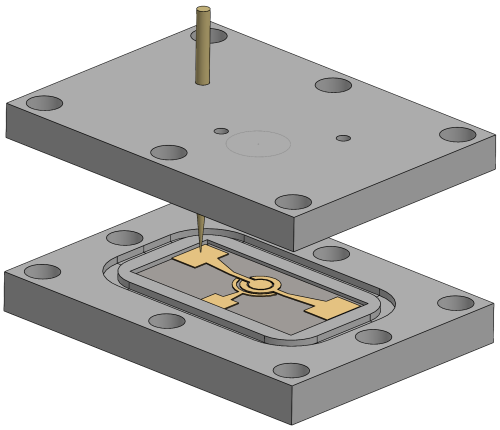

(b) Sketch of the ad ho set up made for the electrochemical measurements

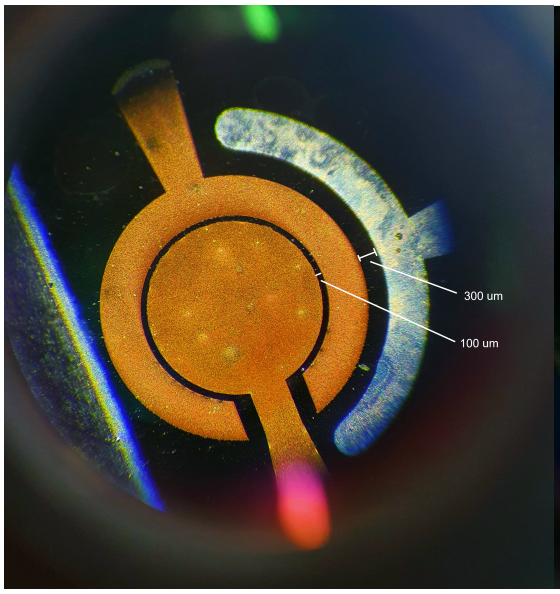

(c) Detail of the micro devices with dendritic gold deposition

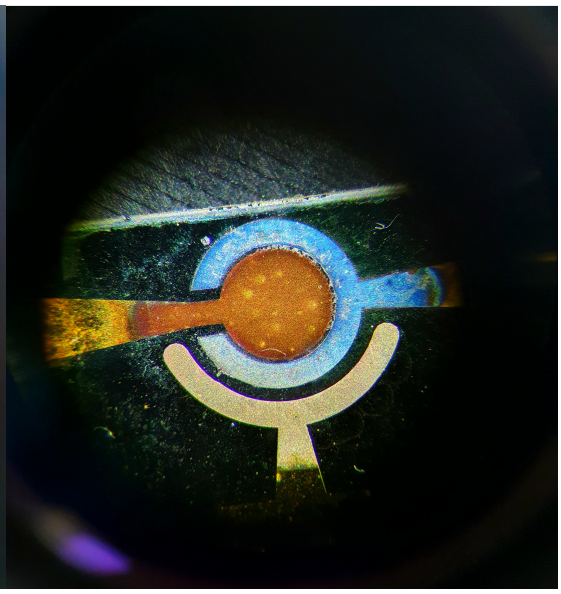

(d) Detail of the device after plating of the iron

Figure 5.23: Micro-Supercap three electrode device.

Chapter 6

Conclusion

The study presented in this work was based on two fundamental initial hypotheses. The first hypothesis aimed to explore the possibility of applying a miniaturization approach, similar to what has been observed in the field of electronics in past years, and which continues to progress towards increasingly stringent challenges. This has led to the development of portable/mobile microelectronics with consequences well known to all. The second hypothesis aimed to demonstrate, as much as possible, that some of the processes involved could adhere to a sustainable research trend. The approach, therefore, focused on researching process compatibility, involving super-capacitive materials that are also sustainable with modern electronic processes.

The initial study focused on material selection and how these materials responded through physical vapor deposition to complex geometries, such as fractal H-tree structures. Subsequently, after patterning our metallic films, electrochemical and electrophoretic deposition techniques were developed on these surfaces, which served as seed layer for current collectors, along with the study of deposition solutions. The processes for loading the active material can be considered entirely green-like, as only low-impact materials were used during the process through the use of an aqueous-based solution. Additionally, the involved materials are easily available in nature, facilitating their sourcing. This is one of the fundamental strengths of this approach is that it will facilitate the transition to sustainable large-scale production. The gold and manganese plating solution on dendritic gold for electrode fabrication was tested and characterized by a mass loading curve. After consolidating the technique, in-depth investigations were conducted, using different analysis techniques physical and electrochemical. Via XPS, Raman, and XRD on the manganese oxide phase, one of the main protagonists of this study, with particular attention to the area covered by the dendritic material. Subsequently, similar devices were defined to those proposed in the literature for direct comparison, but with the aim of improving and making the technology more appealing for substrates and techniques. As mentioned in the initial stages of device development, flexible

substrates were used to facilitate proof of concept demonstration; subsequently, the application was also consolidated on rigid devices. A comprehensive preparation of a flexible and rigid planar micro-hybrid supercapacitor by combining two deposition techniques applied to the same substrate led to a significant improvement in electrode performance. The hybrid capacitor presented, with a negative active carbon composite electrode and a positive manganese oxide-based composite electrode, operates in a neutral aqueous electrolyte. Furthermore, the hybrid capacitor with a negative iron oxide electrode and a positive manganese oxide electrode, operates in a 1 M Na_2SO_4 neutral aqueous electrolyte. Physical analyses were conducted to understand the morphology and quality of the electrode surface. Electrochemical analyses were successfully performed on the dendritic gold electrode, denoting its significant surface enhancement effect. By adding a dendritic gold layer between the current collector and the active material layer, we obtained a roughness factor of approximately 22. A predominant presence of the αMn_2O_3 phase (Bixbyite) was observed. This indicates an improvement in the surface factor by about 400%. We observed that the electrode with the multi-layer electrode could alter the surface behavior after cycling, modifying the slope of the PEIS curve. The final experimental results demonstrate a device with a wide voltage window of 1.6 V in an aqueous-based electrolyte, a surface capacitance of 20 mF cm^{-2}, a lifetime exceeding 1500 cycles, and a stable capacitance retention of over 90%. After developing the flexible device to overcome the physical limitations posed by the colloidal solution, a fully metal-oxide based micro-supercapacitor was fabricated on silicon, involving iron oxide and manganese dioxide. It was found that the tested device has similar performances. However, result are promising but long cycling instability was observed, in these new challenge more caution is needed. Further research efforts are required in this area; not enough tests have been conducted to guarantee long-term use in also disadvantageous and non-ideal situations. Further development need to be conducted in this direction to be certain of future concrete applications. In closing, the aim of this work, namely simplifying the procedures inherently linked to microfabrication, can be considered a necessary step to bring this technology to the level of large-scale production. The original approach proposed in this work, involving eco-friendly processes and low-impact active materials, is considered very promising and impactful.

Future Development

Among the future prospects, undoubtedly, is the adoption of more effective strategies to extend the potential window and consequently the energy stored by the device, reflecting the macro trend of recent years. Today's modern microelectronics processes have extremely low production defect tolerances, so it is necessary to standardize procedures as much as possible to increase reproducibility a factor that is currently also a weakness and requires a high volume of samples produced due

to the complexity and variety of processes adopted. Additionally, entirely in a low-contamination environment, this cannot always be achieved for logistical reasons. This could be realized through partnerships with companies in the sector.

Exploring a solid strategy for different electrolyte confinement, such as using a gel, limiting the use of gold by seeking an alternative, lower-cost metallic element that exhibits dendritic growth, and then using more sophisticated deposition techniques like ALD to perform fine covering of the rough profile obtained, without sacrificing the protective effect of gold, is another aspect that needs to be analyzed due to the complexity and cost of the technique, use alternative natural based substrate, such as cellulose, instead the kapton® that can be dispersed in environment with no risk. These are some choices that could give further boost to this research field on on-chip supercapacitor devices. Finally, the paths we can take in the field of integration are virtually divided into two branches. Namely, moving towards on-chip architecture, where all systems are built on the same substrate, or towards system-in-package, with the latter being more promising due to the fragmentation of technological efforts. This would obviously pave the way concretely for multi-device systems where we find sensors, harvester batteries, data transmission modules, and more..., all coexisting in a single "box".

Lastly, the environmental impact and possible material recovery are aspects that should never be underestimated and require constant development and research. The final considerations, although the devices presented here are a simplified version, can have a significant impact on common usage, making the "human/device" paradigm, once again, the focus of the discussion. Their use involves humans as an integral part of the operation and is seen as both users and power sources, but all this applications can be extend not only for human being but also for other form of life such as plants or animals, to supervise and guarantee biodiversity. Only by approaching future electronics development in this way can we say that we have adopted a research style consistent with the idea of sustainable electronics for IoT. This aspect is now a must and undoubtedly represents the added value of this research.

Bibliography

[1] Sarinn Pech et al. "Ultrahigh-power micrometre-sized supercapacitors based on onion-like carbon." In: *Nature nanotechnology* 5 (Sept. 2010), pp. 651–4. DOI: 10.1038/nnano.2010.162.

[2] Thierry Brousse, Daniel Bélanger, and Jeffrey W. Long. "To Be or Not To Be Pseudocapacitive?" In: *Journal of The Electrochemical Society* 162.5 (Mar. 2015), A5185. DOI: 10.1149/2.0201505jes. URL: https://dx.doi.org/10.1149/2.0201505jes.

[3] Pietro Zaccagnini et al. "Laser-Induced Graphenization of PDMS as Flexible Electrode for Microsupercapacitors." In: *Advanced Materials Interfaces* 8 (23 Dec. 2021), p. 2101046. ISSN: 2196-7350. DOI: 10.1002/admi.202101046.

[4] URL: https://www.britannica.com/science/sustainability.

[5] Jinfang Tian et al. "Global low-carbon energy transition in the post-COVID-19 era." In: *Applied Energy* 307 (Feb. 2022), p. 118205. ISSN: 03062619. DOI: 10.1016/j.apenergy.2021.118205.

[6] Songpu Ai, Antorweep Chakravorty, and Chunming Rong. "Household Power Demand Prediction Using Evolutionary Ensemble Neural Network Pool with Multiple Network Structures." In: *Sensors* 19.3 (2019). ISSN: 1424-8220. DOI: 10.3390/s19030721. URL: https://www.mdpi.com/1424-8220/19/3/721.

[7] Guneet Bedi et al. "Review of Internet of Things (IoT) in Electric Power and Energy Systems." In: *IEEE Internet of Things Journal* 5.2 (2018), pp. 847–870. DOI: 10.1109/JIOT.2018.2802704.

[8] Patrik Söderholm. "The green economy transition: the challenges of technological change for sustainability." In: *Sustainable Earth* 3 (1 Dec. 2020), p. 6. ISSN: 2520-8748. DOI: 10.1186/s42055-020-00029-y.

[9] Alberto Scalia et al. "Tragacanth Gum as Green Binder for Sustainable Water-Processable Electrochemical Capacitor." In: *ChemSusChem* 14 (1 Jan. 2021), pp. 356–362. ISSN: 1864-5631. DOI: 10.1002/cssc.202001754.

[10] Jos F. M. Oudenhoven, Loïc. Baggetto, and Peter H. L. Notten. "All-Solid-State Lithium-Ion Microbatteries: A Review of Various Three-Dimensional Concepts." In: *Advanced Energy Materials* 1.1 (2011), pp. 10–33. DOI: https://doi.org/10.1002/aenm.201000002. URL: https://onlinelibrary.wiley.com/doi/abs/10.1002/aenm.201000002.

[11] Onorato d'Angelis et al. "IoT architecture for continuous long term monitoring: Parkinson's Disease case study." In: *Internet of Things* 20 (2022), p. 100614. ISSN: 2542-6605. DOI: https://doi.org/10.1016/j.iot.2022.100614. URL: https://www.sciencedirect.com/science/article/pii/S2542660522000968.

[12] Alan A. Helal et al. "An integrated solution of software and hardware for environmental monitoring." In: *Internet of Things* 19 (Aug. 2022), p. 100518. ISSN: 25426605. DOI: 10.1016/j.iot.2022.100518.

[13] Yang Wang et al. "Inkjet printing of -MnO2 nanosheets for flexible solid-state micro-supercapacitor." In: *Nano Energy* 49 (July 2018), pp. 481–488. ISSN: 22112855. DOI: 10.1016/j.nanoen.2018.05.002.

[14] P. Simon and Y. Gogotsi. "Perspectives for electrochemical capacitors and related devices." In: *Nature Materials* 19 (Aug. 2020). DOI: 10.1038/s41563-020-0747-z.

[15] S. Trasatti. "Electrochemistry and environment: The role of electrocatalysis." In: *International Journal of Hydrogen Energy* 20.10 (1995), pp. 835–844. ISSN: 0360-3199. DOI: https://doi.org/10.1016/0360-3199(95)00014-5. URL: https://www.sciencedirect.com/science/article/pii/0360319995000145.

[16] John Miller and Andrew Burke. "Electrochemical Capacitors: Challenges and Opportunities for Real-World Applications." In: *The Electrochemical Society Interface* 17 (Mar. 2008), pp. 53–57. DOI: 10.1149/2.F08081IF.

[17] Jarkko Hyysalo et al. "Smart mask – Wearable IoT solution for improved protection and personal health." In: *Internet of Things* 18 (2022), p. 100511. ISSN: 2542-6605. DOI: https://doi.org/10.1016/j.iot.2022.100511. URL: https://www.sciencedirect.com/science/article/pii/S2542660522000166.

[18] GiriBabu Sinnapolu and Shadi Alawneh. "Intelligent wearable heart rate sensor implementation for in-vehicle infotainment and assistance." In: *Internet of Things* 12 (Dec. 2020), p. 100277. ISSN: 25426605. DOI: 10.1016/j.iot.2020.100277.

[19] Amjid Rafique et al. "Binder Free and Flexible Asymmetric Supercapacitor Exploiting Mn3O4 and MoS2 Nanoflakes on Carbon Fibers." In: *Nanomaterials* 10.6 (2020). ISSN: 2079-4991. DOI: 10.3390/nano10061084. URL: https://www.mdpi.com/2079-4991/10/6/1084.

[20] Jos F. M. Oudenhoven, Loïc. Baggetto, and Peter H. L. Notten. "All-Solid-State Lithium-Ion Microbatteries: A Review of Various Three-Dimensional Concepts." In: *Advanced Energy Materials* 1 (1 Jan. 2011), pp. 10–33. ISSN: 16146832. DOI: 10.1002/aenm.201000002.

[21] Vinsensia Ade Sugiawati et al. "Direct Pre-lithiation of Electropolymerized Carbon Nanotubes for Enhanced Cycling Performance of Flexible Li-Ion Micro-Batteries." In: *Polymers* 12 (2 Feb. 2020), p. 406. ISSN: 2073-4360. DOI: 10.3390/polym12020406.

[22] Anju Toor et al. "Stencil-printed Lithium-ion micro batteries for IoT applications." In: *Nano Energy* 82 (2021), p. 105666. ISSN: 2211-2855. DOI: https://doi.org/10.1016/j.nanoen.2020.105666. URL: https://www.sciencedirect.com/science/article/pii/S2211285520312398.

[23] Thibaud Guillemin et al. "Solid-state 3D micro-supercapacitors based on ionogel electrolyte: Influence of adding lithium and sodium salts to the ionic liquid." In: *Energy Storage Materials* 50 (2022), pp. 606–617. ISSN: 2405-8297. DOI: https://doi.org/10.1016/j.ensm.2022.05.041. URL: https://www.sciencedirect.com/science/article/pii/S2405829722002926.

[24] Alberto Scalia et al. "Electrolytes based on N-Butyl-N-Methyl-Pyrrolidinium 4,5-Dicyano-2-(Trifluoromethyl) Imidazole for High Voltage Electrochemical Double Layer Capacitors." In: *ChemElectroChem* 6.2 (2019), pp. 552–557. DOI: https://doi.org/10.1002/celc.201801172. URL: https://chemistry-europe.onlinelibrary.wiley.com/doi/abs/10.1002/celc.201801172.

[25] B. E. Conway. *Electrochemical Capacitors Based on Pseudocapacitance*. 1999. DOI: 10.1007/978-1-4757-3058-6_10.

[26] S. W. Zhang and G. Z. Chen. "Manganese oxide based materials for supercapacitors." In: *Energy Materials* 3.3 (2008), pp. 186–200. DOI: 10.1179/174892409X427940. URL: https://doi.org/10.1179/174892409X427940.

[27] Min-Kyu Song et al. "Anomalous Pseudocapacitive Behavior of a Nanostructured, Mixed-Valent Manganese Oxide Film for Electrical Energy Storage." In: *Nano Letters* 12 (7 July 2012), pp. 3483–3490. ISSN: 1530-6984. DOI: 10.1021/nl300984y.

[28] Veronica Augustyn, Patrice Simon, and Bruce Dunn. "Pseudocapacitive oxide materials for high-rate electrochemical energy storage." In: *Energy Environ. Sci.* 7 (5 2014), pp. 1597–1614. DOI: 10.1039/C3EE44164D. URL: http://dx.doi.org/10.1039/C3EE44164D.

[29] M. J. N. Pourbaix. "Atlas of Electrochemical Equilibria in Aqueous Solutions." In: (1974). URL: https://api.semanticscholar.org/CorpusID:93126068.

[30] Pietro Pedeferri (Deceased). "Pourbaix Diagrams." In: *Corrosion Science and Engineering*. Cham: Springer International Publishing, 2018, pp. 57–72. ISBN: 978-3-319-97625-9. DOI: 10.1007/978-3-319-97625-9_4. URL: https://doi.org/10.1007/978-3-319-97625-9_4.

[31] Peter Wilkinson. "Understanding gold plating." In: *Gold Bulletin* 19 (1986), pp. 75–81. URL: https://api.semanticscholar.org/CorpusID:135489836.

[32] P. Simon and Yury Gogotsi. "Materials for Electrochemical Capacitors." In: *Nature materials* 7 (Dec. 2008), pp. 845–54. DOI: 10.1038/nmat2297.

[33] Bouchra Asbani et al. "Asymmetric micro-supercapacitors based on electrodeposited Ruo2 and sputtered VN films." In: *Energy Storage Materials* 37 (2021), pp. 207–214. ISSN: 2405-8297. DOI: https://doi.org/10.1016/j.ensm.2021.02.006. URL: https://www.sciencedirect.com/science/article/pii/S2405829721000490.

[34] A.J. Paleo et al. "Lifetime assessment of solid-state hybrid supercapacitors based on cotton fabric electrodes." In: *Journal of Power Sources* 434 (Sept. 2019), p. 226735. ISSN: 03787753. DOI: 10.1016/j.jpowsour.2019.226735.

[35] Mara Serrapede et al. "Fiber-shaped asymmetric supercapacitor exploiting rGO/Fe2O3 aerogel and electrodeposited MnOx nanosheets on carbon fibers." In: *Carbon* 144 (Apr. 2019), pp. 91–100. ISSN: 00086223. DOI: 10.1016/j.carbon.2018.12.002.

[36] Kyung-Wan Nam et al. "Electrodeposited manganese oxides on three-dimensional carbon nanotube substrate: Supercapacitive behaviour in aqueous and organic electrolytes." In: *Journal of Power Sources* 188 (1 Mar. 2009), pp. 323–331. ISSN: 03787753. DOI: 10.1016/j.jpowsour.2008.11.133.

[37] Myoung Shin Hong, Seok Hyun Lee, and Sun Wook Kim. "Use of KCl Aqueous Electrolyte for 2 V Manganese Oxide/Activated Carbon Hybrid Capacitor." In: *Electrochemical and Solid-State Letters* 5 (10 2002), A227. ISSN: 10990062. DOI: 10.1149/1.1506463.

[38] Silvana Dimitrijevic, Mirjana Rajčić-Vujasinović, and V. Trujic. "Non-Cyanide Electrolytes for Gold Plating - A Review." In: *International journal of electrochemical science* 8 (May 2013), pp. 6620–6646.

[39] Zuozhao Zhai et al. "A review of carbon materials for supercapacitors." In: *Materials & Design* 221 (2022), p. 111017. ISSN: 0264-1275. DOI: https://doi.org/10.1016/j.matdes.2022.111017. URL: https://www.sciencedirect.com/science/article/pii/S0264127522006396.

[40] Alireza Cheraghi, Hossein Yoozbashizadeh, and Jafar Safarian. "Gaseous Reduction of Manganese Ores: A Review and Theoretical Insight." In: *Mineral Processing and Extractive Metallurgy Review* (Aug. 2019). DOI: 10.1080/08827508.2019.1604523.

[41] Thomas Cottineau et al. "Nanostructured Transition Metal Oxides for Aqueous Hybrid Electrochemical Supercapacitors." In: *Applied Physics A* 82 (Mar. 2006), pp. 599–606. DOI: 10.1007/s00339-005-3401-3.

[42] Jie Chen, Kelong Huang, and Suqin Liu. "Hydrothermal preparation of octadecahedron Fe3O4 thin film for use in an electrochemical supercapacitor." In: *Electrochimica Acta* 55.1 (2009), pp. 1–5. ISSN: 0013-4686. DOI: https://doi.org/10.1016/j.electacta.2009.04.017. URL: https://www.sciencedirect.com/science/article/pii/S0013468609005179.

[43] Thi Ngoc Nga Dau et al. "In-situ electrochemically deposited Fe3O4 nanoparticles onto graphene nanosheets as amperometric amplifier for electrochemical biosensing applications." In: *Sensors and Actuators B: Chemical* 283 (2019), pp. 52–60. ISSN: 0925-4005. DOI: https://doi.org/10.1016/j.snb.2018.11.152. URL: https://www.sciencedirect.com/science/article/pii/S0925400518321087.

[44] Sagar Mitra et al. "Growth and Electrochemical Characterization versus Lithium of Fe3O4 Electrodes Made by Electrodeposition." In: *Advanced Functional Materials* 16 (Nov. 2006), pp. 2281–2287. DOI: 10.1002/adfm.200500753.

[45] URL: https://www.dupont.com/electronics-industrial/kapton-polyimide-film.html.

[46] Andrea Balducci and Lars Henning Heß. "The impact of carbonate solvents on the self-discharge, thermal stability and performance retention of high voltage electrochemical double layer capacitors." In: *Physical chemistry chemical physics : PCCP* 21 (2019). DOI: 10.1039/C9CP00483A.

[47] Lars H. Hess and Andrea Balducci. "1,2-butylene carbonate as solvent for EDLCs." In: *Electrochimica Acta* 281 (Aug. 2018), pp. 437–444. ISSN: 00134686. DOI: 10.1016/j.electacta.2018.05.168.

[48] A. Krause et al. "Electrochemical double layer capacitor and lithium-ion capacitor based on carbon black." In: *Journal of Power Sources* 196 (20 Oct. 2011), pp. 8836–8842. ISSN: 03787753. DOI: 10.1016/j.jpowsour.2011.06.019.

[49] Simon Fleischmann et al. "Continuous transition from double-layer to Faradaic charge storage in confined electrolytes." In: *Nature Energy* 7 (Mar. 2022), pp. 1–7. DOI: 10.1038/s41560-022-00993-z.

[50] Mathieu Toupin, Thierry Brousse, and Daniel Bélanger. "Influence of Microstucture on the Charge Storage Properties of Chemically Synthesized Manganese Dioxide." In: *Chemistry of Materials* 14 (9 Sept. 2002), pp. 3946–3952. ISSN: 0897-4756. DOI: 10.1021/cm020408q.

[51] Kyung-Wan Nam et al. "Electrodeposited manganese oxides on three-dimensional carbon nanotube substrate: Supercapacitive behaviour in aqueous and organic electrolytes." In: *Journal of Power Sources* 188.1 (2009), pp. 323–331. ISSN: 0378-7753. DOI: https://doi.org/10.1016/j.jpowsour.2008.11.133. URL: https://www.sciencedirect.com/science/article/pii/S0378775308022805.

[52] Mathieu Toupin, Thierry Brousse, and Daniel Bélanger. "Charge Storage Mechanism of MnO ₂ Electrode Used in Aqueous Electrochemical Capacitor." In: *Chemistry of Materials* 16 (16 Aug. 2004), pp. 3184–3190. ISSN: 0897-4756. DOI: 10.1021/cm049649j.

[53] Muhammad Atiq Ur Rehman et al. "Electrophoretic deposition of carbon nanotubes: recent progress and remaining challenges." In: *International Materials Reviews* 66 (Oct. 2020). DOI: 10.1080/09506608.2020.1831299.

[54] R. W. Powers. "The Electrophoretic Forming of Beta-Alumina Ceramic." In: *Journal of The Electrochemical Society* 122.4 (Apr. 1975), p. 490. DOI: 10.1149/1.2134246. URL: https://dx.doi.org/10.1149/1.2134246.

[55] H. C. Hamaker. "Formation of a deposit by electrophoresis." In: *Trans. Faraday Soc.* 35 (0 1940), pp. 279–287. DOI: 10.1039/TF9403500279. URL: http://dx.doi.org/10.1039/TF9403500279.

[56] H. Koelmans and J. Th. G. Overbeek. "Stability and electrophoretic deposition of suspensions in non-aqueous media." In: *Discussions of The Faraday Society* 18 (1954), pp. 52–63. URL: https://api.semanticscholar.org/CorpusID:97040837.

[57] François Grillon, Dominique Michel Maur Fayeulle, and Michel Jeandin. "Quantitative image analysis of electrophoretic coatings." In: *Journal of Materials Science Letters* 11 (1992), pp. 272–275. URL: https://api.semanticscholar.org/CorpusID:135875545.

[58] Masaru Shimbo et al. "Electrophoretic Deposition of Glass Powder for Passivation of High Voltage Transistors." In: *Journal of The Electrochemical Society* 132 (1985), pp. 393–398. URL: https://api.semanticscholar.org/CorpusID:97100993.

[59] Jin Mizuguchi, Koichiro Sumi, and Tsuneo Muchi. "A Highly Stable Nonaqueous Suspension for the Electrophoretic Deposition of Powdered Substances." In: *Journal of The Electrochemical Society* 130 (1983), pp. 1819–1825. URL: https://api.semanticscholar.org/CorpusID:96918747.

[60] Partho Sarkar and Patrick S. Nicholson. "Electrophoretic Deposition (EPD): Mechanisms, Kinetics, and Application to Ceramics." In: *Journal of the American Ceramic Society* 79.8 (1996), pp. 1987–2002. DOI: https://doi.org/10.1111/j.1151-2916.1996.tb08929.x. URL: https://ceramics.onlinelibrary.wiley.com/doi/abs/10.1111/j.1151-2916.1996.tb08929.x.

[61] Fikri Erdem Sesen. "Practical reduction of manganese oxide." In: *Journal of Chemical Technology and Applications* 01 (01 2017). DOI: 10.35841/chemical-technology.1.1.26-27.

[62] L. J. van der PAUW. "A METHOD OF MEASURING SPECIFIC RESISTIVITY AND HALL EFFECT OF DISCS OF ARBITRARY SHAPE." In: *Semiconductor Devices: Pioneering Papers* (Mar. 1991), pp. 174–182. DOI: 10.1142/9789814503464_0017.

[63] Marcin Wojdyr. "Fityk : a general-purpose peak fitting program." In: *Journal of Applied Crystallography* 43 (5 Oct. 2010), pp. 1126–1128. ISSN: 0021-8898. DOI: 10.1107/S0021889810030499.

[64] Sanliang Zhang and Ning Pan. "Supercapacitors Performance Evaluation." In: *Advanced Energy Materials* 5.6 (2015), p. 1401401. DOI: https://doi.org/10.1002/aenm.201401401. URL: https://onlinelibrary.wiley.com/doi/abs/10.1002/aenm.201401401.

[65] Mark C. Biesinger et al. "Resolving surface chemical states in XPS analysis of first row transition metals, oxides and hydroxides: Cr, Mn, Fe, Co and Ni." In: *Applied Surface Science* 257 (7 Jan. 2011), pp. 2717–2730. ISSN: 01694332. DOI: 10.1016/j.apsusc.2010.10.051.

[66] Masaya Chigane and Masami Ishikawa. "Manganese Oxide Thin Film Preparation by Potentiostatic Electrolyses and Electrochromism." In: *Journal of The Electrochemical Society* 147 (6 2000), p. 2246. ISSN: 00134651. DOI: 10.1149/1.1393515.

[67] V. R. Galakhov et al. "Mn 3s exchange splitting in mixed-valence manganites." In: *Physical Review B* 65 (11 Feb. 2002), p. 113102. ISSN: 0163-1829. DOI: 10.1103/PhysRevB.65.113102.

[68] V. Di Castro and G. Polzonetti. "XPS study of MnO oxidation." In: *Journal of Electron Spectroscopy and Related Phenomena* 48 (1 Jan. 1989), pp. 117–123. ISSN: 03682048. DOI: 10.1016/0368-2048(89)80009-X.

[69] Ming Sun et al. "Controlled synthesis of nanostructured manganese oxide: crystalline evolution and catalytic activities." In: *CrystEngComm* 15 (35 2013), p. 7010. ISSN: 1466-8033. DOI: 10.1039/c3ce40603b.

[70] Yanqing Xin et al. "A systematic spectroscopic study of laboratory synthesized manganese oxides relevant to Mars." In: *Journal of Raman Spectroscopy* 53 (3 Mar. 2022), pp. 340–355. ISSN: 0377-0486. DOI: 10.1002/jrs.6231.

[71] Lauren M. Garten et al. "Phase formation of manganese oxide thin films using pulsed laser deposition." In: *Materials Advances* 2 (1 2021), pp. 303–309. ISSN: 2633-5409. DOI: 10.1039/D0MA00417K.

[72] Alejandra Ramirez Caro et al. "Evaluation of MnOx, Mn2O3, and Mn3O4 Electrodeposited Films for the Oxygen Evolution Reaction of Water." In: *The Journal of Physical Chemistry C* 118 (June 2014), pp. 14073–14081. DOI: 10.1021/jp500939d.

[73] M. Karuppaiah et al. "Solvent dependent morphological modification of micro-nano assembled Mn2O3/NiO composites for high performance supercapacitor applications." In: *Ceramics International* 45 (4 Mar. 2019), pp. 4298–4307. ISSN: 02728842. DOI: 10.1016/j.ceramint.2018.11.104.

[74] Taher Yousefi et al. "Synthesis, characterization, and supercapacitor studies of manganese (IV) oxide nanowires." In: *Materials Science in Semiconductor Processing* 16.3 (2013), pp. 868–876. ISSN: 1369-8001. DOI: https://doi.org/10.1016/j.mssp.2013.01.012. URL: https://www.sciencedirect.com/science/article/pii/S1369800113000218.

[75] Qurat-ul-ain Javed et al. "Canted antiferromagnetic and optical properties of nanostructures of Mn2O3 prepared by hydrothermal synthesis." In: *Chinese Physics B* 21 (11 Nov. 2012), p. 117311. ISSN: 1674-1056. DOI: 10.1088/1674-1056/21/11/117311.

[76] D.A.J. Rand and R. Woods. "The nature of adsorbed oxygen on rhodium, palladium and gold electrodes." In: *Journal of Electroanalytical Chemistry and Interfacial Electrochemistry* 31 (1 June 1971), pp. 29–38. ISSN: 00220728. DOI: 10.1016/S0022-0728(71)80039-6.

[77] Anaïs Ferris et al. "3D Interdigitated Microsupercapacitors with Record Areal Cell Capacitance." In: *Small* 15 (27 July 2019), p. 1901224. ISSN: 1613-6810. DOI: 10.1002/smll.201901224.

[78] Nishuang Liu and Yihua Gao. "Recent Progress in Micro-Supercapacitors with In-Plane Interdigital Electrode Architecture." In: *Small* 13 (45 Dec. 2017), p. 1701989. ISSN: 16136810. DOI: 10.1002/smll.201701989.

[79] Davide Arcoraci et al. "Enhancing the performance and mechanical stability of 2D-based hybrid micro-supercapacitors using dendritic-gold as framework layer." In: *Electrochimica Acta* 453 (2023), p. 142346. ISSN: 0013-4686. DOI: https://doi.org/10.1016/j.electacta.2023.142346. URL: https://www.sciencedirect.com/science/article/pii/S0013468623005248.

[80] Deepak P. Dubal et al. "3D hierarchical assembly of ultrathin MnO2 nanoflakes on silicon nanowires for high performance micro-supercapacitors in Li- doped ionic liquid." In: *Scientific Reports* 5 (1 Sept. 2015), p. 9771. ISSN: 2045-2322. DOI: 10.1038/srep09771.

[81] Wen-Wen Liu et al. "Superior Micro-Supercapacitors Based on Graphene Quantum Dots." In: *Advanced Functional Materials* 23 (33 Sept. 2013), pp. 4111–4122. ISSN: 1616301X. DOI: 10.1002/adfm.201203771.

[82] Shuijian He et al. "Al/C/MnO2 sandwich nanowalls with highly porous surface for electrochemical energy storage." In: *Journal of Power Sources* 299 (Dec. 2015), pp. 408–416. ISSN: 03787753. DOI: 10.1016/j.jpowsour.2015.09.029.

[83] Haibo Hu et al. "3D Interdigital Au/MnO2 /Au Stacked Hybrid Electrodes for On-Chip Microsupercapacitors." In: *Small* 12 (22 June 2016), pp. 3059–3069. ISSN: 16136810. DOI: 10.1002/smll.201503527.

[84] R.-Z. Li et al. "High-rate in-plane micro-supercapacitors scribed onto photo paper using in situ femtolaser-reduced graphene oxide/Au nanoparticle microelectrodes." In: *Energy & Environmental Science* 9 (4 2016), pp. 1458–1467. ISSN: 1754-5692. DOI: 10.1039/C5EE03637B.

[85] Jieqiong Qin et al. "2D mesoporous MnO2 nanosheets for high-energy asymmetric micro-supercapacitors in water-in-salt gel electrolyte." In: *Energy Storage Materials* 18 (Mar. 2019), pp. 397–404. ISSN: 24058297. DOI: 10.1016/j.ensm.2018.12.022.

[86] Buddha Deka Boruah, Arnab Maji, and Abha Misra. "Flexible Array of Microsupercapacitor for Additive Energy Storage Performance Over a Large Area." In: *ACS Applied Materials and Interfaces* 10 (18 May 2018), pp. 15864–15872. ISSN: 1944-8244. DOI: 10.1021/acsami.8b02660.

[87] Fan Xia et al. "On-Chip High-Power Supply Unit: Micro Supercapacitor With Superb Capacitance Density and Fast Charge/Discharge Ability." In: *IEEE Electron Device Letters* 42 (4 Apr. 2021), pp. 625–628. ISSN: 0741-3106. DOI: 10.1109/LED.2021.3063474.

[88] Bouchra Asbani et al. "Asymmetric micro-supercapacitors based on electrodeposited Ruo2 and sputtered VN films." In: *Energy Storage Materials* 37 (May 2021), pp. 207–214. ISSN: 24058297. DOI: 10.1016/j.ensm.2021.02.006.

[89] Alan A. Helal et al. "An integrated solution of software and hardware for environmental monitoring." In: *Internet of Things* 19 (2022), p. 100518. ISSN: 2542-6605. DOI: https://doi.org/10.1016/j.iot.2022.100518. URL: https://www.sciencedirect.com/science/article/pii/S254266052200021X.

[90] GiriBabu Sinnapolu and Shadi Alawneh. "Intelligent wearable heart rate sensor implementation for in-vehicle infotainment and assistance." In: *Internet of Things* 12 (2020), p. 100277. ISSN: 2542-6605. DOI: https://doi.org/10.1016/j.iot.2020.100277. URL: https://www.sciencedirect.com/science/article/pii/S2542660520301104.

[91] GiriBabu Sinnapolu and Shadi Alawneh. "Integrating wearables with cloud-based communication for health monitoring and emergency assistance." In: *Internet of Things* 1-2 (2018), pp. 40–54. ISSN: 2542-6605. DOI: https://doi.org/10.1016/j.iot.2018.08.004. URL: https://www.sciencedirect.com/science/article/pii/S2542660518300404.

[92] Pietro Zaccagnini et al. "Laser-Induced Graphenization of PDMS as Flexible Electrode for Microsupercapacitors." In: *Advanced Materials Interfaces* 8.23 (2021), p. 2101046. DOI: https://doi.org/10.1002/admi.202101046. URL: https://onlinelibrary.wiley.com/doi/abs/10.1002/admi.202101046.

[93] Lu Yin and Joseph Wang. "Wearable energy systems: what are the limits and limitations?" In: *National Science Review* 10.1 (Mar. 2022), nwac060. ISSN: 2095-5138. DOI: 10.1093/nsr/nwac060. URL: https://doi.org/10.1093/nsr/nwac060.

[94] Vinsensia Ade Sugiawati et al. "Direct Pre-lithiation of Electropolymerized Carbon Nanotubes for Enhanced Cycling Performance of Flexible Li-Ion Micro-Batteries." In: *Polymers* 12.2 (2020). ISSN: 2073-4360. DOI: 10.3390/polym12020406. URL: https://www.mdpi.com/2073-4360/12/2/406.

[95] Brian E. Conway. *Electrochemical Supercapacitors*. Springer New York, NY, 1999.

[96] Jinfang Tian et al. "Global low-carbon energy transition in the post-COVID-19 era." In: *Applied Energy* 307 (2022), p. 118205. ISSN: 0306-2619. DOI: https://doi.org/10.1016/j.apenergy.2021.118205. URL: https://www.sciencedirect.com/science/article/pii/S0306261921014720.

[97] Patrik Söderholm. "The green economy transition: the challenges of technological change for sustainability." In: *Sustainable Earth* 3 (June 2020). DOI: 10.1186/s42055-020-00029-y.

[98] Qi Kang et al. "A single wire as all-inclusive fully functional supercapacitor." In: *Nano Energy* 32 (2017), pp. 201–208. ISSN: 2211-2855. DOI: https://doi.org/10.1016/j.nanoen.2016.12.020. URL: https://www.sciencedirect.com/science/article/pii/S2211285516305857.

[99] A. Krause et al. "Electrochemical double layer capacitor and lithium-ion capacitor based on carbon black." In: *Journal of Power Sources* 196.20 (2011), pp. 8836–8842. ISSN: 0378-7753. DOI: https://doi.org/10.1016/j.jpowsour.2011.06.019. URL: https://www.sciencedirect.com/science/article/pii/S0378775311011311.

[100] A.J. Paleo et al. "Lifetime assessment of solid-state hybrid supercapacitors based on cotton fabric electrodes." In: *Journal of Power Sources* 434 (2019), p. 226735. ISSN: 0378-7753. DOI: https://doi.org/10.1016/j.jpowsour.2019.226735. URL: https://www.sciencedirect.com/science/article/pii/S0378775319307062.

[101] Mara Serrapede et al. "Fiber-shaped asymmetric supercapacitor exploiting rGO/Fe2O3 aerogel and electrodeposited MnOx nanosheets on carbon fibers." In: *Carbon* 144 (2019), pp. 91–100. ISSN: 0008-6223. DOI: https://doi.org/10.1016/j.carbon.2018.12.002. URL: https://www.sciencedirect.com/science/article/pii/S0008622318311217.

[102] Aldo R. Boccaccini et al. "Electrophoretic deposition of carbon nanotubes." In: *Carbon* 44.15 (2006), pp. 3149–3160. ISSN: 0008-6223. DOI: https://doi.org/10.1016/j.carbon.2006.06.021. URL: https://www.sciencedirect.com/science/article/pii/S0008622306003502.

[103] Mohammad Mahmudul Huq, Chien-Te Hsieh, and Chia-Yin Ho. "Preparation of carbon nanotube-activated carbon hybrid electrodes by electrophoretic deposition for supercapacitor applications." In: *Diamond and Related Materials* 62 (2016), pp. 58–64. ISSN: 0925-9635. DOI: https://doi.org/10.1016/j.diamond.2015.12.014. URL: https://www.sciencedirect.com/science/article/pii/S092596351530114X.

[104] Taeuk Kim, Seong-Hoon Yi, and Sang-Eun Chun. "Electrophoretic deposition of a supercapacitor electrode of activated carbon onto an indium-tin-oxide substrate using ethyl cellulose as a binder." In: *Journal of Materials Science & Technology* 58 (2020), pp. 188–196. ISSN: 1005-0302. DOI: https://doi.org/10.1016/j.jmst.2020.03.072. URL: https://www.sciencedirect.com/science/article/pii/S1005030220304837.

[105] Renpeng Yu et al. "Overcurrent Electrodeposition of Fractal Plasmonic Black Gold with Broad-Band Absorption Properties for Excitation-Immune SERS." In: *ACS Omega* 5.14 (2020). PMID: 32309740, pp. 8293–8298. DOI: 10.1021/acsomega.0c00698. URL: https://doi.org/10.1021/acsomega.0c00698.

[106] Amjid Rafique et al. "Binder Free and Flexible Asymmetric Supercapacitor Exploiting Mn3O4 and MoS2 Nanoflakes on Carbon Fibers." In: *Nanomaterials* 10 (6 May 2020), p. 1084. ISSN: 2079-4991. DOI: 10.3390/nano10061084.

[107] Taeuk Kim, Seong-Hoon Yi, and Sang-Eun Chun. "Electrophoretic deposition of a supercapacitor electrode of activated carbon onto an indium-tin-oxide substrate using ethyl cellulose as a binder." In: *Journal of Materials Science & Technology* 58 (Dec. 2020), pp. 188–196. ISSN: 10050302. DOI: 10.1016/j.jmst.2020.03.072.

[108] Mohammad Mahmudul Huq, Chien-Te Hsieh, and Chia-Yin Ho. "Preparation of carbon nanotube-activated carbon hybrid electrodes by electrophoretic deposition for supercapacitor applications." In: *Diamond and Related Materials* 62 (Feb. 2016), pp. 58–64. ISSN: 09259635. DOI: 10.1016/j.diamond.2015.12.014.

[109] Aldo R. Boccaccini et al. "Electrophoretic deposition of carbon nanotubes." In: *Carbon* 44 (15 Dec. 2006), pp. 3149–3160. ISSN: 00086223. DOI: 10.1016/j.carbon.2006.06.021.

[110] Amjid Rafique et al. "Highly Uniform Anodically Deposited Film of MnO2 Nanoflakes on Carbon Fibers for Flexible and Wearable Fiber-Shaped Supercapacitors." In: *ACS Applied Materials and Interfaces* 9 (34 Aug. 2017), pp. 28386–28393. ISSN: 1944-8244. DOI: 10.1021/acsami.7b06311.

[111] S. W. Zhang and G. Z. Chen. "Manganese oxide based materials for supercapacitors." In: *Energy Materials* 3 (3 Sept. 2008), pp. 186–200. ISSN: 1748-9237. DOI: 10.1179/174892409X427940.

[112] Pietro Zaccagnini and Andrea Lamberti. "A perspective on laser-induced graphene for micro-supercapacitor application." In: *Applied Physics Letters* 120 (10 Mar. 2022), p. 100501. ISSN: 0003-6951. DOI: 10.1063/5.0078707.

[113] H. Keiser, K.D. Beccu, and M.A. Gutjahr. "Abschätzung der porenstruktur poröser elektroden aus impedanzmessungen." In: *Electrochimica Acta* 21 (8 Aug. 1976), pp. 539–543. ISSN: 00134686. DOI: 10.1016/0013-4686(76)85147-X.

[114] Hasimur Rahaman et al. "Fabrication of Mn2O3 nanorods: an efficient catalyst for selective transformation of alcohols to aldehydes." In: *RSC Advances* 5 (43 2015), pp. 33923–33929. ISSN: 2046-2069. DOI: 10.1039/C5RA02504D.

[115] Z.W. Chen, J.K.L. Lai, and C.H. Shek. "Influence of grain size on the vibrational properties in Mn2O3 nanocrystals." In: *Journal of Non-Crystalline Solids* 352 (30-31 Sept. 2006), pp. 3285–3289. ISSN: 00223093. DOI: 10.1016/j.jnoncrysol.2006.04.011.

[116] Guneet Bedi et al. "Review of Internet of Things (IoT) in Electric Power and Energy Systems." In: *IEEE Internet of Things Journal* 5 (2 Apr. 2018), pp. 847–870. ISSN: 2327-4662. DOI: 10.1109/JIOT.2018.2802704.

[117] Songpu Ai, Antorweep Chakravorty, and Chunming Rong. "Household Power Demand Prediction Using Evolutionary Ensemble Neural Network Pool with Multiple Network Structures." In: *Sensors* 19 (3 Feb. 2019), p. 721. ISSN: 1424-8220. DOI: 10.3390/s19030721.

[118] Alejandra Ramirez Caro et al. "Evaluation of MnOx, Mn2O3, and Mn3O4 Electrodeposited Films for the Oxygen Evolution Reaction of Water." In: *The Journal of Physical Chemistry C* 118 (June 2014), pp. 14073–14081. DOI: 10.1021/jp500939d.

[119] Wei Chen et al. "Facile synthesis of manganite nanowires: phase transitions and their electrocatalysis performance." In: *Nanotechnology* 20 (44 Nov. 2009), p. 445601. ISSN: 0957-4484. DOI: 10.1088/0957-4484/20/44/445601.

[120] D. Jarosch. "Crystal structure refinement and reflectance measurements of hausmannite, Mn3O4." In: *Mineralogy and Petrology* 37 (1 Aug. 1987), pp. 15–23. ISSN: 0930-0708. DOI: 10.1007/BF01163155.

[121] Sujit Kumar Ghosh. "Diversity in the Family of Manganese Oxides at the Nanoscale: From Fundamentals to Applications." In: *ACS Omega* 5 (40 Oct. 2020), pp. 25493–25504. ISSN: 2470-1343. DOI: 10.1021/acsomega.0c03455.

[122] Jeffrey E. Post. "Manganese oxide minerals: Crystal structures and economic and environmental significance." In: *Proceedings of the National Academy of Sciences* 96 (7 Mar. 1999), pp. 3447–3454. ISSN: 0027-8424. DOI: 10.1073/pnas.96.7.3447.

[123] Kalyan Ghosh and Martin Pumera. "MXene and $MoS_(3-x)Coated3D-PrintedHybridElectr$ In: *Small Methods* 5 (8 Aug. 2021), p. 2100451. ISSN: 2366-9608. DOI: 10.1002/smtd.202100451.

[124] S. A. Hashmi et al. "Conducting polymer-based electrochemical redox supercapacitors using proton and lithium ion conducting polymer electrolytes." In: *Polymer International* 47 (1 Sept. 1998), pp. 28–33. ISSN: 0959-8103. DOI: 10.1002/(SICI)1097-0126(199809)47:1<28::AID-PI3>3.0.CO;2-C.

[125] Lei Li et al. "High-Performance Pseudocapacitive Microsupercapacitors from Laser-Induced Graphene." In: *Advanced Materials* 28 (5 Feb. 2016), pp. 838–845. ISSN: 09359648. DOI: 10.1002/adma.201503333.

[126] Kai Shen, Junwei Ding, and Shubin Yang. "3D Printing Quasi-Solid-State Asymmetric Micro-Supercapacitors with Ultrahigh Areal Energy Density." In: *Advanced Energy Materials* 8 (20 July 2018), p. 1800408. ISSN: 16146832. DOI: 10.1002/aenm.201800408.

[127] Andrea Massa et al. "Electro-oxidation of phenol over electrodeposited MnOx nanostructures and the role of a TiO2 nanotubes interlayer." In: *Applied Catalysis B: Environmental* 203 (Apr. 2017), pp. 270–281. ISSN: 09263373. DOI: 10.1016/j.apcatb.2016.10.025.

[128] Renpeng Yu et al. "Overcurrent Electrodeposition of Fractal Plasmonic Black Gold with Broad-Band Absorption Properties for Excitation-Immune SERS." In: *ACS Omega* 5 (14 Apr. 2020), pp. 8293–8298. ISSN: 2470-1343. DOI: 10.1021/acsomega.0c00698.

[129] Alberto Scalia et al. "Electrolytes based on N-Butyl-N-Methyl-Pyrrolidinium 4,5-Dicyano-2-(Trifluoromethyl) Imidazole for High Voltage Electrochemical Double Layer Capacitors." In: *ChemElectroChem* 6 (2 Jan. 2019), pp. 552–557. ISSN: 21960216. DOI: 10.1002/celc.201801172.

[130] Qi Kang et al. "A single wire as all-inclusive fully functional supercapacitor." In: *Nano Energy* 32 (Feb. 2017), pp. 201–208. ISSN: 22112855. DOI: 10.1016/j.nanoen.2016.12.020.

[131] S TRASATTI. "Electrochemistry and environment: The role of electrocatalysis*1." In: *International Journal of Hydrogen Energy* 20 (10 Oct. 1995), pp. 835–844. ISSN: 03603199. DOI: 10.1016/0360-3199(95)00014-5.

[132] Thibaud Guillemin et al. "Solid-state 3D micro-supercapacitors based on ionogel electrolyte: Influence of adding lithium and sodium salts to the ionic liquid." In: *Energy Storage Materials* 50 (Sept. 2022), pp. 606–617. ISSN: 24058297. DOI: 10.1016/j.ensm.2022.05.041.

[133] Anju Toor et al. "Stencil-printed Lithium-ion micro batteries for IoT applications." In: *Nano Energy* 82 (Apr. 2021), p. 105666. ISSN: 22112855. DOI: 10.1016/j.nanoen.2020.105666.

[134] Lu Yin and Joseph Wang. "Wearable Energy Systems: What are the Limits and Limitations?" In: *National Science Review* (Mar. 2022). ISSN: 2095-5138. DOI: 10.1093/nsr/nwac060.

[135] Lars H. Hess, Ladyna Wittscher, and Andrea Balducci. "The impact of carbonate solvents on the self-discharge, thermal stability and performance retention of high voltage electrochemical double layer capacitors." In: *Physical Chemistry Chemical Physics* 21 (18 2019), pp. 9089–9097. ISSN: 1463-9076. DOI: 10.1039/C9CP00483A.

[136] GiriBabu Sinnapolu and Shadi Alawneh. "Integrating wearables with cloud-based communication for health monitoring and emergency assistance." In: *Internet of Things* 1-2 (Sept. 2018), pp. 40–54. ISSN: 25426605. DOI: 10.1016/j.iot.2018.08.004.

[137] Jarkko Hyysalo et al. "Smart mask – Wearable IoT solution for improved protection and personal health." In: *Internet of Things* 18 (May 2022), p. 100511. ISSN: 25426605. DOI: 10.1016/j.iot.2022.100511.

[138] Joseph Abys. "Modern Electroplating, Fifth Edition." In: Feb. 2011, pp. 327–368. ISBN: 9780470167786. DOI: 10.1002/9780470602638.ch12.

[139] Qiancheng Zhu et al. "A New View of Supercapacitors: Integrated Supercapacitors." In: *Advanced Energy Materials* 9.36 (2019), p. 1901081. DOI: https://doi.org/10.1002/aenm.201901081. URL: https://onlinelibrary.wiley.com/doi/abs/10.1002/aenm.201901081.

[140] Simone Bernardini et al. “Raman spectra of natural manganese oxides.” In: *Journal of Raman Spectroscopy* 50.6 (2019), pp. 873–888. DOI: https://doi.org/10.1002/jrs.5583. URL: https://analyticalsciencejournals.onlinelibrary.wiley.com/doi/abs/10.1002/jrs.5583.

This Ph.D. thesis has been typeset by means of the TEX-system facilities. The typesetting engine was LuaLATEX. The document class was `toptesi`, by Claudio Beccari, with option `tipotesi=scudo`. This class is available in every up-to-date and complete TEX-system installation.